UNIVERSITY OF OKLAHOMA

GRADUATE COLLEGE

CATALYTIC CONVERSION OF FURFURAL TO MORE UPGRADABLE

PRODUCTS OVER BIFUNCTIONAL CATALYST

A THESIS

SUBMITTED TO THE GRADUATE FACULTY

in partial fulfillment of the requirements for the

Degree of

MASTER OF SCIENCE

By

LEIDY VALERIA HERRERA ARAQUE
Norman, Oklahoma
2017

CATALYTIC CONVERSION OF FURFURAL TO MORE UPGRADABLE
PRODUCTS OVER BIFUNCTIONAL CATALYST

A THESIS APPROVED FOR THE
SCHOOL OF CHEMICAL, BIOLOGICAL AND MATERIALS ENGINEERING

BY

_____
Dr. Steven P. Crossley, Chair

_____
Dr. Daniel Resasco

_____
Dr. Lance Lobban

To my family Hugo Herrera, Yolanda Araque and Catherin Herrera.

Acknowledgements

Thanks to the merciful God for all the countless gifts and opportunities He has given to me.

To my parents and sister for giving me so much love and support. They help me in the way of accomplishing my dreams always believing in me. I do not know what I would do without my family, and I appreciate everything they have done for me.

My advisor Dr. Steven Crossley who provided an endless amount of support, positivity, and guidance throughout my time at the graduate school. He spent an enormous amount of time discussing research with me and promoting my professional skills. His encouragement and enthusiasm helped me big time in this process.

Dr. Daniel Resasco for giving me the opportunity to live and study at the University of Oklahoma. He believed in me when I came looking for an opportunity and opened space in his investigation group for me to learn and become a better researcher. I consider myself lucky to be guided by such an incredible professor who every day teaches me something new. Thanks to him, I am now making a dream come true by achieving my Master's degree. Also, many thanks to Dr. Lobban and Dr. Wang for being always open to answer my questions and trying their best to give me a complete and accurate answer.

Santiago Umbarila thanks for being next to me in each step of my journey. Thank you for being light in the darkest days. I am lucky to count on someone so kind, lovely and intelligent like you.

Table of Contents

List of Tables

List of Figures

x

Abstract

Furanics are produced in high abundance from the decomposition of biomass. The thermal and chemical instability of these species leads to the formation of humins upon condensation. The ring rearrangement of furfural via the Piancatelli mechanism to form 2-cyclopentenone/cyclopentanone is a well-established reaction known to occur in the aqueous phase, but this requires a prior condensation where humin formation readily occurs. The upgrading of furfural to cyclopentanone in a single step over supported TiO_2 catalysts in the vapor phase is studied. Role of water, nature of active site and mechanism were evaluated over different catalyst. This reaction was also investigated in presence of acetic acid and water that are the most abundant oxygenated chemicals obtained from biomass. Selectivity for ring rearrangement vs. C-O cleavage over TiO_2 supported Ru and Pd catalysts can be tuned by manipulating the water partial pressure. Furfural and acetic acid compete for active sites. The presence of acetic acid influences the adsorption of furfural facilitating the breaking of the ring. Finally, combining the ability to synthesize carbon nanotubes with different properties, the location of the active site and important kinetics pathways for this rearrangement reaction are discussed.

Chapter 1: Introduction

Biomass is an ideal alternative to traditional resources because it is environmentally friendly, abundant and renewable[1]. Lignocellulosic biomass is composed mostly of three polymers: hemicellulose, cellulose and lignin. The specific ratios of these compounds depend on the source, normally ranged between 40−50%, 25−35%, and 15−20% of lignocellulose, respectively [2].

Fractionation of the bio-oil in stages, with a less complex distribution of chemical functionalities facilitates the subsequent catalytic upgrading, which is a more promising process to remove oxygen from the bio-oil [3]. By carrying out the treatment at successively higher temperatures different vapor product streams are obtained, which individually are far less complex than whole pyrolysis oil. At each stage, the nature of the chemical compounds formed depend on their thermal stability. The first stage is initial heating at 270 °C resulting in the formation of small oxygenates, primarily acetic acid and furfural; increasing to 350 °C breaks down cellulose forming sugars as levoglucosan and furfural; finally, at the highest pyrolysis temperature, degradation of the lignin and fractions remaining in the solid results in a mixture of multiple methoxylated phenolics (e.g., guaiacol, syringol), catechols, phenol, and other lignin monomers, as well as smaller amounts of lignin dimers, trimers, etc, **Figure 1** [4-6].
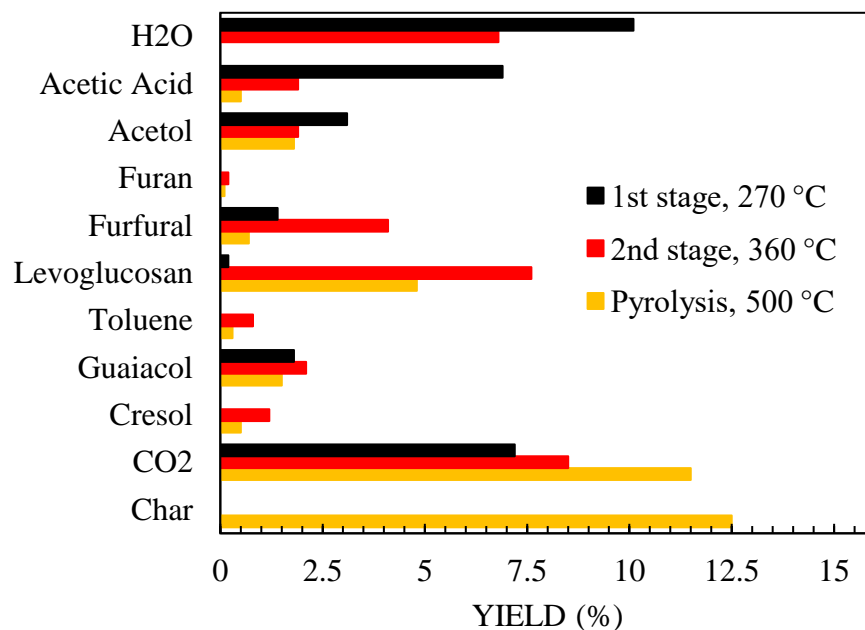
Figure 1 Yields for a three-stage torrefaction process of raw oak [7]

The conversion of biomass to fuels and chemicals through fast pyrolysis presents great economic potential over alternative methods such as liquefaction, hydrolysis or gasification. However, the obtained mixture contains over 400 different oxygenated compounds with a variety of functional groups and many undesirable properties due to its intrinsic chemistry. Therefore, the upgrading of the mixture is required to obtain suitable compounds for fuels and chemicals[1,8,9].

Upgrading of furfural

The first stage of torrefaction requires a low temperature (~270 °C) to mainly degrade hemicellulose and release vapors that include acetic acid and furfural as major oxygenates, together with lesser amounts of C_1–C_4 oxygenates [10]. Furfural is an almond-scented, oily, colorless liquid. It is used as a solvent for refining lubricating oils, as a fungicide and in the production of different chemicals as furfuryl alcohol,

2

tetrahydrofuran, methylfuran, etc, **Figure 2** [11]. It has been selected as one of the top 30 biomass derived building block compounds by the U.S. Department of Energy based on several criteria such as the raw material, estimated processing cost, technical complexity, and market potential [12].
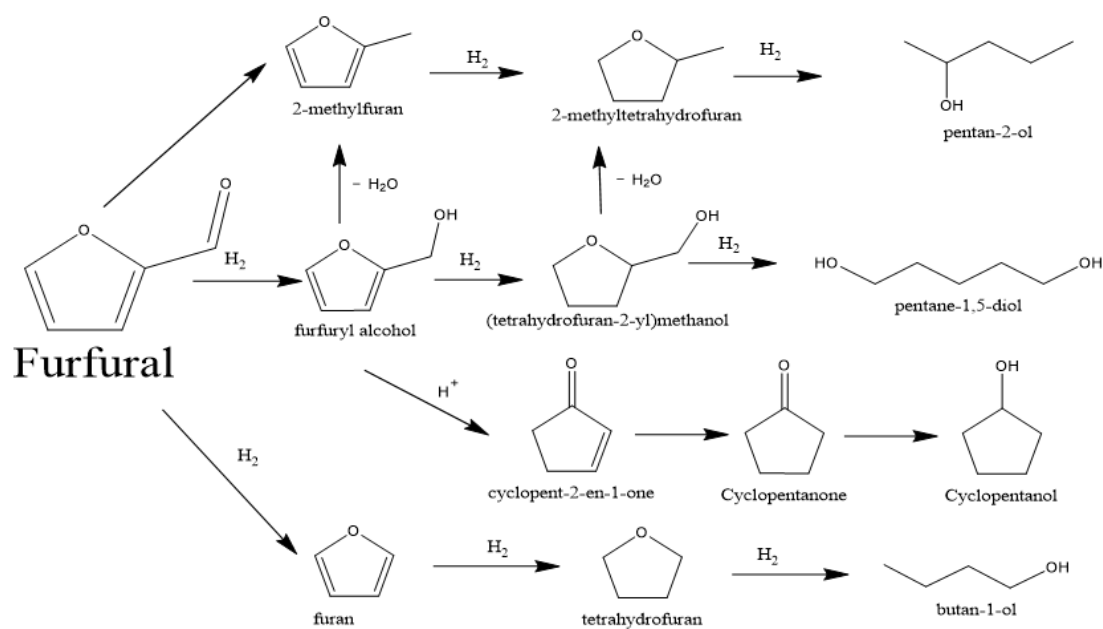
Figure 2 Value-added chemicals derived from furfural

Besides pyrolysis of biomass, furfural can be also produced by acid–catalyzed dehydration of xylose, a pentose sugar, obtained from hemicellulose [13,14]. However, furfural presents an obstacle for catalytic upgrading processes. First of all, the number of carbons in a furfural molecule after deoxygenation is too low to be added with gasoline. Secondly, furfural is thermally unstable and rapidly polymerizes forming humins. Furfural is highly reactive under typical biomass processing conditions and even at room temperature. This rapid polymerization complicates the condensation approach since the furfural will have already polymerized. Therefore, the possibility to convert furfural in

the dilute vapor phase prior to condensing in the liquid phase can significantly increase yields and improve the characteristics of the final product [4,15].

Furfural hydrogenation to furfuryl alcohol

Furfural holds two useful functional groups, a carbonyl and a conjugated furan ring, making its role as a versatile building block for various applications. The carbonyl (C=O) group of the furfural ring can be reduced leading to furfuryl alcohol, which is the main hydrogenation product obtained from furfural [16]. The industrial production of furfuryl alcohol is performed by selective hydrogenation of furfural in the gas or liquid phase using Cu−Cr catalysts. Chromium causes serious environmental problems due to its high toxicity. As a consequence of the high toxicity of chromium, experimental and theoretical methods have studied the selective hydrogenation of furfural over a variety of environmentally acceptable metal catalysts (Cu, Pd, Pt, Co, and Zn) leading to different reaction pathways[17-19]. Among those reaction mechanisms proposed, Cu-based catalysts and group VIII metal catalysts are the most widely accepted, **Figure 3a, b**. Resasco *et al.* showed furfural tends to adsorb perpendicular through the carbonyl group directly bonded to the surface via a lone pair of electrons of oxygen in a η^1(O)-aldehyde binding mode over Cu, and consequently favors hydrogenation of the C=O bond yielding mainly furfuryl alcohol [20]. The further hydrogenation of the η^1(O)-adsorbed species to furfuryl alcohol can proceed via either an alkoxide intermediate or a hydroxyalkyl intermediate, **Figure 3a**. The lower activation barrier for hydroxyalkyl intermediate indicates that the first H atom prefers to attack at the O atom rather than the C atom of the carbonyl group [21].
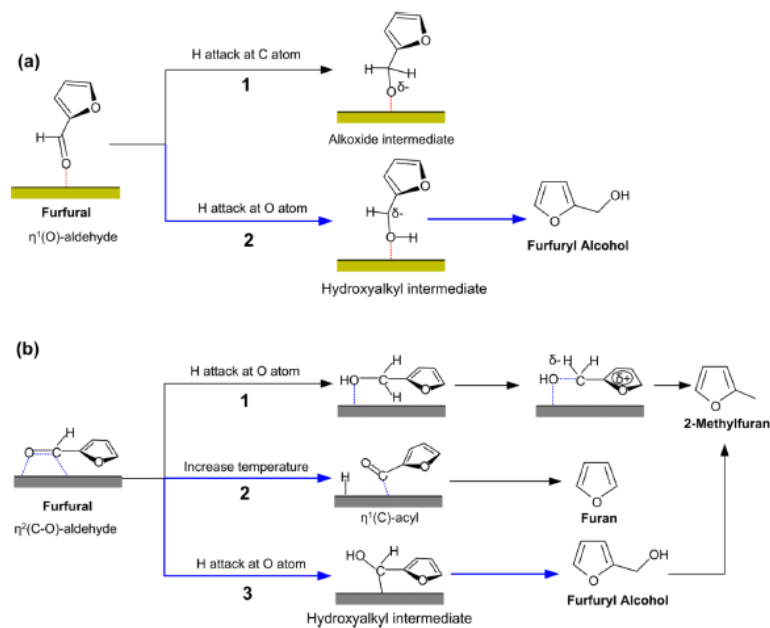
Figure 3 Mechanisms of furfural hydrogenation to furfuryl alcohol over a Cu and b group VIII metals based on DFT calculations and experimental results [22]

Vlachos *et al.* investigated the group VIII metal surfaces finding that the most stable adsorption mode of furfural is flat in the η^2(C,O)-aldehyde configuration with both the C and O atoms of the carbonyl group bonded to the metal surface, **Figure 3b**. The further hydrogenation occurs preferentially with a hydroxyalkyl intermediate to furfuryl alcohol [22]. Due to the electron-withdrawing and space effect of the carbonyl group, the furan ring of furfural is less accessible to the cleavage of the ring. The hydrogenation of C=C bonds in the furan ring of furfural can produce tetrahydrofurfural and tetrahydrofurfuryl alcohol. Since the furan ring is stable, metals with strong affinities for C=C bonds allow furfural to adsorb parallel to the metal surface, facilitating the saturation of the ring [20].

Furfural decarbonylation to furan

Experimental and theoretical studies have shown when the reaction temperature increases, the preferred binding mode of furfural changes from the $\eta^2(C,O)$-aldehyde configuration to the $\eta^1(C)$-acyl configuration, leading to the formation of furan via decarbonylation [20]. Different catalysts have been investigated for this reaction, including supported noble metal catalysts and mixed metal oxides based on non-noble metals such as Zn−Fe, Zn−Fe−Mn, Zn−Cr, etc. Pd has been identified as the more selective catalyst for furfural decarbonylation, at high temperature and H_2 pressure, while catalysts with oxophilic sites have been shown to stabilize the metal oxygen bond more strongly and hinder the formation of surface acyl species, leading to decreased selectivity of decarbonylation products [23,24]. Although Pd catalysts are more active than other catalysts, the yield of furan decreases sharply with time on stream. Among the various possible reasons for the observed deactivation, the most commonly proposed is carbon deposition, which could be due to side reactions, such as condensation and/or decomposition of furfural. The change of oxidation state and the sintering of the particles can also promote deactivation. The further hydrogenation of C=C bonds in the furan ring can produce tetrahydrofuran, which has been widely used as a solvent and intermediate for chemical production [20].

Furfural conversion to methyfuran

From the point of view of fuel production, either hydrogenation or decarbonylation are desirable. While the hydrogenation does not remove O, decarbonylation loses C in

the process. On the other hand, 2-methylfuran is an important component for producing perfume intermediates, fine chemicals and medicines. More interestingly, this molecule is desirable since it not only has intrinsically good fuel properties (high octane number, RON = 131, low water solubility, 7 g/L) but also can be considered an archetypical product of the desired reaction paths in bio-oil upgrading [25]. 2-methyl furan is produced from the hydrogenolysis of the C-O bond of furfuryl alcohol. Sitthisa *et al.* have shown that the combination of metals with oxophilic sites can facilitate the selective cleavage of this bond, for example through the use of Ni-Fe alloys. In the same study the DFT calculations suggest that the oxophilic nature of Fe makes the di-bonded η^2(C, O)-aldehyde more stable than on the pure Ni surface which indicates that the overall stronger interaction of the C=O group with the Ni-Fe alloy surface results in the weakening of the C-O bond of the furfuryl alcohol, **Figure 4** [20,26].
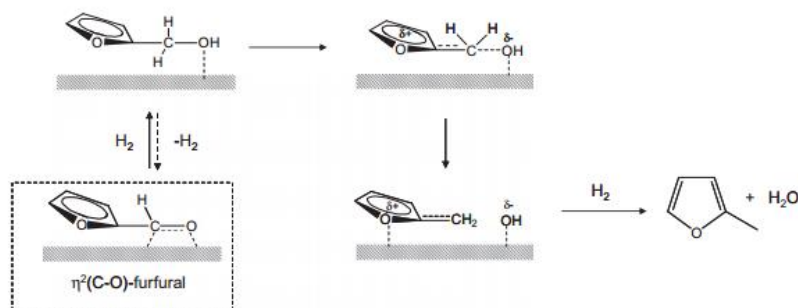
Figure 4 Possible species on the surface during conversion of furfural to 2-methylfuran over Ni-Fe [26]

Ring rearrangement of furfural to 2-Cyclopentenone and cyclopentanone

The rearrangement of furfural to cyclopentanone is a promising route since cyclopentanone is more stable than furfural and furfuryl alcohol even in hot water at

higher temperatures. Furthermore, its ketone group and the α-hydrogen allow the coupling of cyclopentanone with other ketones, aldehydes, and also with itself via self-aldol condensation. Cyclopentanone can be prepared by vapor-phase catalytic cyclization of 1,6-hexanediol or adipic esters, liquid phase oxidation of cyclopentene by nitrous oxide, and hydrogenation of phenol. However, all of these petroleum based processes are less developed because of the high cost of the feedstocks and environmental concerns [27].

The most studied catalysts for the transformation of furfural to cyclopentanone are Cu-based catalysts, with yields in the range of 60−80%. Hronec *et al.* was the first to report the furfural ring rearrangement. Recently they obtained 92.1 mol% yield over carbon-supported Pd−Cu catalysts, suggesting that the distribution of Pd^0 and Cu^+ was responsible for the catalyst activity and selectivity [28]. Yang *et al.* investigated this reaction over Ni−Cu/SBA-15 bimetallic catalysts in aqueous media under a H_2 atmosphere and obtained a 62% yield of cyclopentanone [29], while Li *et al.* obtained a 67% yield over Cu−Co bimetallic catalysts . Several noble metals have also been tested showing good activity [25]. Hronec and co-workers found that in the presence of 5% Pt/C catalyst, a 76.5% yield was obtained in water at 160 °C and 8.0 MPa H_2. They also studied the effect of the solvent and the metal type (Ni, Pt, Pd, or Ru) on the rearrangement of the furan ring to cyclopentanone, showing that Pt was more selective to produce cyclopentanone than other metals and that the acid−base properties of the solvent as well as the furfural concentration influenced the product distribution [30,31].

The mechanism of the ring rearrangement of furanic species to cyclopentanone was first reported by Piancatelli *et al.* who observed the rearrangement of 2-furylcarbinol into a 4-hydroxycyclopent-2-enone in an acidic aqueous system. The same rearrangement has

been also reported with 2-furylcarbinol and furfuryl alcohol. From furfural, this mechanism requires an initial hydrogenation step for the formation of furfuryl alcohol [31], which is typically achieved over metals in the presence of hydrogen. The subsequent ring rearrangement to cyclopentanone is thought to be acid catalyzed by water.

The nucleophilic attack of the furan ring by H_2O in the Piancatelli mechanism, as well as the influence of an aqueous environment on stabilization of the intermediate species on the metal surface have been stated as explanations for water's role. Even in the absence of added acid, H_2, or catalyst, 4-hydroxy-2-cyclopentenone has been reported to result from the heating of furfuryl alcohol in water [32]. The required acidity in this case was reported to result from the hydronium ions inherently present in water. However, in the absence of water furfural conversion is mainly to tetrahydrofurfuryl alcohol and methyltetrahydrofuran rather than the ring closure products [29].

Hronec *et al* [30], proposed a mechanism for the ring rearrangement reaction that involves water and claims as first step the formation of carbocation. They based this hypothesis in the fact that not ring rearrangement reaction proceeds with 2-methylfuran as the reactant. The carbocation specie is produced in an excess of hydrogen by scission of the C-O bond in the alkoxide or hydroxyalkyl intermediates, but not by dissociation of strong C-H bond in the methyl group of 2-methylfuran. The stabilization of the carbocation plays a very important role as well. If the reactive carbocation is not stabilized, it is quickly transformed to undesirable products. The stabilization of carbocation is achieved by its strong binding on the metal surface and by additional interaction with co-adsorbed water and furfural or furfuryl alcohol. Besides influencing the adsorption characteristics of the carbocation on the metal surface, water can attack

9

the carbocation and thus favor the cleavage of the C-O bond and subsequently the rearrangement of formed species to cyclopentanone.
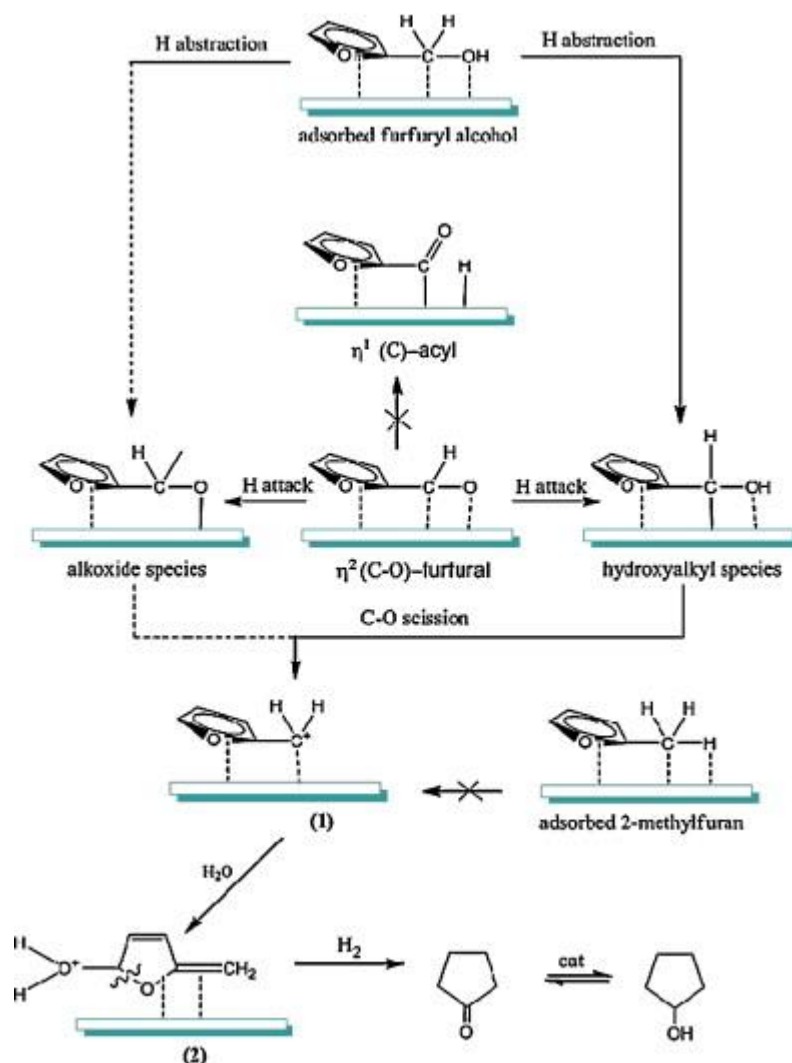
Figure 5 Proposed reaction mechanism for the furan ring rearrangement to cyclopentanone [31]

The ring rearrangement of furfural via the Piancatelli mechanism to form 2-cyclopentenone/cyclopentanone is a desired reaction because it does not involve the loss of any carbon and cyclopentanone can undergo aldol condensation reactions to more valuable molecules [27]. The transformation of furfural to cyclopentanone is a well-established reaction known to occur in the aqueous phase, but currently requires a prior

condensation where humin formation readily occurs[29-31]. However, the vapor phase conversion of furfural to cyclopentanone has not been studied. Therefore, this work focuses on the upgrading of furfural, investigates the reaction chemistry as well as the nature of the active sites and the influence of biomass derived co-adsorbates on furfural conversion to cyclopentanone in the vapor phase over different bifunctional catalyst.

Chapter 2: Stabilization of furanics to cyclic ketone building blocks in the vapor phase

Introduction

Furanic species are well known products of biomass degradation. While a variety of techniques can be used to produce furanic species from biomass in high abundance, ranging from hydrolysis to pyrolysis, the selective conversion of furanics to higher value products while minimizing side reactions such as humins formation remains a challenge. A wide range of reactions have been proposed to yield higher value products from furanics,[26,33,34] the ring rearrangement reaction to form cyclic ketones, commonly referred to as a Piancatelli ring rearrangement, carries significant promise.

The formation of cyclopentanone (CPNO) and its derivatives from the ring rearrangement of furanic molecules such as furfural (FAL) is promising for a variety of reasons. Cyclopentanone is more stable than FAL and more amenable to long term storage and transportation than its furanic counterpart. In addition, CPNO is capable of undergoing self-aldol condensation reactions to form jet fuel precursors, unlike furfural.[27,35,36] CPNO is a valuable specialty chemical as well, serving as an important intermediate for the production of a variety of polymers and pharmaceutical chemicals.[29,37]

Initial studies focusing on this reaction proposed a pathway via the rearrangement of a 2-furylcarbinol into 4-hydroxycyclopent-2-enone in the aqueous phase in an acidic aqueous environment.[38] It has been shown that the presence of water is necessary for this reaction to occur, and that the reaction rate is enhanced in acidic environment[28-30,32].

12

Unfortunately, the conditions that are known to favor the ring rearrangement (acidic aqueous conditions) are also the same conditions that are known to benefit undesirable humin formation.

Among the different techniques that can be used to convert biomass into biofuels and more valuable compounds, torrefaction is considered an attractive technique where undergoing a mild heat treatment from 200-330 °C biomass partially decomposes, releasing mostly water and to a lesser extent organic compounds. This step leads to an increase in energy density of the solid residue, that is, the resulting carbon/oxygen ratio is higher than the initial [4,39] and decreases costs associated with producing oxygenated monomers.[1,40] However, the cellulose and hemicellulose are converted to anhydrosugars in the process at elevated temperatures, and the bio-oil, once condensed is not thermally stable. Furanic species have a well-known propensity to form humin species when stored even at room temperature in bio-oil mixtures.[1,5,41,42] The possibility to convert these furanic species in the dilute vapor phase prior to condensing to a liquid phase has the potential to significantly increase yields and improve the overall thermal stability of the resulting product.

While a great deal of effort has been dedicated to the transformation of FAL and other furanics in the vapor phase, [43-47] products observed are typically limited to furfuryl alcohol (FOL), 2-methylfuran (2MF), furan (FUR) and cracking products. [48-52] Here we show that TiO_2 supported catalysts in the presence of water vapor at elevated temperature and atmospheric pressure can catalyze ring rearrangement reactions in the absence of a condensed phase. Water exhibits the remarkable role of shifting the selectivity from 2MF to 2-cyclopentenone (2CPNE) and subsequently CPNO, while also decreasing excess

13

hydrogenolysis to form light gases. The model compound studies were found to be in good agreement with the reaction of Red Oak torrefaction feeds which contained a mixture of furfurals, acids/esters and an excess of water where both cyclopentanone and 2-methylfuran were produced. The role of the metal/support interface as well as defects on the TiO_2 support on this reaction is discussed.

Experimental

Catalyst Preparation

Ru and Pd catalysts were synthesized using the incipient wetness impregnation method of an aqueous solution of hexaamineruthenium (III) chloride (98% Sigma Aldrich) and palladium (II) nitrate dehydrated, respectively, on the TiO_2 support (Aeroxide P25, 0.25 ml/g pore volume) or SiO_2 support (Hisil-210, 0.96 ml/g pore volume). The catalysts were then dried at room temperature in air for 48 h, at 120 °C for 12 h in an oven before reducing at 400 °C for 2 h in hydrogen flow. The catalysts were pelletized and sieved to yield pellet sizes from 250-420 μm.

Catalyst Characterization

Nicholas Briggs performed the characterization of the different catalyst by TEM.

Inductively coupled plasma mass spectrometry (ICP-AES) was utilized to determine Ru content of the synthesized catalysts, since Ru is known to have high mobility during reduction and form gases which makes the total amount of the metal in

the catalyst smaller [53]. Ru and Pd particle size distribution was obtained using Transmission Electron Microscopy (TEM, JEOL JEM-2100 model). Before imaging, the catalysts were pre-reduced in hydrogen flow at 400 °C for 1 h and cooled down to room temperature in nitrogen before dispersion in isopropanol and sonication to obtain a uniform suspension. A few drops of the suspension were dispersed on carbon-coated copper TEM grids. At least 200 particles were counted in order to obtain particle size distributions, which are shown in Figure S1 to S10.

Catalytic Activity Tests

Catalytic activity was tested in a quartz tube packed bed flow reactor (0.25 in OD) at atmospheric pressure and 400 °C. Catalyst particles (250-420 μm) were mixed with inert acid-washed glass beads (Sigma Aldrich, Part number: G1277) with a particle size range of 212-300 μm and packed between two layers of quartz wool inside the reactor. In a typical experiment, pure distilled furfural (obtained from Sigma Aldrich; distilled and stored at -15 °C) with a feed flow rate of 0.1 ml/h or co-fed with water 0.25mL/h, was vaporized at the inlet zone of the reactor before introduction into a 30 ml/min hydrogen flow. The outlet stream of the reactor was heated to 250 °C to prevent condensation of compounds in the transfer lines and then flows through a six-port valve to allow for injection into a GC for product analysis. Product distribution was analyzed by online gas chromatography equipped with flame ionization detector (Agilent 5890), and HP-INNOWAX column (30 m, 0.25 µm). Identification of products was confirmed using a Shimadzu QP-2010 GCMS and standards were used to quantify the various products in the FID. Before introduction of the feed, the catalysts were reduced in situ at 400 °C for 1 h in 100 ml/min hydrogen flow. Mass balances for all the reactions were > 94 %.

Oak Torrefaction Experiments

For these experiments using the real biomass vapors Red Oak sawdust was ground to 0.25-0.45 mm and dried in a vacuum oven (0.02 MPa) at 60 °C for 24 hours. Sample sizes consisting of 0.7-1.0 mg red oak were packed in a quartz sample tube for use in the pyroprobe CDS analytical Model 5250 with autosampler. The heating chamber in the pyroprobe is a quartz chamber that was heated to 270 °C for 20 min in 20 ml/min inert helium carrier gas. The vapors produced over the 20 min travel through the transfer lines where a 20 ml/min hydrogen stream is introduced. Hydrogen is introduced after the torrefaction step to ensure torrefaction is carried out under an inert environment. After passing through the catalyst bed the vapors are collected in a sorbent trap at -50 °C by use of N_2. The trap is then desorbed at 300 °C for 3 minutes and the vapors passed through 1/16" Silcosteel transfer lines at 300 °C to a separate quartz reactor setup for ex situ upgrading. An 8" quartz reactor tube placed inside a 2" ID x 6" Fibercraft Heater was connected to the pyroprobe transfer lines. 1.0 mg of Ru/TiO_2 catalyst was mixed thoroughly with 200 mg acid washed borosilicate beads (Sigma Aldrich G1145) to prevent channelling. The catalyst bed was maintained halfway through the quartz reactor by use of 30 mg of quartz wool. Temperature was measured directly outside of the quartz reactor tube by use of an Omega Type K thermocouple.

Analysis of the vapor product stream was carried out using an online Shimadzu QP2010 GCMS-FID system equipped with a RTX-1701 column (60m×0.25mm with 0.25 µm film thickness). The column oven heating ramp was set to hold at 4 min at 45 °C then ramp at 3°C/min to 280°C and hold for 20 min. A helium carrier gas was used with a total flowrate of 90 ml/min and a column flowrate of 1 ml/min. The products were

identified by literature mass spectral data and quantified using FID peak area. Calibration injections of known torrefaction products were applied to determine the molar amounts of each compound in the product stream.

The mass spectrum allowed for identification of each product using the mass fragmentation patterns and literature while yields were determined using the FID area of a peak normalized to 1 mg of biomass fed. The FID/MS split ratio was set to 10:1. A calibration was then applied to determine the μg of carbon/mg biomass. This was done using an effective carbon number (ECN) model which is the number of carbons in the molecule that are effective in producing FID signal therefore it takes into account the various effects of C-O bonds on the FID signal. Due to the large amount of compounds seen in pyrolysis/torrefaction, traditional model compound injection calibrations were not feasible. This model has been used extensively for the quantification of compounds found in oak pyrolysis. The model was validated with our own experimental calibrations of 42 compounds, including typical compounds of light oxygenates, sugar derivatives and phenolic categories.

Results and discussion

Reaction of pure furfural over Ru/TiO$_2$

Product distributions for furfural conversion over Ru/TiO$_2$ in the vapor phase are shown in **Figure 6b**. The most abundant product is 2MF (yield = 59.7 % at 0.9 h), is produced from the hydrogenolysis of the C-O bond of FOL. Others have shown that the combination of metals with oxophilic sites can facilitate the selective cleavage of this

bond, for example through the use of NiFe alloys[26]. While it is known that this hydrogenolysis can occur on metal surfaces,[20,26,54,55] interfacial sites formed as a result of the interaction between Ru and the reducible oxide TiO_2 can play an important role in the formation of 2MF from FOL as seen by the importance of these sites in reactions such as Fischer- Tropsch[56] and alkane hydrogenolysis.[57]

The unanticipated reaction product observed under these conditions is 2CPNE and CPNO. Both of these products appear to increase at higher contact times (W/F, defined as grams of catalyst/grams of furfural fed per hour), while FOL yields pass through a maximum (yield = 5.5 % at 0.3 h). This result implies that FOL is subsequently converted to 2MF or possibly 2CPNE/CPNO at higher W/F values. FOL can be formed from direct hydrogenation of the carbonyl C-O bond of FAL on the Ru metal. This reaction has been shown to occur over various metal catalysts such as Pt, Pd, Cu and Ni in liquid and gas phase[21,26,30,54] To obtain FOL, the O atom in the carbonyl group of FAL can adsorb on top of the Ru surface in an η^1 configuration as has been reported over Cu catalysts.[21,58] FAL can also adsorb on metal surfaces with both C and O atoms bound to the surface in a η^2 mode.[20,59,60] At higher temperatures, the metal oxygen bond of the η^2 intermediate may break to form a surface acyl, which is a precursor to decarbonylation to produce FUR. Catalysts with oxophilic sites have been shown to stabilize the metal oxygen bond more strongly and hinder the formation of surface acyl species,[26] leading to decreased selectivity to decarbonylation products. This may be occurring at the Ru/TiO_2 interface in this case.

The unexpected formation of 2CPNE and the subsequent hydrogenation of the olefin to form CPNO represent the most interesting products observed here. From **Figure**

6b, the yield of these products increase steadily as the W/F increases. The yield of the

ring rearrangement products increased at higher W/F values, with the H_2O partial pressure

also increasing with W/F due to the in-situ water generated from 2MF production.
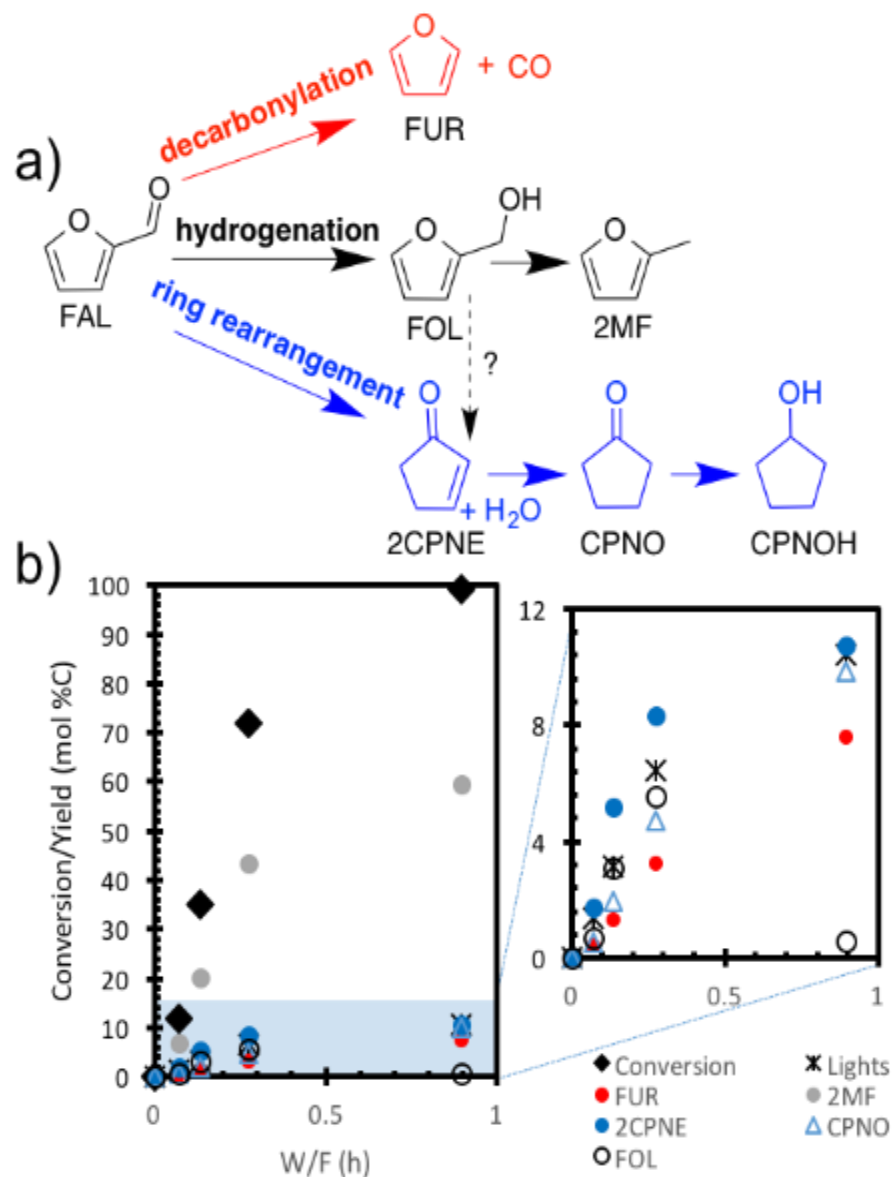
Figure 6 a. Reaction pathway of furfural conversion over Ru/TiO2. b. Furfural conversion and product yield with W/F over 4.4% Ru/TiO2 at 400°C. 1 atm, TOS: 30 min. Carbon balance ~ 95% all reactions

Role of water for furfural conversion to cyclopentanone

The importance of water for the Piancatelli rearrangement to occur in the liquid phase has been discussed extensively in literature [28-30,38], but this reaction has not been investigated in the vapor phase. It should be noted that even though water was not introduced as a reactant in the results presented above, the CPNO/2CPNE products were still observed. Water can be produced in-situ via the hydrogenolysis of FOL to form 2MF as discussed earlier.

To determine whether gas phase water is involved in this rearrangement, furfural was co-fed with excess water in a molar ratio 12:1, the results are presented in **Figure 7a**. With the introduction of water, the sum of the CPNO/2CPNE products (yield = 16 %) is similar to the yield of 2MF (yield = 17 %). Comparing this with the values obtained without water in the feed, CPNO/2CPNE (yield = 7 %), 2MF (yield = 20 %) an enhancement in the rate of the ring rearrangement reaction is clearly observed upon the introduction of water to the system. The role of the support on this reaction will be discussed in the following section.
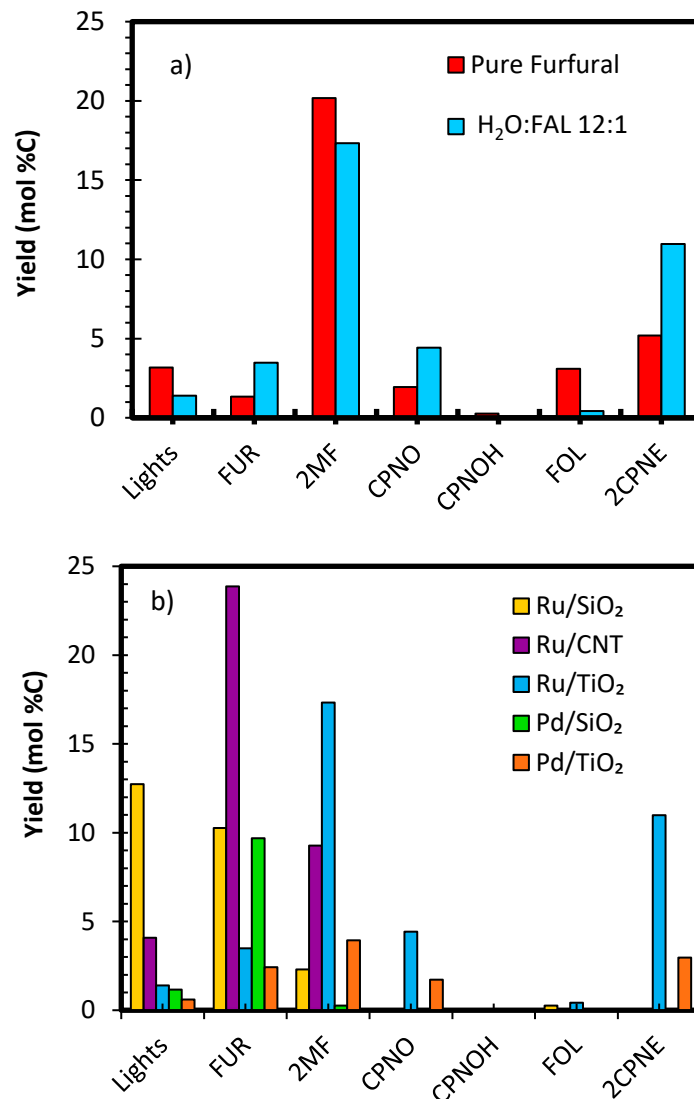
Figure 7 a) Product distribution for pure furfural and furfural co-fed with excess water at different molar ratios. 4.4% Ru/TiO2 at 400°C, 1 atm, and 30 minutes time on stream. Conversion=35%. Carbon balance ~ 95% all reactions. b) Product Yield for water/furfural (12:1 molar ratio) feed mixture over TiO₂, Ru/SiO₂ , Ru/CNT and Ru/TiO₂ catalysts W/F = 1.85h (TiO₂) and 0.13h (Ru/SiO₂ and Ru/TiO₂) and 0.39h(Ru/CNT) Conversion = 10% (TiO₂); 25%(5.3% Ru/SiO₂); 38% (4.4% Ru/TiO₂) and 37% (1% Ru/CNT) T = 400 °C, P = 1 atm, TOS = 30 mins. Carbon balance ~ 94% all reactions

Active sites responsible for conversion over Ru/TiO₂ and Pd/TiO₂

TiO$_2$ supported catalysts have been shown to exhibit several possible types of active sites for the selective cleavage of C-O bonds, ranging from the creation of new sites at the metal support perimeter to the presence of defects, or promoter effects on the support.[61] For the conversion of phenolic oxygenates, enhanced rates of C-O cleavage have been reported when the reducible oxide TiO$_2$ was introduced as a support, which was attributed to the synergy between Ru and TiO$_2$. While it was not clear if these sites were around the perimeter of the Ru metal or defects on the TiO$_2$ support far away from the metal, further studies showed that defect sites on the TiO$_2$ support are the active sites for the initial transalkylation step of guaiacol conversion, while the same is not necessarily the case for the subsequent C-O bond cleavage reactions such as the conversion of cresol to toluene [53,62].

To investigate the importance of active sites on the support for this rearrangement, pure Ru catalysts (supported on SiO$_2$ and CNT) and a bare TiO$_2$ catalyst with no metal loading were compared with Ru/TiO$_2$. The results obtained from feeding a water/furfural (12:1 molar ratio) mixture over these catalysts are presented in **Figure 7b**. Ru can facilitate the splitting of water leading to decoration of the metal surface with OH groups, which could potentially play a role in this reaction.[63-65] We shall proceed by discussing the difference in product selectivity observed over the pure Ru catalysts on inert supports (Ru/SiO$_2$ and Ru/CNT) and Ru/TiO$_2$. The following are evident: 1) CPNO and 2CPNE are only observed over Ru catalysts supported on TiO$_2$; 2) An enhancement in FAL conversion to 2MF, which is also a valuable product, is observed when compared to Ru

supported on the other tested supports. 3) Decarbonylation and C-C hydrogenolysis rates are inhibited on Ru/TiO$_2$ when compared to other supported Ru catalysts.

This enhancement to form desired products (CPNO/2CPNE and 2MF) as a result of the introduction of TiO$_2$ as a support could be due to either sites located around the perimeter of the metal particle, or defects in the TiO$_2$. To understand this further, the same reaction was conducted over pure TiO$_2$ without the Ru metal. As seen in **Table 1**, when passing FAL and water over TiO$_2$ alone, some 2CPNE/CPNO is observed, but due to the lack of a metal that promotes the dissociation of hydrogen, nearly an order of magnitude higher TiO$_2$ catalyst amount is necessary to achieve the same level of conversion as with metal supported in TiO$_2$.

If sites at the metal/support interface are directly involved in the ring rearrangement reaction, one would anticipate significant shifts in reaction rate with the carbon-metal and carbon-oxygen bond strength should play an important role in this reaction. To further probe the role of the metal, the FAL reactions with water were carried out over Pd supported on TiO$_2$, with Pd forming much weaker bonds with both carbon and oxygen than Ru.[66] The role of Pd at opening the furanic ring at interfacial sites is anticipated to be very different. Considering spillover to the TiO$_2$ support to create defects, however, Rekoske and Barteau reported indistinguishable isothermal reduction profiles when the two metals were added in similar quantities to a TiO$_2$ support.[67] This implies that the different behaviour between the two catalysts likely involves the direct interaction of the metal with the furanic species, as opposed to a simple shift in the number of defects on the TiO$_2$ support at steady state. In **Figure 7b** the production of

CPNO/2CPNE over Pd/TiO$_2$ is clearly lower than observed for Ru/TiO$_2$, but it is still present.

Table 1 shows the rate of formation of various products normalized per metal exposed (Ru or Pd), per TiO$_2$ surface area, and per perimeter area surrounding the nanoparticles for TiO$_2$ supported catalysts. Ru/TiO$_2$ is the most effective catalyst tested for forming ring rearrangement products. When compared with the TiO$_2$ support alone, the reaction rate is enhance by approximately 40x when Ru is incorporated, implying that the reaction can occur over defects alone, but the rate of this reaction is negligible when compared to rate in the presence of a metal.
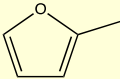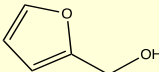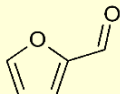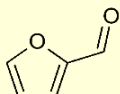
Table 1 Rate of products normalized per exposed metal, support, or metal-support perimeter

Catalyst	Conversion (%)	Rate product/exposed metal (mol/m^2.h)			Rate /Per TiO$_2$ (mol/m^2.h)	Rate/Per Perimeter (mol/m.h)	Carbon balance (%)
		FUR	LIGHTS	2CPNE+CPNO	2CPNE + CPNO	2CPNE + CPNO	
Ru/SiO$_2$	25	$1.23*10^{-03}$	$1.53*10^{-03}$	-	-	-	95
Ru/CNT	37	$5.55*10^{-03}$	$9.51*10^{-04}$	-	-	-	94
Ru/TiO$_2$	38	$4.42*10^{-04}$	$1.78*10^{-04}$	$1.95*10^{-03}$	$1.96*10^{-04}$	$3.52*10^{-12}$	95
Pd/SiO$_2$	11	$4.98*10^{-03}$	$6.02*10^{-04}$	-	-	-	96
Pd/TiO$_2$	12	$6.22*10^{-04}$	$1.57*10^{-04}$	$1.21*10^{-03}$	$5.96*10^{-05}$	$1.03*10^{-12}$	96
TiO$_2$	10	-	-	-	$5.14*10^{-06}$	-	94

*All reactions conducted at a water/FAL (12:1 molar ratio) feed mixture. W/F = 0.13h (Pd/SiO2 and Pd/TiO2), Conversion = 11.12% (1%Pd/SiO2) and 13.05%(1% Pd/TiO2), W/F = 1.85h (TiO2) and 0.13h (Ru/SiO2 and Ru/TiO2) and 0.39h(Ru/CNT) Conversion = 10% (TiO2); 25% (5.3% Ru/SiO2); 38% (4.4% Ru/TiO2) and 37% (1% Ru/CNT) T = 400 °C, P = 1 atm, TOS = 30 mins.

In the condensed aqueous phase ring rearrangement reaction, it is generally accepted that the role of the metal is to hydrogenate the FAL to form FOL, with subsequent ring rearrangement reactions occurring in the acidic solvent.[31,35] Rates of 2CPNE/CPNO production when feeding intermediate products (FOL and 2MF) can be used to determine the kinetic relevance of pathways involving these intermediates. As shown in **Table 2** when feeding 2MF no CPNO/2CPNE was observed, which illustrates that it is not a relevant intermediate for the reaction. Surprisingly, when feeding FOL, the yield of CPNO/2CPNE is lower when than was observed when FAL was fed over Pd/TiO_2. This indicates that FAL itself can undergo CPNO/2CPNE the furanic rearrangement prior to desorbing from the surface, and the role of the metal is not to simply supply hydrogen to create defects and yield alcohol intermediates that react on the TiO_2 support. These results suggest that the active site for this reaction lies at the interface of the metal and the TiO_2 support. The presence of water accelerates this reaction, even under vapor phase conditions. The mechanism by which water interacts with this catalyst at elevated temperatures, as well as the role of carbon-metal and carbon-oxygen bond strength should be the focus of follow up studies.

Table 2 Yield of products for reactions feeding different possible intermediates for the ring rearrangement

Catalyst	Entry*	Yield Products (%)					
		2CPNE	CPNO	2MF	Lights	FUR	CB**
Pd/TiO$_2$		-	-	-	0.59	-	93
		2.42	0.12	7.72	0.95	-	89
		2.96	1.7	3.94	0.61	2.42	96
Ru/TiO$_2$		6.82	1.69	5.98	1.40	3.47	95

*Reaction conditions: water/2MF: 12:1 (W/F = 0.13h (Pd/TiO$_2$, Conversion: 9.15%), water/FOL: 12:1 (W/F = 0.13h Pd/TiO$_2$, Conversion: 21.8%), water/FAL: 12:1 (W/F = 0.13h Pd/TiO$_2$, Conversion: 13.05%), and water/FAL: 12:1(W/F = 0.13 h Ru/TiO$_2$, Conversion: 38%), T = 400 °C, P = 1 atm, TOS = 30 mins. **CB: Carbon Balance*

Oak Torrefaction Experiments

As this reaction showed promise in model compound studies, it was of interest to study if the same reaction results would take place with real biomass stream. The effect of Ru/TiO$_2$ was studied flowing the Stage 1 torrefaction vapors of red oak to an *ex situ* pulse reactor. The torrefaction stream consisted primarily of water and C2-C3 acids and esters. The red oak also yielded 0.21 μmol of furfural specie. The upgrading results over Ru/TiO$_2$ for the first biomass pulse have been summarized in **Figure 8a**. As expected the acids and esters underwent ketonization reactions under these conditions to form C3-C4.

High levels of ketonization were observed to yield acetone and butanone from acetic acid and propionic acid-methyl ester. As shown **Figure 8b** once condensed, these compounds have stable behaviour that limits acid catalyzed reactions, this is of great importance as one of the main reasons for separation of the different chemical compounds via thermal fractionation is to improve catalyst life.

However, the most significant finding from this work is, remarkably, the FAL species reacted to produce 2CPNE/CPNO and 2MF similar to the model compound studies. Furfural conversion levels of 94% were observed in the initial biomass pulse. It is important to note that molar ratios of water/furfural levels are even higher with this feed than with model compound studies. Competitive adsorption due to the many compounds in the torrefaction vapor stream could be playing a major role in shifting the product selectivity and reactivity with these real feeds.

With the real torrefaction stream an increased selectivity to ring rearrangement products (74.86 %) was observed compared to dehydration products 2MF (17.18%). A summary of product selectivities can be seen in **Figure 9a**. Converted furfural not accounted is likely cracked into light gases over the metal catalyst.

During pulse experiments ten pulses of red oak was torrefied approximately two hours apart, each time the vapors passed through the reactor with the Ru/TiO_2 catalyst. As it can be seen in **Figure 9b**, the conversion to cyclopentenone/cyclopentanone and 2MF is fairly stable throughout the pulses. It was also observed that the ketonization reactions stayed at a stable conversion as well. It would be expected scaling up this upgrading process would lead to a stable liquid product. These results also show the

promise of the torrefaction process. This is the first evidence of a Piancatelli type rearrangement using actual biomass feeds. It is well known if a full pyrolysis of oak was carried out catalyst deactivation would be significant and unwanted side reactions would dominate. As this strategy limits the amount of different organic compounds that pass over the catalyst surface, targeted chemistries can occur. This promising product could then be upgraded in the liquid phase as discussed previously to form gasoline and/or diesel range products.
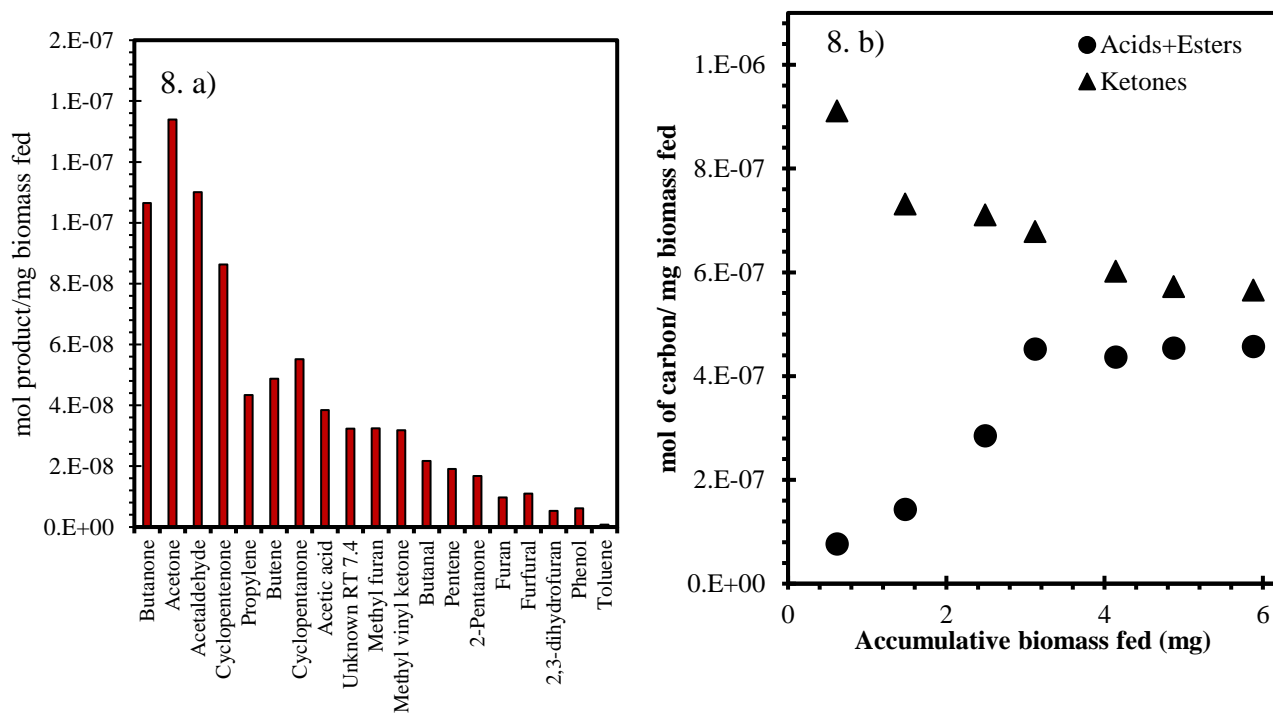
Figure 8 a. Product distribution of 1st pulse of Stage 1 torrefaction with 5% Ru/TiO2 catalyst. 3b. Sum of moles of acids + esters and ketones as a function of the biomass that is pulsed over the reactor
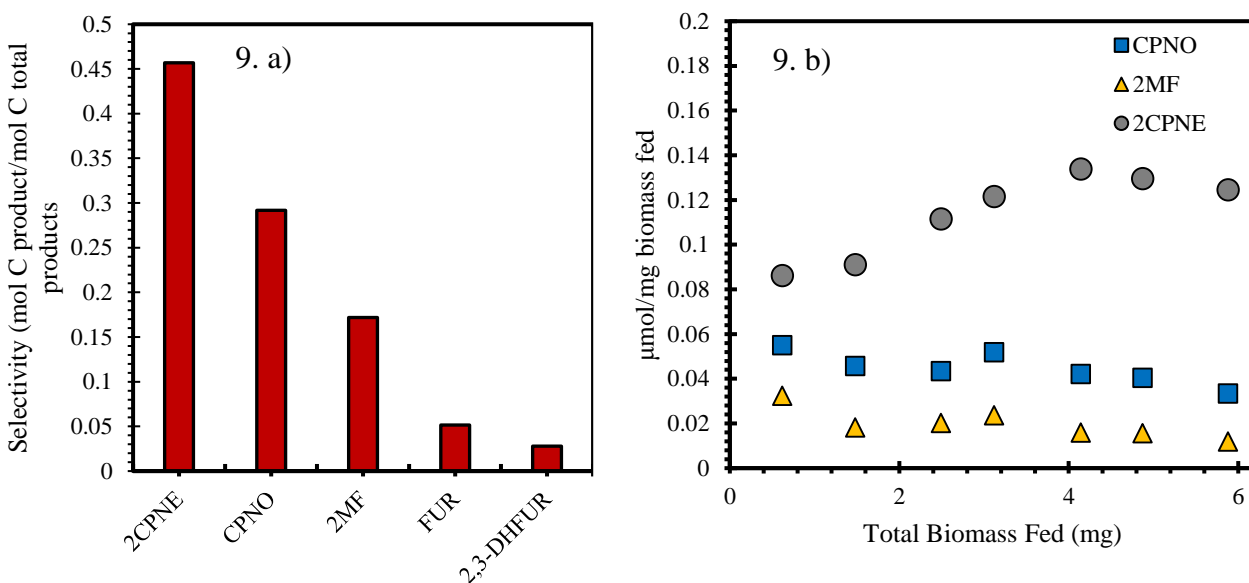
Figure 9 a Product yields derived from furfural on the first biomass pulse for torrefaction studies at 400°C, 4.4% Ru/TiO2 b. Yield of products from furfural as a function of biomass fed for torrefaction studies at 400°C, 4.4% Ru/TiO₂

Conclusions

The carbon efficient reaction of furfural to cyclopentanone/2-cyclopentenone to cyclopentanone/2-cyclopentenone was also observed with subsequent hydrogenation to form cyclopentanol. Water was demonstrated to play a role in shifting the selectivity from 2-methylfuran to cyclopentanone and 2-cyclopentenone. The support plays an important role in determining the product distribution as pure Ru catalysts produced mainly light gases and furan when compared with Ru/TiO₂. Experiments feeding various intermediates indicate that the vapor phase reaction does not proceed through an alcohol intermediate that desorbs from the catalyst surface, as is accepted in condensed phased reactions. Experiments over Pd supported catalysts imply that carbon-metal and oxygen-metal bond strength at the metal/support interface likely play an important role on this reaction.

Using Red Oak as a biomass source, the reaction was also observed with real torrefaction feeds in a pulse reactor. With the biomass feeds the selectivity to cylcopentanone was enhanced due to the adsorption effects of the numerous compounds found in the vapor stream.

Chapter 3: Influence of biomass derived co-adsorbates on furfural conversion over Ru/TiO₂
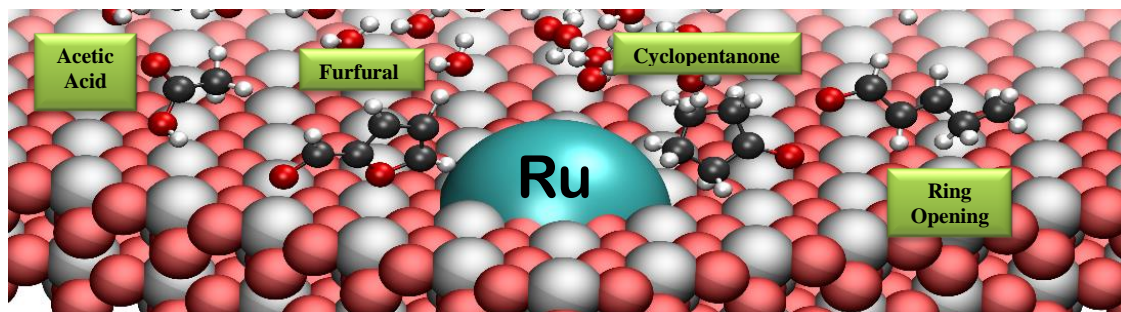
Introduction

Biomass torrefaction yields a significant amount of light oxygenates (acids, aldehydes, esters) and sugar derived products (furanics, pyrans) [2]. Furanic species such as furfural tend to form humins when stored even at room temperature. An upgrading of these species in the dilute vapor phase prior to condensing in the liquid phase can significantly increase yields and improve the overall characteristics of the final product [1,5,41,42].

Furfural (FAL) is considered as a building block for transportation fuels [68]. The carbonyl group of the furan ring can be reduced leading to furfuryl alcohol (FOL), which is the main hydrogenation product obtained from furfural. Depending on the type of metal catalyst use decarbonylation [69] and hydrogenolysis[26] of the etheric C-O bond can also proceed yielding furan (FUR) or methyl furan (2MF) respectively. It has been shown the consecutively ring opening of FUR and 2MF can happen over Ni/SiO₂ and Pd/SiO₂ obtaining products in the C4 and C5 range which can further alkylate the furan ring [20,23].

More interestingly we have reported the gas phase reaction of FAL co-feeding water over bifunctional catalyst such as Ru/TiO_2 can undergo selectively transformation to 2-cyclopentenone (2CPNE)/cyclopentanone (CPNO). While this reaction is well-known in the liquid phase as the ring rearrangement reaction [30,31], our previous report showed for the first time this mechanism occurring in the gas phase and with real biomass streams. The formation of CPNO is desirable because is more stable than furfural, its transformation does not involve a loss of carbon and CPNO can undergo further self-aldol condensation reaction to products in the jet fuel range [27].

Various starting reactant molecules have been tested in liquid phase for this rearrangement such as FAL, FOL, 4-hydrxoxy-2-carbynol and it has been demonstrated that water has an important role for the reaction to occur via key intermediates [29]. Furthermore, it has been shown that an appropriate addition of weak acids such as acetic acid (AcOH) has a positive effect on the production of CPNO over a Ni-based catalyst while the addition of basic molecules shows the opposite trend[29]. Similarly, results over Pt and Pd-Cu catalyst showed [28] the addition of weak acids such as AcOH, NaH_2PO_4 preferred the CPNO formation while the addition of Na_2CO_3, Na_2HPO_4 favored the hydrogenation of FOL to tetrahydrofurfuryl alcohol (THFOL).

This work investigates the role of water and primarily carboxylic acids in biomass such as AcOH for the FAL conversion over Ru/TiO_2 to 2CPNE/CPNO in gas phase which avoids the formation of humins [7]. The ring rearrangement products are observed in the presence of the mixture with high water partial pressure and acetic acid. The selectivity can be tuned to produce methylfuran vs. cyclopentanone via water partial pressure. Competition between the acid and the furfural is observed, the sites for 2CPNE/CPNO

production are inhibited by carboxyilic acids. However, water was found to play an important role in enhancing the 2CPNE/CPNO production even in presence of the acid. The adsorption/desorption of AcOH over the metal may change the adsorption of FAL facilitating the breaking of the ring to trans-2-pentenal, this product is observed at high selectivity only when co-feeding the acid.

Experimental

Catalyst Preparation

Ru catalysts were synthesized using the incipient wetness impregnation method of an aqueous solution of ruthenium (III) nitrosyl nitrate solution (1.5% Ru, Sigma Aldrich), on the TiO_2 support (Aeroxide P25, 0.25 ml/g pore volume) or carbon nanotube support. The catalysts were then dried at room temperature in air for 48 h, at 120 °C for 12 h in an oven before reducing at 400 °C for 2 h in hydrogen flow. The catalysts were pelletized and sieved to yield particles sizes from 90-250 μm.

Catalyst Characterization

Nicholas Briggs performed the characterization of the different catalyst by TEM.

Inductively coupled plasma mass spectrometry (ICP-AES) was utilized to determine Ru content of the synthesized catalysts. Ru particle size distribution was obtained using Transmission Electron Microscopy (TEM, JEOL JEM-2100 model). For this process, the catalysts were pre-reduced in hydrogen flow at 400 °C for 1 h and cooled

down to room temperature in nitrogen before their dispersion in isopropanol and sonication to obtain a uniform suspension. Few drops of the suspension were dispersed on carbon-coated copper TEM grids. At least 200 particles were counted in order to obtain particle size distributions.

Catalytic Activity Tests

Catalytic activity was tested in a quartz tube reactor (0.25 in OD) at atmospheric pressure and 250°C to 400 °C. Catalyst particles (90 – 250 μm) were mixed with inert acid washed glass beads (Sigma Aldrich, Part number: G1277) with a particle size range of 212-300 μm and packed between two layers of quartz wool inside the reactor when required. In a typical experiment, pure distilled furfural (obtained from Sigma Aldrich; distilled and stored at -15 °C) with a feed flow rate of 0.1 ml/h or co-fed with water or acetic acid at different ratios, was vaporized at the inlet zone of the reactor before introduction into a 30 ml/min hydrogen flow. The outlet stream of the reactor was heated to 250 °C to prevent condensation of compounds in the transfer lines and then flows through a six-port valve to allow for injection into a GC for product analysis. Product distribution was analyzed by online gas chromatography equipped with flame ionization detector (Agilent 5890), and HP-INNOWAX column (30 m, 0.25 µm). Identification of products was confirmed using a Shimadzu QP-2010 GCMS and standards were used to quantify the various products in the FID. Before introduction of the feed, the catalysts were reduced in situ at 400 °C for 1 h in 100 ml/min hydrogen flow.

Results and discussion

Catalyst characterization

The total metal loading is 4.1% for Ru/TiO_2 calculated with ICP. The Ru particles size supported on carbon nanotubes (CNT) was 1.5 nm, in the case of Ru/TiO_2 the particle size was 3.1 nm. TEM micrographs of the catalysts are shown in **Figure 10**.
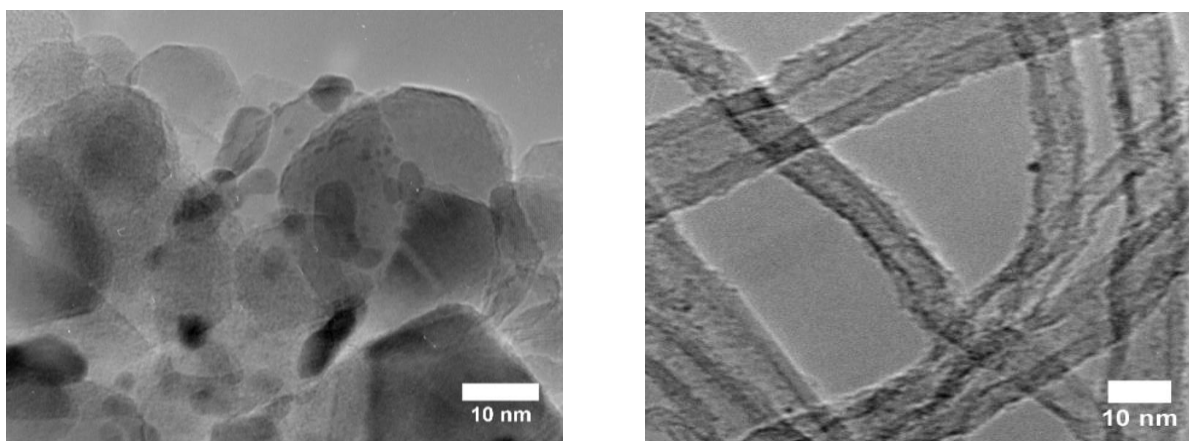
Figure 10 Representative TEM images for Ru catalysts a) 4.1% Ru/TiO₂ b) 1% Ru/CNT

Role of water in furfural conversion over Ru/TiO₂

As the most abundant product from biomass, the role of water was investigated in detail for the conversion of FAL using H_2 and different ratios of H_2O/FAL (H_2O/FAL: 5, 12, 15, 20, 25, and 30). The reduction of furfural is known to proceed in four ways: i) the hydrogenation of C=O bond, ii) the hydrogenation of the furan ring, iii) the hydrogenolysis of the C=O bond, iv) decarbonylation [9]. However, over Ru/TiO_2 as the partial pressure of water in the system is increased the yield of the rearrangement products

2-CPNE/CPNO increments too as shown in **Figure 11**. There is a clear shift in selectivity from FAL to 2MF (yield: 6.39% at H2O/FAL: 30) to FAL to CPNO/2CPNO (yield: 14.81% at H2O/FAL: 30).

Figure 11 Product Distribution for pure furfural and furfural co-fed with water at different molar ratios (H2O/FAL: 5, 12, 15, 20, 25 and 30) over 4.1% Ru/TiO2, T= 400°C, P= 1 atm, TOS= 30 mins, W/FFAL: 0.13 h Conversion ~ 22%

In liquid phase it was proposed that the hydronium ions formed from the dissociation of water can catalyze the furan ring rearrangement reaction by shuttling which will require a liquid film that it is not formed in gas phase [32]. Furthermore, it is believed the water is responsible for initiating the opening and closure of the furan ring via nucleophile attack in the 5-position of the furan ring which can make the reaction faster [29] . On the other hand, from density functional theory (DFT) calculations it was recently proposed the mechanism for the direct deoxygenation of phenol to benzene over

Ru/TiO$_2$ is by direct proton-assisted of H$_2$O Caryl-OH cleavage mechanism across the Ru/TiO$_2$ interface. The last can explain the enhancement of the ring rearrangement products in presence of water since the protolytic effect will help with the opening or closure of the furan ring to form 2CPNE [70,71].

An interesting component of this Ru/TiO$_2$ catalyst is the relatively low selectivity to furan even under high temperature of 400°C used here. This implies that the Ru/TiO$_2$ interface may play an important role in this reaction. Oxophilic additions to a metal that is capable of decarbonylation are known to destabilize the tendency of the O to lift from the surface and stabilize the acyl intermediate. This would inherently reduce the selectivity to furan. This can be observed by the addition of the oxophilic metal Fe to Ni or Pd catalysts [26].

The metal/support perimeter has been proposed as the active site for bond activation for a variety of reactions. In Ru/TiO$_2$ systems, perimeter sites for C-O bond activation have been implicated for phenol dehydroxylation and in Fischer-Tropsch (FT) synthesis [56]. Furthermore, it was shown that surface water on TiO$_2$ donates protons across the Au/TiO$_2$ interface, thus acting as a co-catalyst for CO oxidation on Au nanoparticles [72]

By varying the water partial pressure the rate of 2CPNE production exhibits a 1.2 order with respect to water as shown in **Figure 12a**. In the case of the hydrogenolysis to lights the order obtained with respect to water is -0.5 showing an inhibition with the addition of H$_2$O (**Figure 12b**).

.
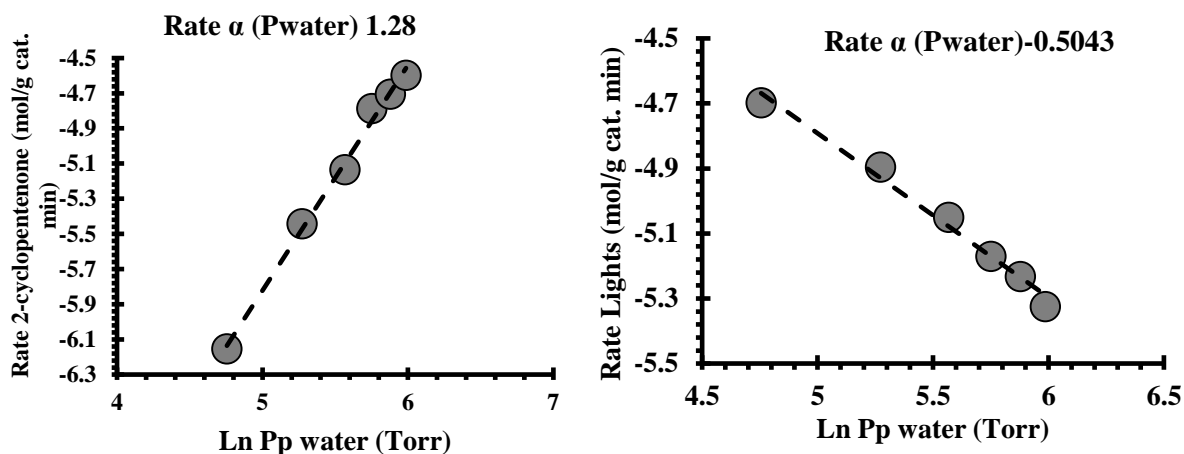
Figure 12 Rate of 2-cyclopentenone and Lights with respect to order of water. Conditions are vs water partial pressure over 5% Ru/TiO2 at 400°C, 15.5 mg catalyst. TOS = 30 min

Role of acetic acid in furfural conversion over Ru/TiO$_2$

AcOH is one of the most abundant carboxylic acid present in torrefaction of biomass [7]. AcOH has also showed a positive enhancement in the furan ring rearrangement yields obtained from conversion of FAL in liquid phase [29]. Therefore, it is important to investigate its role in the reaction of furfural over Ru/TiO$_2$ in gas phase. We conducted studies by gradually increasing the partial pressure of AcOH in the system (AcOH/FAL: 3 and 5).

The product distribution of the reactions are shown in **Figure 13**. When AcOH is co-fed with FAL in absence of water the overall yield of the furan ring rearrangement products and 2MF decreased while the yield of acetone produced by ketonization of acetic acid increases [73]. More interesting, upon introduction of AcOH there is an appearance of

a new ring opening product, trans-2-pentenal which can be formed from hydrolysis of the furan ring.

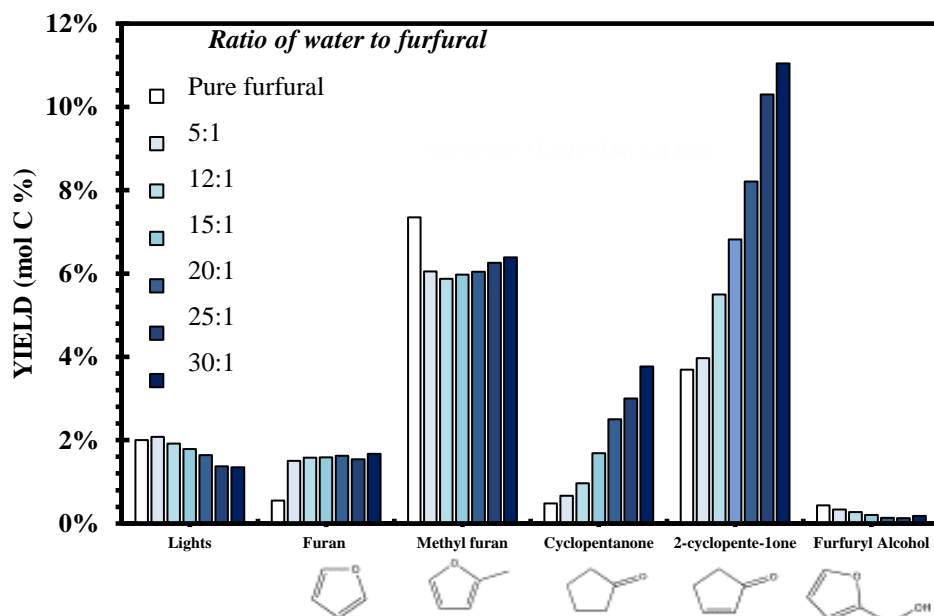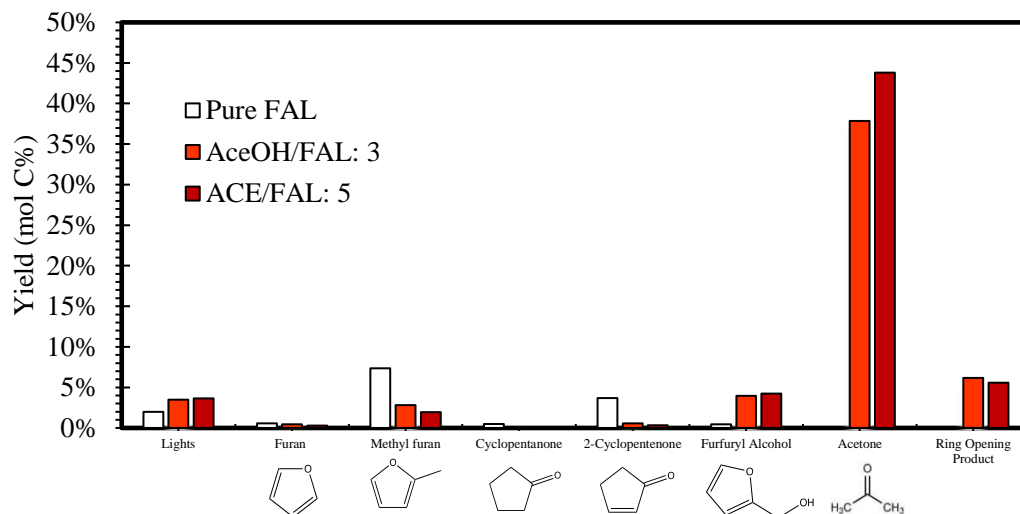**Figure 13 Product Distribution for pure furfural and furfural co-fed with acetic acid at different molar ratios (AceOH/FAL: 3 and 5) over 4.1% Ru/TiO2, T= 400°C, P= 1 atm, TOS= 30 mins, W/FFAL: 0.13 h Conversion ~ 18%**

To further investigate the mechanism of formation of the new ring opening product we carried out the reaction co-feeding AcOH and FAL over Ru/C. From the results showed in **Figure 14** it is possible to confirm this product is obtained by the interaction of FAL with the metal in the presence of the acid. The AcOH does not participate directly as a reactant for this product. This implies the adsorption/desorption of acetic acid over the metal may be changing the adsorption of furfural which can facilitate the braking of the ring.
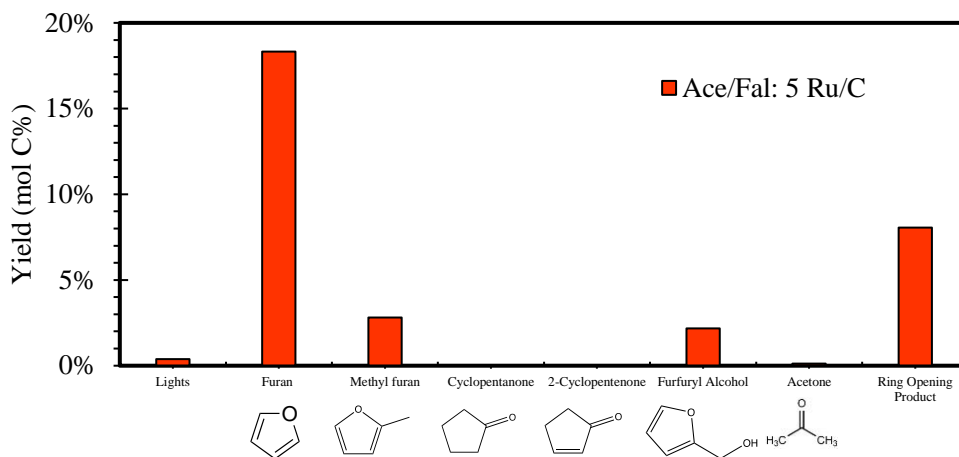
Figure 14 Product Distribution for furfural co-fed with acetic acid at different molar ratios (AceOH/FAL: 5) over 5% Ru/C, T= 400°C, P= 1 atm, TOS= 30 mins, W/FFAL: 0.13 h Conversion 33%

Role of mixture acetic acid and water in furfural conversion over Ru/TiO₂
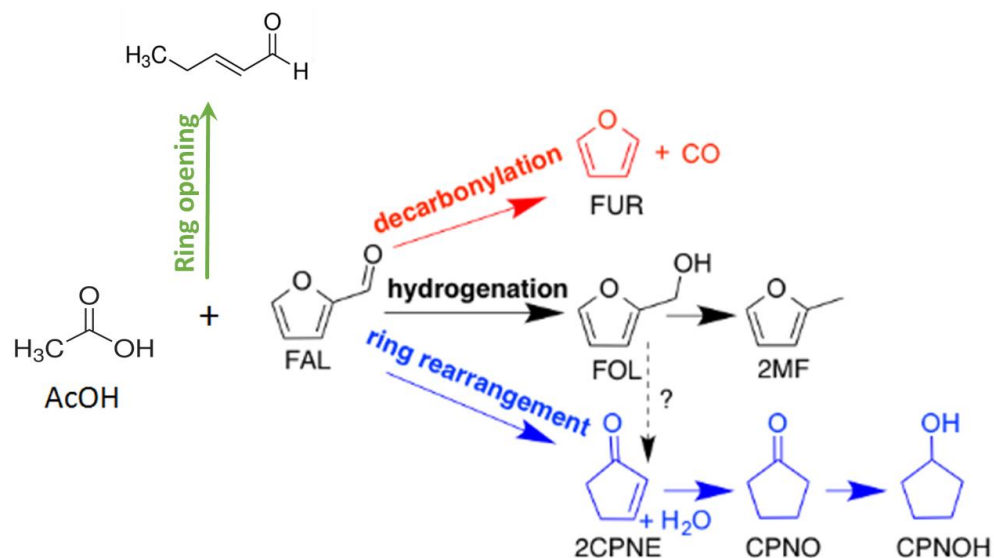
Schematic 1 Reaction pathway for furfural reactions cofeeding acetic acid and water over Ru/TiO₂

In real biomass torrefaction stream, FAL is in presence of AcOH and water at the same time as well as other molecules. To simulate this torrefaction stream closely, we carried out experiments increasing the partial pressure of water while co-feeding FAL and AcOH **Figure 15**. In contrast of the results obtained just co-feeding FAL and AcOH, where the FAL absorbs strong in the metal yielding ring opening products while the yield of ring rearrangement products is dramatically decreased. The water enhances the yield of the furan ring rearrangement products even in the presence of the acid. This also evidences a competition between the acid and the aldehyde.
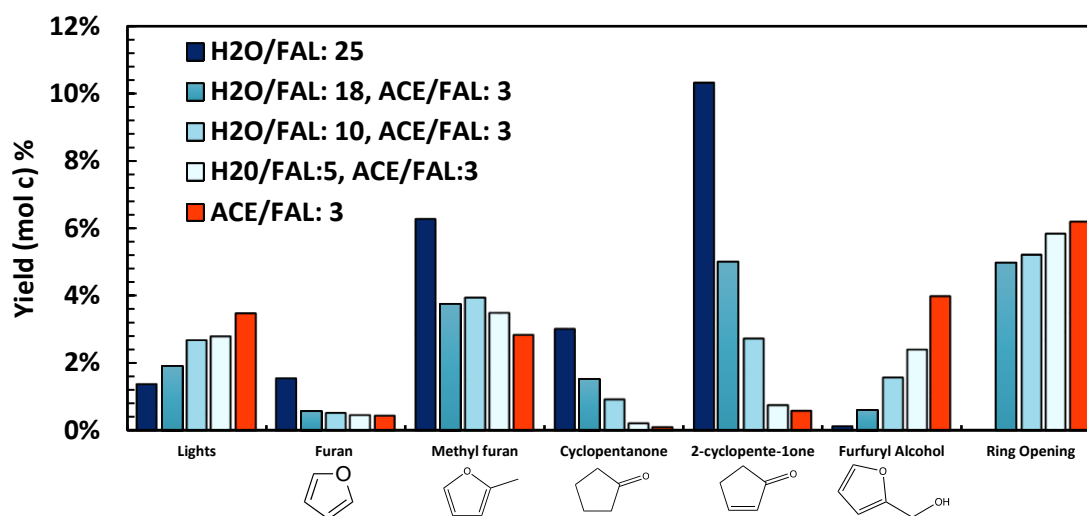
Figure 15 Product Distribution for furfural co-fed with acetic acid and water at different molar ratios (H2O/FAL: 5, 10, 18, 25) over 4.1% Ru/TiO2, T= 400°C, P= 1 atm, TOS= 30 mins, W/FFAL: 0.13 h, W/FACE: 0.25 h Conversion ~ 22%

It is also important to note the ketonization reaction of AcOH is inhibited by water while at the same time it enhances the FAL conversion to 2MF and 2CPNE/CPNO **Figure 16 a y b**. This means there is not a simply competition for active sites, water is necessary to accelerate the rate of FAL. Resasco *et al* studied the kinetics of ketonization over

Ru/TiO$_2$ in gas phase. The water inhibiton order reported was -0.1 [73]. This confirms the competition between the two reactants FAL and ACE since in the present study the calculated order of ketonization inhibition in the mixture is -0.53.
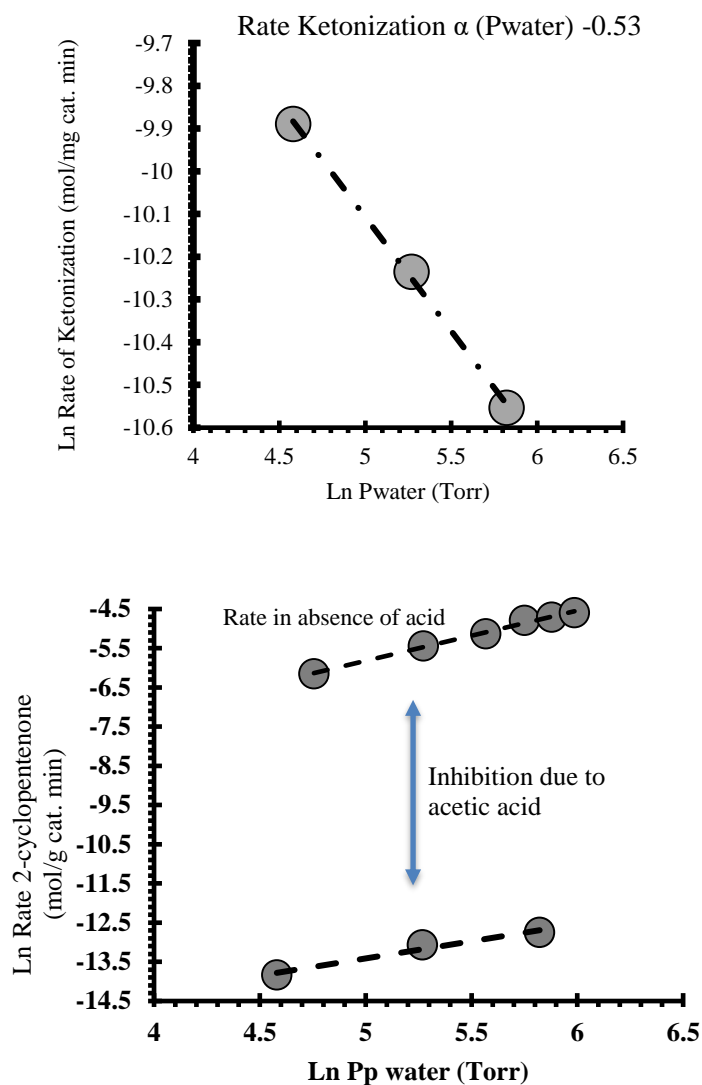
Figure 16 a. Rate of 2-cyclopentenone and b. ketonization with respect to order of water in a mixture of FAL, ACE and H2O. Conditions are vs water partial pressure over 4.1% Ru/TiO$_2$ at 400°C, 15.5 mg catalyst. TOS = 30 min

Role of temperature in furfural conversion over Ru/TiO₂

To obtain kinetic parameters that can be used to evaluate a given reaction mechanism, it is important to conduct the measurements in the absence of mass transport limitations. When the reaction is controlled by external diffusion, the measured rate is proportional to the mass transfer coefficient *"K_c"* as presented in Equation (1).

$$(1) \quad -r_{obs} = k_c(C_{AS})$$

$$(2) \quad \bar{k}_c \propto \frac{D_{AB}Sh}{R_p} \propto \frac{D_{AB}}{R_p} Re^{1/2} Sc^{1/3} \propto \frac{D_{AB}}{R_p} \left(\frac{R_p u \rho}{\bar{\mu}}\right)^{1/2} \left(\frac{\bar{\mu}}{\rho D_{AB}}\right)^{1/3} \propto \frac{(D_{AB})^{2/3} u^{1/2} \rho^{1/6}}{(R_p)^{1/2}(\bar{\mu})^{1/6}}$$

At the same time, the mass transfer coefficient is a function of the viscosity, density, diffusivity, velocity, and catalyst particle size as can be observed in Equation (2). However, because of the isothermal conditions, the diffusivity, density, and viscosity are considered to be constant during reaction. This leads to a proportionality dependence of the mass transfer coefficient with the square root of the ratio of the velocity and the pellet radius. Therefore, to ensure operation in a regime devoid of mass transport effects, the carrier gas flow and catalyst pellet sizes were varied to determine the regime where external mass transfer limitations are eliminated. Hydrogen carrier gas flow was varied between 20 and 100 ml/min while catalyst pellet size was changed within the range of 90 to 425 μm. It is important to mention that the W/F (weight of catalyst in g/feed flow rate in g/h) and the partial pressure of furfural were maintained constant during this study.

Results presented in **Figure 17** show that rate increases with the parameter (carrier gas velocity/particle size)$^{1/2}$ in the region where the reaction is mass transfer limited. This

effect disappears above 30 ml/min of gas flow suggesting the reaction is devoid of external diffusion corruptions above this flow rate. All kinetic experiments were therefore conducted with a carrier gas flowrate of 40 ml/min[74].
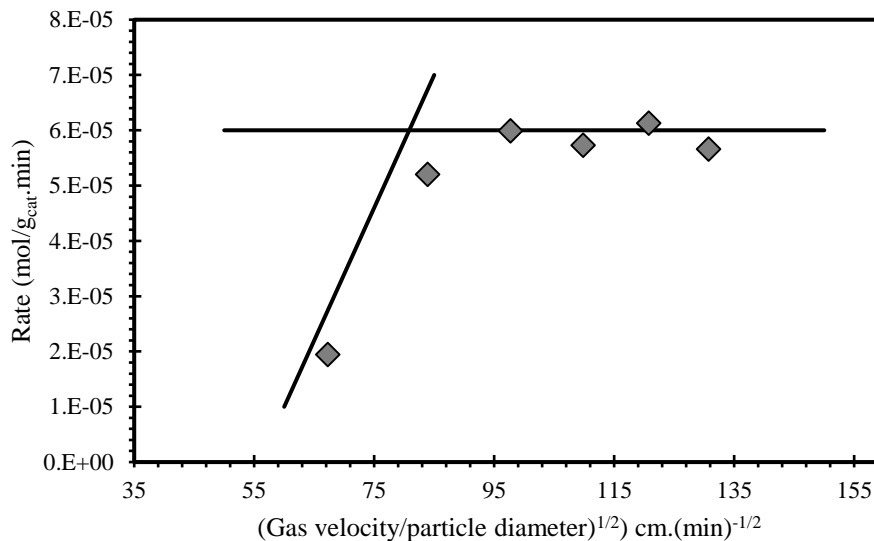
Figure 17 Effect of varying carrier gas velocity and catalyst pellet size on rate of furfural conversion over 4.1% Ru/TiO$_2$. T= 400 $^{\circ}$C, P = 1atm

Even though this rules out the presence of external mass transport effects in this regime, it does not guarantee the absence of internal diffusion effects within the pores. Therefore, internal diffusion limitations were also tested by applying Weisz–Prater criterion[75] (Equation 3), that is:

$$(3) \quad N_{w-P} = \frac{rR_r^2}{C_s D_{eff}} \leq 0.3$$

To apply this criteria the most severe reaction conditions were chosen. That is at 400°C, largest pellet size (250 µm) and cofeeding FAL and H_2O since those reactions showed the highest rate of FAL disappearance. The rates were taken at 30 min time on stream. Accordingly, the following operating conditions were used: r (reaction rate per volume of catalyst) = 3.59×10^{-5} mol/sec/cm³; R_p (catalyst particle radius) = 1.25×10^{-2} cm; C_s (reactant concentration at particle surface) = 1.006×10^{-9} mol/cm³. D_{eff} (effective diffusivity) = 2.05×10^{1} cm²/s, calculated with Ru/TiO₂ average pore size diameter of around 11.92 nm[76].

$$D_{eff} = \frac{v d_p}{3} = \frac{(5.16 x 10^7 cm/s)(11.92 x 10^{-7} cm)}{3} = 2.05 x 10^1 cm^2/s$$

Where v is average velocity of furfural molecules in gas phase at 400 °C and 1 atm and d_p is average pore size diameter of the catalyst. Accordingly, the calculated Weisz–Prater number obtained over Ru/TiO₂ at 400 °C is 0.158, which assured the absence of internal mass transfer limitations.

The study of the product distribution of FAL and FAL co-fed with water was carried out in a range of temperature between 250°C to 400°C. Resasco et al. showed that Ni and Pd supported over inert supports like SiO_2 yield mainly FUR, FOL and C_4 ring opening products for the reduction of FAL in gas phase at low temperatures [20]. For the bifunctional catalyst Ru/TiO₂, the main product of the reaction is 2MF with and without water with an exception at 400°C where 2CPNE becomes the dominant product **Figure 18 b**. 2MF is a desirable product not only because it has intrinsically good properties for fuels but it can also undergo to several reactions such as acylation reaction.
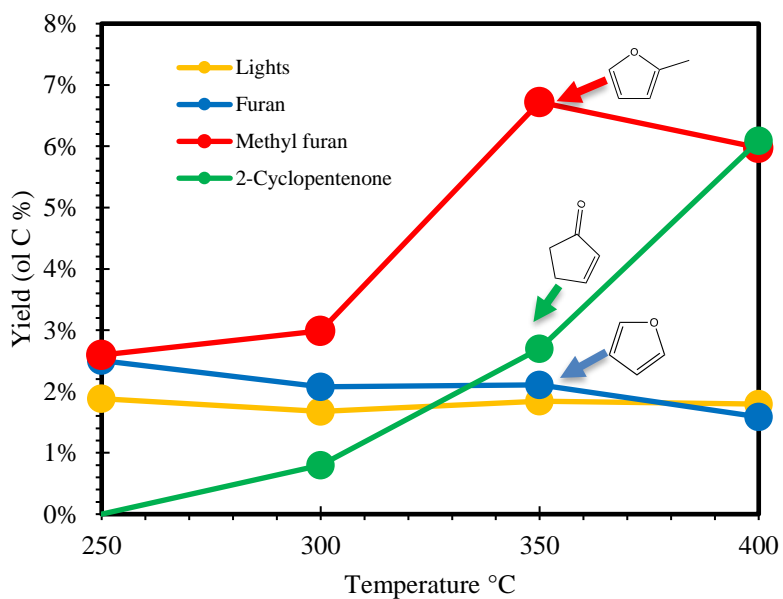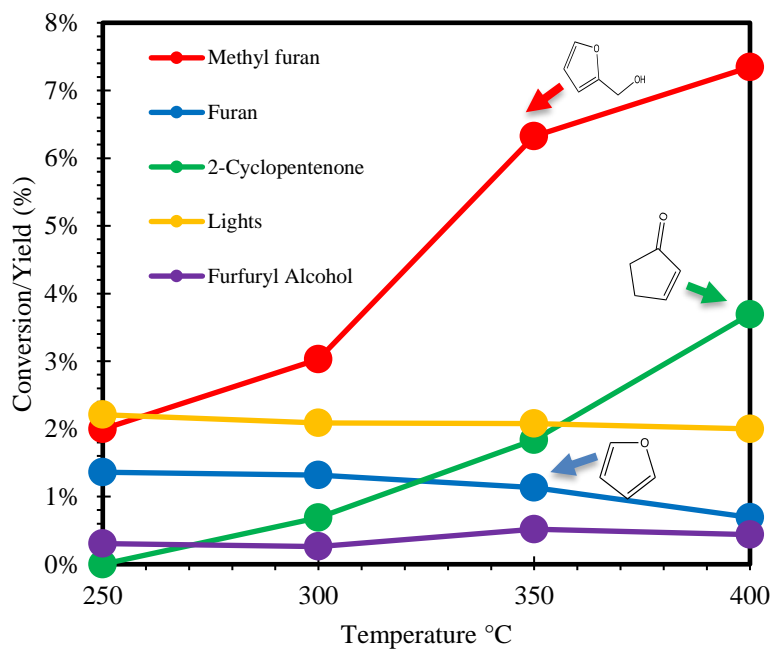
Figure 18 a. Product distribution for furfural conversion at b. lower temperatures with and without water. Conditions are 4.1% Ru/TiO₂ at 250°C - 400°C, 15.5 mg catalyst. TOS = 30 min

Ring rearrangement products have a higher energetic barrier of production compared with the other products from FAL, it is produced until the temperature reaches 300°C. The effect of water is clear visible even at lower temperatures. The yield of 2CPNE increases exponentially with temperature when the water is fed **Figure 19**. However, the apparent activation energy calculated for the reaction cofeeding water is higher (65KJ/mol) than the one feeding only FAL (53 KJ/mol). In the former case, the presence of water may affect the coverage of FAL and at the same time the heat of adsorption. That change will compensate in the true activation energy barrier for the reaction.
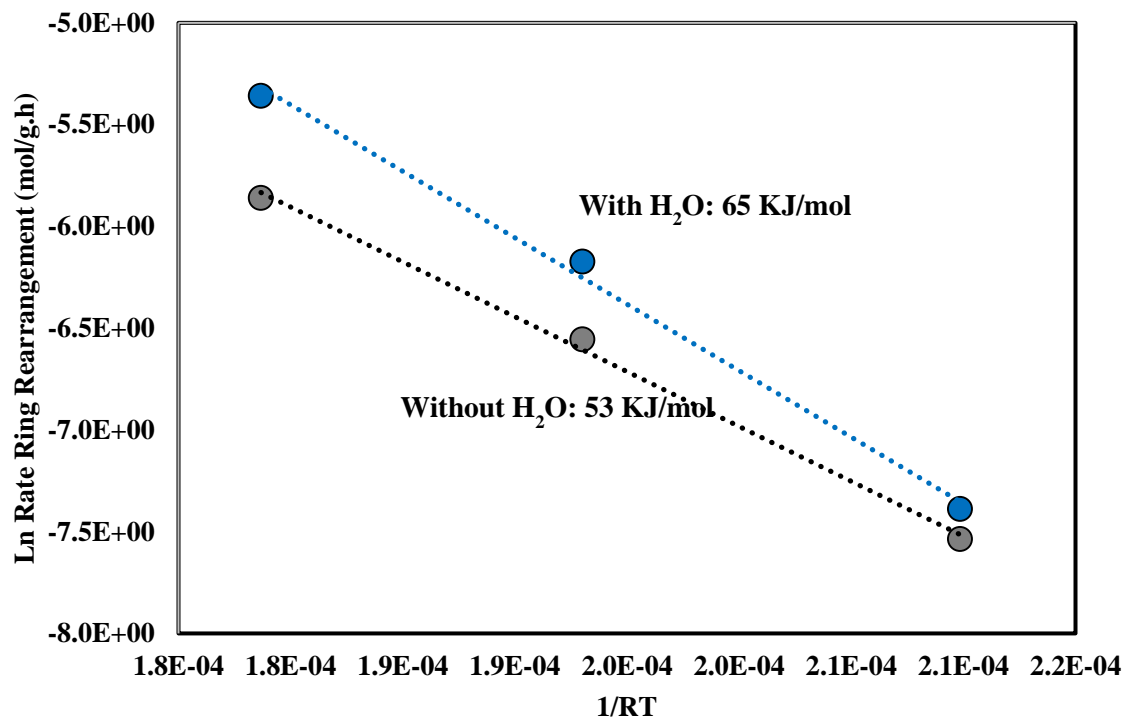
Figure 19 Apparent activation energy for ring rearrangement products with and without water. Conditions are 4.1% Ru/TiO2 at 250°C - 400°C, 15.5 mg catalyst. TOS = 30 min

Conclusions

The role of water and acetic acid in the furfural conversion in vapor phase at 400 $^{\circ}$C has been studied over Ru/TiO$_2$ and a number of reactions such as hydrogenation, ring opening, hydrogenolysis were observed over the catalyst to form products such as furfuryl alcohol, *trans*-2-pentenal and 2-methylfuran. The carbon efficient ring rearrangement reaction of furfural to produce 2-cyclopentenone was also observed with subsequent hydrogenation to form cyclopentanone occurring over the Ru metal. Furfural and acetic acid compete for active sites however the selectivity can be tuned to produce cyclopentanone via water partial pressure even in the presence of the acid. The presence of acetic acid influences the adsorption of furfural facilitating the braking of the ring to *trans*-2-pentenal. We believe the approach here will help bridge the gap between fundamental studies and real streams.

Chapter 4: Identification of Active Sites in Bifunctional Catalysts with Carbon Nanotube Hydrogen Highways

Introduction

Bifunctional catalysts have shown significant promise in terms of both activity and selectivity for the conversion of many families of compounds to more valuable products. While examples of superior catalytic activity and selectivity when combining two different types of active sites in close proximity are abound, the fundamental reason for this enhanced activity is often unknown. One of the most common forms of bifunctional catalysts are metals deposited on a catalytically active oxide support, with promising activity demonstrated for numerous reactions including C-C cleavage, C-O cleavage, and C-O oxidation reactions. Many of these oxide supports are also reducible oxides, capable of exhibiting OH groups and oxygen vacancies at elevated temperatures.

The interaction of a reducible metal oxide with a metal capable of dissociating hydrogen can be complex due to the creation of several potential catalytic active sites under reduction conditions. These active sites can be separated into two general categories, short-range interactions and long-range interactions. Short-range interactions are in close proximity to the metal particle and include the highly reducible interface along the perimeter of the metal, electronic perturbations to the exposed metal surface due to interaction with the support, as well as thin oxide films forming over the metal surface. Surface defects, subsurface defects, and surface OH groups that are created due to spillover from the metal nanoparticle to the support can be considered long-range

interactions, or promoter effects, as the primary active sites are found on the support itself [77,78]

Understanding the location and nature of the catalytic active site is critical for controlling a catalyst's activity and selectivity. A variety of methods have been applied to determine the active sites responsible for the activity observed over bifunctional catalysts. One approach is to change the particle size of the metal supported on the oxide which changes the perimeter of the metal oxide interface[56,79-81]. By systematically modifying the perimeter and particle size, correlations with the observed rate can be developed between perimeter sites and sites on the metal with various coordination. Lack of direct correlation with perimeter or metal surface are often correlated with promoter effects. However, the metal oxide interface can change due to strong metal support interaction involving decoration or encapsulation of the metal particle by the reducible oxide support[81-84]. Spectroscopic techniques are also used to propose active sites, however, the possibility of observable vibrations from spectator species that are often difficult to distinguish from catalytically relevant intermediates complicates this approach.

Furthermore, either the majority of the literature does not address this question or authors simply speculate on the location of the active site without any direct proof. In this work vertically grown carbon nanotubes are used to segregate direct catalytic interactions from promoter effects. This is accomplished by separating metal and oxide catalysts by a precise distance through a conductive bridge of carbon nanotubes serving as hydrogen highways. This approach eliminates direct contact of the metal nanoparticle with the oxide support while maintaining the formation and regeneration of prospective

51

active sites on the oxide. Promoter effects of the metal on the oxide are still possible in this scenario due to the fact that carbon nanotubes are known to facilitate spillover of dissociated hydrogen from the metal as illustrated in **Figure 20** [85-89]
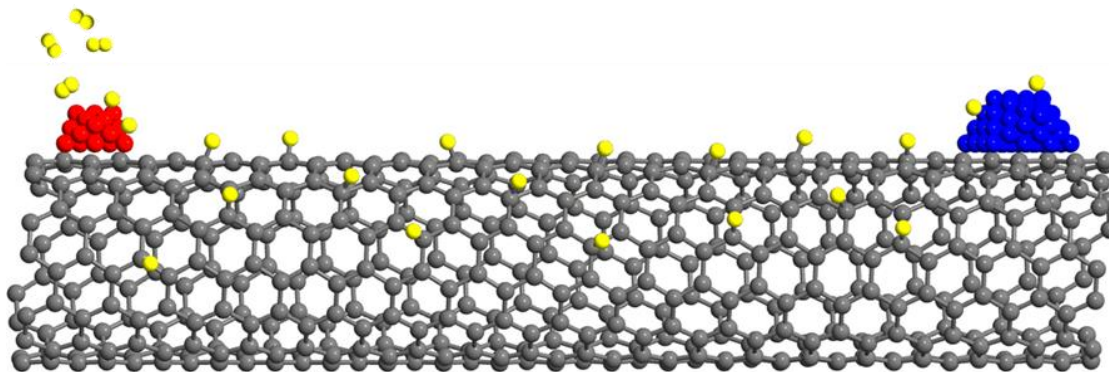
Figure 20 Novel catalyst for locating catalytic active sites for bifunctional catalyst. The catalyst consists of a metal (red) capable of dissociating hydrogen (yellow) onto a carbon nanotube (grey) where hydrogen can travel along to a metal oxide (blue) that can be reduced by the hydrogen

Experimental

Materials

Chemicals used for multi-walled carbon nanotube growth were isopropanol, iron nitrate nonahydrate, cobalt nitrate hexahydrate, aluminum nitrate nonahydrate, and 2-hydroxyethyl cellulose ($M_w \sim 1,300,000$). All of the chemicals used were purchased from Sigma Aldrich. Silicon wafers of n-type were purchased from Wafer World, Inc. (SKU: 1186). 18 MΩ water was obtained from an in house filtration system and used in this study.

Vertical Multi-walled Carbon Nanotube Growth

Nicholas Briggs grew the carbon nanotubes up, synthetized the catalyst and performed the TPR analysis.

Vertical multi-walled carbon nanotubes (VMWNTs) were grown by spin coating a catalyst solution on silicon wafers. First silicon wafers were cut using a diamond scribe into 22 mm x 22 mm square pieces. A catalyst solution was made containing 1.11 wt% iron nitrate nonahydrate, 0.39 wt% cobalt nitrate hexahydrate, 1.23 wt% aluminum nitrate nonahydrate, and 0.74 wt% 2-hydroxyethyl cellulose all with respect to water. The solution was spin coated on the silicon wafers by putting one millimeter of solution on the silicon wafer and spin coating using two stages which followed one another. The silicon wafer was first spin coated at 500 rpm for 10 seconds and then the spin speed increased to 2000 rpm for 30 seconds. The silicon wafers with the solution were then allowed to dry overnight and calcined the next day.

The silicon wafer spin coated with catalyst solution was calcined the next day by placing the sample in a one inch quartz diameter tube and connecting one end to an inlet line and the other an outlet line. The one inch quartz diameter tube was placed in a furnace oriented horizontally. With a continuous flow of 150 sccm of air through the quartz tube the furnace was ramped to 450°C at 10°C per minute and then held at 450°C for two hours. After heating at 450°C the reactor was allowed to cool to room temperature and the sample removed from the quartz tube.

For the growth of vertically aligned MWNTs the silicon wafer with catalyst was placed in a one inch quartz diameter tube and connected to inlet and outlet gas lines. The

quartz tube was placed in a furnace oriented horizontally for heating. With a flow of 300 sccm of hydrogen passing through the quartz tube the furnace was heated to 650°C at a rate of 10°C per minute and then held at 650°C for 30 minutes. The flow of hydrogen was stopped and a flow of 300 sccm of argon was flowed through the quartz tube and the quartz tube ramped to a reaction temperature of 675°C at a rate of 10°C per minute. Then the flow of argon was changed to 200 sccm and flowed with ethylene at 200 sccm for 20 minutes. After the reaction the flow of ethylene was stopped and argon continued to flow through the quartz tube as the temperature decreased to room temperature.

Depositing different catalyst on opposite ends of VMWNTs

To facilitate the removal of the VMWNTs from the silicon wafer the sample was heated in air to help weaken the interaction between the VMWNTs and catalyst particles on the silicon wafer [78,90] . The sample was loaded into a one inch diameter quartz tube and the quartz tube connected to inlet and outlet airlines. Next the quartz tube was loaded into a furnace oriented horizontally. Air was flowed through the quartz tube at 150 sccm while the furnace was heated to 480°C at 10°C per minute and then held at 480°C for two hours. After this step the sample was removed from the quartz tube once the temperature of the furnace reached room temperature.

Physical vapor deposition of palladium and titanium onto VMWNTs was completed by using a custom built vacuum evaporator. To evaporate metal onto the VMWNTs the VMWNTs were placed in the vacuum evaporator sample area. Next a tungsten wire, 1mm in diameter, was connected to two brass electrodes which were connected to the power supply. Titanium wire, with a diameter of 0.050 cm, palladium

54

wire, with a diameter of 0.025 cm, or copper wire, with a diameter of 0.01 cm was wrapped around the tungsten wire. For all metals a length of 2 cm was wrapped around the tungsten wire. A quartz crystal monitor was used to determine the amount of titanium, copper, or palladium deposited on the VMWNTs. For making the catalyst where the palladium and titanium are separated palladium was first deposited on the VMWNTs. After evaporation of the palladium the side of the VMWNTs with palladium was attached to aluminum tape, which contains a carbon adhesive, to remove the VMWNTs from the silicon wafer. Following this the aluminum tape with VMWNTs was placed back into the vacuum evaporator sample area with the end of the VMWNTs without palladium face up.

Titanium was then evaporated resulting in deposition on the other end of the VMWNTs. After evaporation of the titanium the VMWNTs on the aluminum tape the edges of the VMWNTs on the aluminum tape were cut off using a razor blade. This removal of the edges was performed to ensure that any palladium which came into contact with titanium was removed since the edges of the VMWNTs on the aluminum tape could have both catalysts. Next the VMWNTs on aluminum tape were placed in a petri dish filled with isopropanol and soaked for one hour to solubilize the carbon adhesive holding the VMWNTs to the carbon tape. After soaking for one hour the aluminum tape was shaken to help dislodge the VMWNTs from the carbon tape. The VMWNTs were then recovered from the isopropanol. To oxidize the titanium to titania or copper to copper oxide the VMWNTs with catalyst were placed in a one inch quartz diameter tube and connected to inlet and outlet gas lines. The quartz tube was placed in a furnace oriented horizontally for heating. With a flow of 100 sccm of air passing through the quartz tube

the furnace was heated to 350°C at a rate of 10°C per minute and then held at 350°C for 60 minutes. This was done to ensure complete oxidation of titanium to titania and copper to copper oxide [91-94].

Chemical Reactions

Catalytic activity for the four different catalysts was tested in a quartz tube reactor (0.25 in OD) at atmospheric pressure and 400 °C. Catalyst particles (90 – 250 μm) were mixed with inert acid washed glass beads (Sigma Aldrich, Part number: G1277) with a particle size range of 212-300 μm and packed between two layers of quartz wool inside the reactor. The quartz tube was placed in a furnace oriented vertically and connected to an inlet gas line at the top and an outlet gas line at the bottom. The catalyst was reduced by flowing 100 sccm of hydrogen through the quartz tube and heating the furnace up to 400°C and then holding at the same temperature for one hour.

In a typical experiment, pure distilled furfural (obtained from Sigma Aldrich; distilled and stored at -15 °C) was fed with a flow rate of 0.1 ml/h or co-fed with acetic acid and water with flow rates 0.22 mL/h and 0.37 mL/h respectively. The outlet stream of the reactor was heated to 250 °C to prevent condensation of compounds in the transfer lines and then flowed through a six-port valve to allow for injection into a gas chromatography unit equipped with a flame ionization detector, Agilent 6890, using a HP-INNOWAX column (30 m, 0.25 μm) for product quantification. Identification of products was confirmed using a Shimadzu QP-2010 GCMS and standards were used to quantify the various products in the FID.

Catalyst characterization

Scanning electron microscopy of the catalyst was performed using a Zeis Neon 40 EsB scanning electron microscope operating at an accelerating voltage of 5 kV for imaging and 10 kV when performing energy-dispersive x-ray spectroscopy. Transmission electron microscopy was performed by using a JEOL 200 FX equipped with a LaB_6 filament and operating at 200 kV.

Temperature programmed reduction (TPR) of the catalysts was carried out using an in house built system. An SRI 110 thermal conductivity detector (TCD) was used to analyze the effluent gas that was passed over drierite before entering the TCD, which was then analyzed with 5% hydrogen in argon mixture gas flown at the same rate. A flow rate of 30 sccm of 5% hydrogen in argon was passed through a ¼" quartz tube packed with quartz wool and 10 mg of sample. The quartz tube was mounted vertically in a furnace for heating. The temperature was ramped to 800°C at 5°C/minute and then held at 800°C for ten minutes.

Results and discussion

Selective deposition of catalytic sites at a specific distance along the length of a nanotube was accomplished through use of vertically grown carbon nanotube forests followed by selective deposition with a metal evaporator to deposit metals such as Pd, Cu or Ti. Subsequent calcination forms their respective oxides (e.g. TiO_2). Loadings are determined through a quartz crystal microbalance to tune deposition conditions. The amounts of catalyst deposited can be found in the Table S1. **Figure 21** shows an energy

dispersive X-ray spectroscopy (EDS) spectra of the separated catalyst prepared with Pd metal deposited on one end of the forest with TiO_2 on the other. Catalyst particles are known to sinter and migrate at various rates depending on the catalyst support [95,96]. To ensure that migration is not sufficient to induce significant physical contact, EDS spectra were taken after treatment at 400°C in hydrogen to ensure that the particles were not migrating across the length of the nanotube and the two catalysts are not coming into contact.

No significant penetration of Pd or TiO_2 was observed beyond 5 microns depth into the forest on either side. Pd and Ti signals were within the noise range in the center of the forest. The forest length can be adjusted by changing nanotube synthesis conditions, controlling the distance between catalytic particles. In this case, the forest was manipulated by removing from the silicon wafer via aluminum tape containing a carbon adhesive to position the forest for metal deposition on each side. Trace amounts of residue from the tape is removed via a mild thermal treatment in an oxidizing atmosphere.
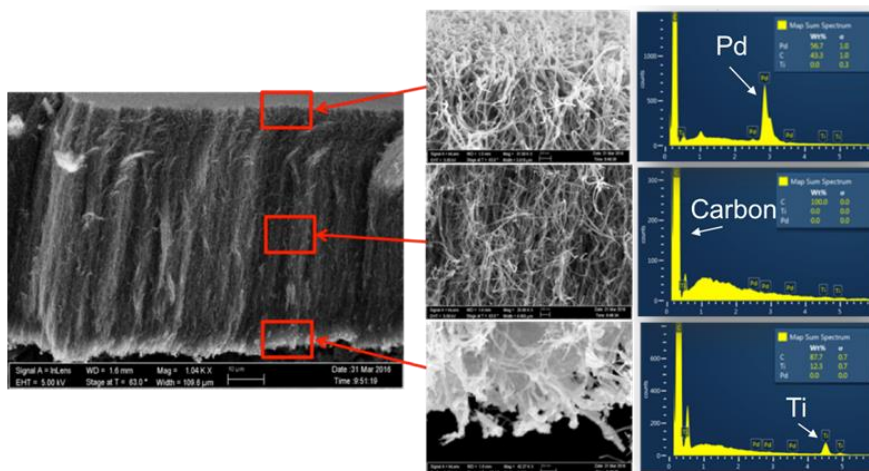
Figure 21 SEM and EDS spectra of a nanotube forest with Pd and TiO2 deposited on opposite ends through metal evaporation and after treatment in hydrogen for one hour at 400°C

58

A combination of probe reactions and characterization, using temperature programmed reduction (TPR), are used to validate this approach for discerning promoter effects from direct catalytic effects in bifunctional catalysts. Prior to conducting catalytic runs, simple shifts in reduction profile of a CuO catalyst supported on a carbon nanotube was conducted in the presence or absence of physically separated Pd on the same nanotube. Pd is well known to reduce and dissociate hydrogen at temperatures well below those required for dissociation on Cu.[i] Pd catalysts can be reduced 100°C or even at room temperature while CuO reduces just above 200°C [23].[i] The TPR profile for Pd and CuO spatially separated on carbon nanotubes (Pd/CNT/CuO) is compared with identically deposited CuO on carbon nanotubes alone (CuO/CNT) in **Figure 22 a**. EDS spectra of this catalyst after high temperature reduction confirming lack of direct Pd-Cu contact can be found in **Figure 22 b**.
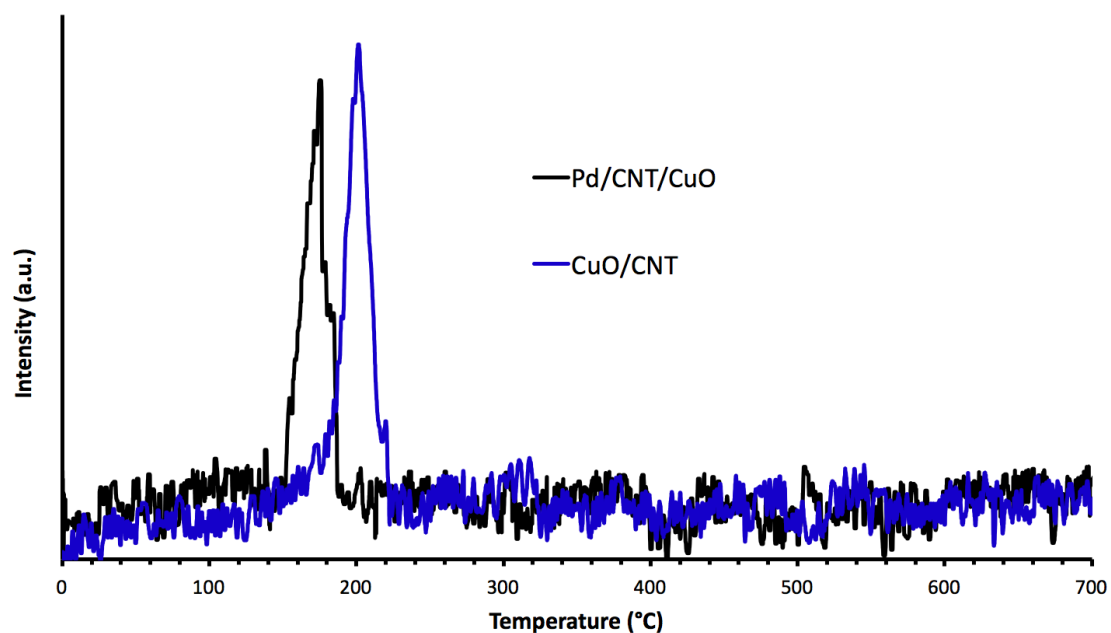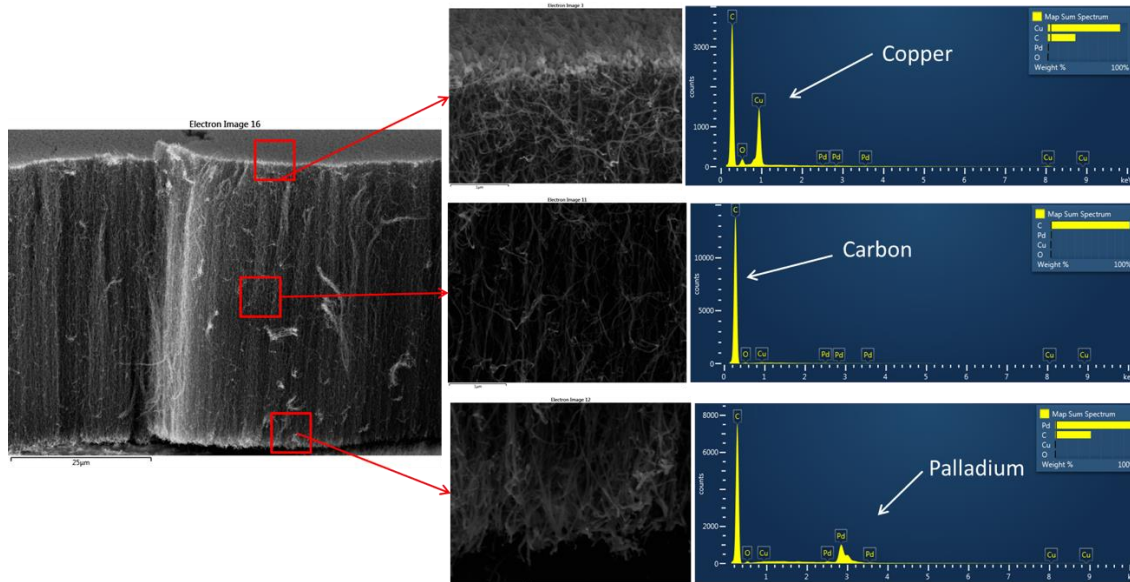
Figure 22 a. TPR profiles of CuO/CNT and Pd/CNT/CuO catalysts. b. SEM and EDS spectra of a nanotube forest with Pd and CuO deposited on each end through metal evaporation and after treatment in hydrogen for one hour at 400°C

As can be seen in Figure 3 b, the reduction temperature for CuO is lowered by 30°C when Pd is present on the same carbon nanotube. Pd is reduced during equilibration of the TPR system at room temperature. Therefore, this reduction temperature shift is associated with CuO and indicates dissociated hydrogen from the Pd is spilling over onto the carbon nanotubes and reaching the CuO causing the CuO to reduce at a lower temperature than normal. Comparable shifts in reduction temperature have been observed when Pd and CuO are in direct contact in the absence of the carbon nanotube bridge [23]. This illustrates that hydrogen is capable of travelling along the length of the carbon nanotube to reach the oxide and facilitate its reduction.

In order to demonstrate the capability of this approach to create promoter effects via continuous reduction of an oxide across a carbon nanotube bridge, a combination of probe molecules were introduced in parallel to a catalyst containing Pd and TiO_2. Acetic acid (AceOH) ketonization is a reaction that is known to occur over TiO_2, with the rate of ketonization to form acetone (ACE) scaling with the number of available oxygen vacancies on the surface [73,97]. While this reaction is enhanced by the presence of oxygen vacancies, these vacancies are not consumed in the process. This makes this reaction an ideal probe of the number of defects on the TiO_2 surface.

Cleavage of oxygen from carbonyl containing species has been proposed over reducible oxide catalysts via a reverse Mars van Krevelin approach [98]. Specifically over TiO_2, the selective conversion of furfural (FAL) to form methyl furan has been proposed to occur over TiO_2 oxygen vacancies that are produced by hydrogen spillover from the metal [99,100]

The selective deoxygenation of furfural has been a subject of many recent research articles due to its prevalence in biomass derived stream [33,78,97,101] This reaction would consume defects, requiring hydrogen spilled over from the Pd to reduce the oxide again and complete the catalytic cycle. By co-feeding AceOH with FAL over a catalyst with physically separated sites, one can test significance of this promotion path under reaction conditions. As can be observed in **Figure 23**, the rate of acetone production from acetic acid is markedly enhanced in the presence of Pd on the other side of the nanotube ($Pd/CNT/TiO_2$) when compared with the catalyst with TiO_2 only on the CNT, (TiO_2/CNT). This reveals that the Pd is capable of generating defects on the TiO_2 support necessary to enhance the rate of the ketonization reaction.

61
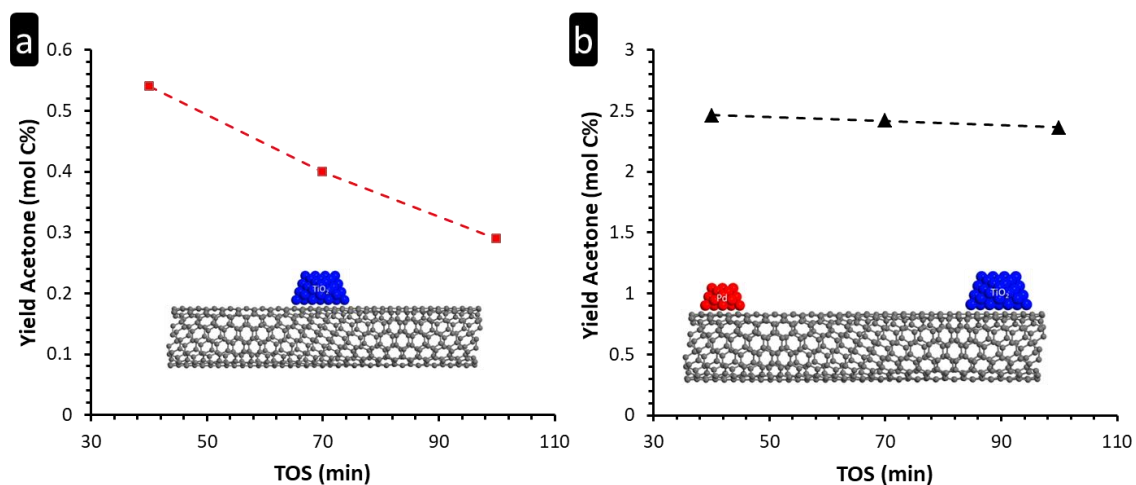
Figure 23 Acetone yield when co-feeding furfural and acetic acid over a) TiO2/CNT and b) Pd/CNT/TiO2. At T= 400 oC, P = 1 atm, under a H2 flow, 30 min TOS

In addition to generating active sites, it should be noted that the catalyst with the separated Pd sites exhibits increased stability. The low stability over the TiO_2/CNT catalyst could be due to furfural deoxygenation yielding methylfuran, which would consume oxygen vacancies in the process. This deactivation is even more pronounced if the TiO_2 contains several oxygen vacancies prior to introducing the reactants. This result can be found in **Figure 24**, where a severely pre-reduced TiO_x exhibits similar rates of acetone formation to the Pd/CNT/TiO_2 catalyst after 40 minutes on stream, but the deactivation rate is clearly diminished when Pd is present.

These results indicate that if furfural deoxygenation to form methylfuran is occurring on TiO_2 defects, the regeneration of active sites by spillover from the Pd is fast enough to maintain a stable level of catalytic activity (oxygen vacancies) necessary for steady acetone production. In other words, defect regeneration is not rate limiting, or one

would expect acetone formation rates to approach levels representative of a non-pre-reduced catalyst. An alternative explanation could be that side reactions such as aldol condensation and eventual coke formation lead to catalyst deactivation when furfural is present. In this case as well, the conclusion that Pd levels are sufficient to maintain a steady population of surface defects necessary for the proposed furfural deoxygenation due to defects on the support under reaction conditions is still valid.
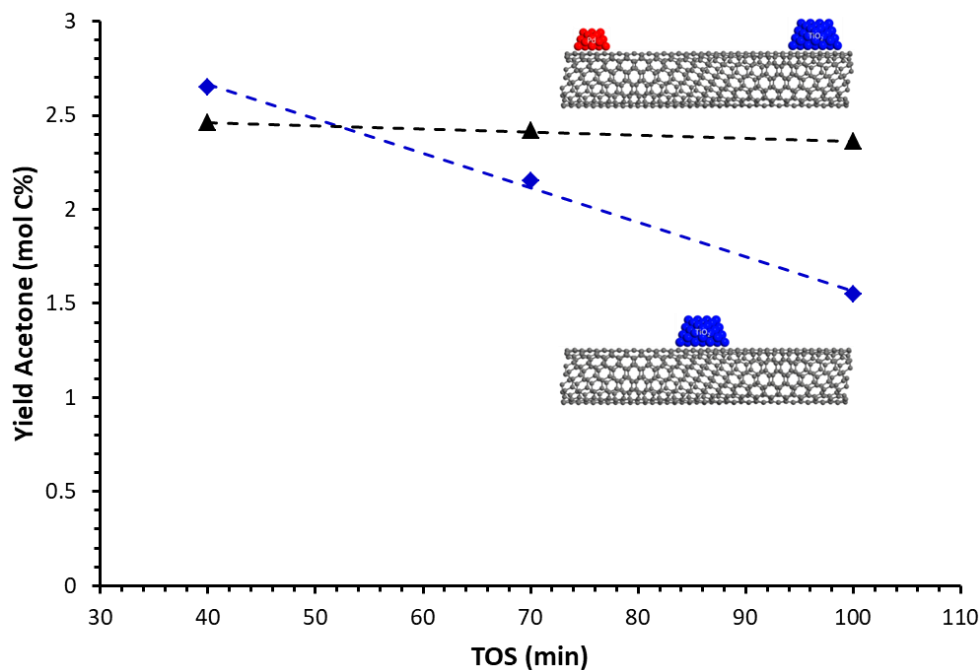
Figure 24 Acetone yield comparison as a function of TOS between TiO2/CNT, not calcined and Pd/CNT/TiO2

Since defects are present on the TiO_2 surface at steady state when the Pd and TiO_2 catalysts are separated on a nanotube bridge, the role of direct contact between the TiO_2 and the Pd nanoparticle may be investigated. Error! Reference source not found.**25** shows that Pd on nanotubes alone (Pd/CNT) yields similar rates and selectivity to furan vs.

methylfuran when compared with Pd and TiO_2 deposited on opposite ends of carbon nanotubes (Pd/CNT/TiO_2). In contrast, selectivity for methyl furan increased significantly, when Pd is deposited on the same side as TiO_2 on the carbon nanotubes (Pd/TiO_2/CNT). It should be noted that furfural conversions were comparable over all catalysts (within 3%). These results suggest that active sites for methylfuran production are due to direct contact between the Pd and the TiO_2, as opposed to on longer range defects as some have claimed [99,100]. Corma *et al.* suggested that selective C-O cleavage reactions may occur at the periphery of the metal particle, and this evidence appears to support this conclusion [102].
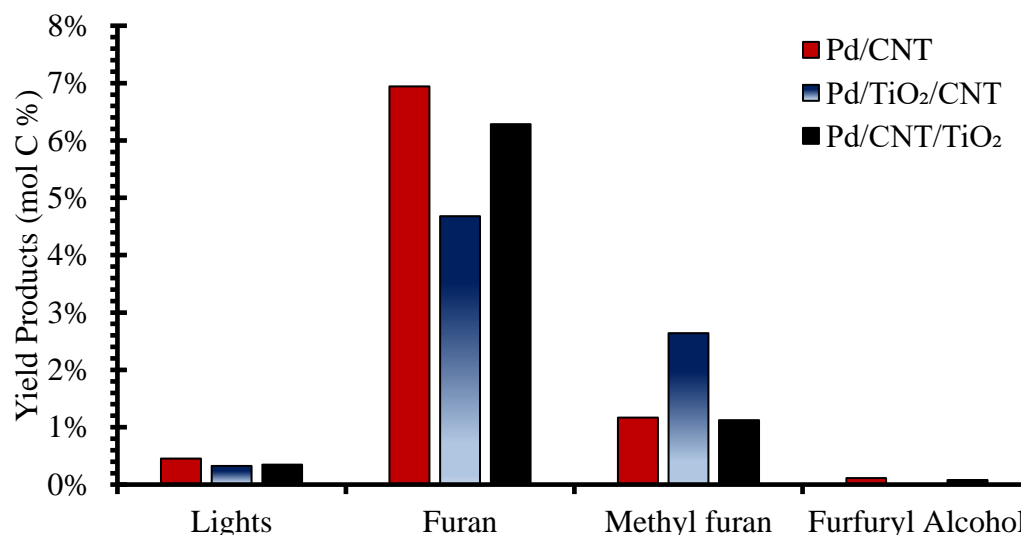
Figure 25 Reaction feeding furfural over Pd and TiO2 catalysts supported on CNTs. T= 400 oC, P = 1 atm, under a H2 flow, 30 min TOS

Conclusions

This method can be used with a variety of different bifunctional catalyst to segregate the role of sites induced by direct contact from promoter effects. Not only does this approach

provide the ability to determine the location of catalytically active sites in bifunctional catalysts, but also further improve our understanding of the role of defects on hydrogen spillover. By coupling precise probe reactions and segregated oxide reduction rates with functional groups present and distance between the catalytic moieties on aligned nanotube supports, this system provides a surrogate for future kinetic studies to quantify the role of functional groups on hydrogen spillover rates on carbon supports as well.

Chapter 5: Concluding remarks

Conversion of furfural in vapor phase at 400°C has been studied and a number of reactions such as hydrogenation, decarbonylation, and hydrogenolysis were observed over the catalyst to form products such as furfuryl alcohol, furan and 2-methylfuran. The carbon efficient reaction of furfural to cyclopentanone/2-cyclopentenone to cyclopentanone/2-cyclopentenone was also observed. Water was demonstrated to play a role in shifting the selectivity from 2-methylfuran to cyclopentanone and 2-cyclopentenone. The support plays an important role in determining the product distribution as pure Ru catalysts produced mainly light gases and furan when compared with Ru/TiO$_2$. Experiments feeding various intermediates indicate that the vapor phase reaction does not proceed through an alcohol intermediate that desorbs from the catalyst surface, as is accepted in condensed phased reactions.

Furfural and acetic acid compete for active sites however the selectivity can be tuned to produce cyclopentanone via water partial pressure even in the presence of the acid. The presence of acetic acid influences the adsorption of furfural facilitating the braking of the ring to *trans*-2-pentenal. Using Red Oak as a biomass source, the reaction was also observed with real torrefaction feeds in a pulse reactor. With the biomass feeds the selectivity to ring rearrangement products was enhanced beyond the levels observed with the model compound studies, illustrating the potential of this reaction to convert furfural in real biomass streams. We believe the approach here will help bridge the gap between fundamental studies and real streams.

Finally, experiments over Pd supported catalysts imply that carbon-metal and oxygen-metal bond strength at the metal/support interface likely play an important role on this reaction. This was also confirmed with the experiments using a separated metal and oxide catalysts by a precise distance through a conductive bridge of carbon nanotubes serving as hydrogen highways.

References

1   Zhang, Q., Chang, J., Wang, T. & Xu, Y. Review of biomass pyrolysis oil properties and upgrading research. *Energy conversion and management* **48**, 87-92 (2007).

2   Yang, H., Yan, R., Chen, H., Lee, D. H. & Zheng, C. Characteristics of hemicellulose, cellulose and lignin pyrolysis. *Fuel* **86**, 1781-1788 (2007).

3   Venderbosch, R. & Prins, W. Fast pyrolysis technology development. *Biofuels, bioproducts and biorefining* **4**, 178-208 (2010).

4   Resasco, D. E. & Crossley, S. P. Implementation of concepts derived from model compound studies in the separation and conversion of bio-oil to fuel. *Catalysis Today* **257**, 185-199 (2015).

5   Meng, J., Park, J., Tilotta, D. & Park, S. The effect of torrefaction on the chemistry of fast-pyrolysis bio-oil. *Bioresource technology* **111**, 439-446 (2012).

6   Shankar Tumuluru, J., Sokhansanj, S., Hess, J. R., Wright, C. T. & Boardman, R. D. REVIEW: A review on biomass torrefaction process and product properties for energy applications. *Industrial Biotechnology* **7**, 384-401 (2011).

7   Herron, J. A. *et al.* A Systems-Level Roadmap for Biomass Thermal Fractionation and Catalytic Upgrading Strategies. *Energy Technology* (2016).

8   French, R. & Czernik, S. Catalytic pyrolysis of biomass for biofuels production. *Fuel Processing Technology* **91**, 25-32 (2010).

9   Bridgwater, A. V. Review of fast pyrolysis of biomass and product upgrading. *Biomass and bioenergy* **38**, 68-94 (2012).

10   Van der Stelt, M., Gerhauser, H., Kiel, J. & Ptasinski, K. Biomass upgrading by torrefaction for the production of biofuels: A review. *Biomass and bioenergy* **35**, 3748-3762 (2011).

11   Ebert, J. Furfural: Future feedstock for fuels and chemicals. *Ethanol Producer Magazine* (2008).

12   Werpy, T. *et al.* Top value added chemicals from biomass. Volume 1-Results of screening for potential candidates from sugars and synthesis gas. (DTIC Document, 2004).

13   Gürbüz, E. I., Wettstein, S. G. & Dumesic, J. A. Conversion of hemicellulose to furfural and levulinic acid using biphasic reactors with alkylphenol solvents. *ChemSusChem* **5**, 383-387 (2012).

14   Dias, A. S., Lima, S., Pillinger, M. & Valente, A. A. Furfural and Furfural-Based Industrial-Chemicals. *Ideas in Chemistry and Molecular Sciences: Advances in Synthetic Chemistry* **8**, 167-186 (2010).

15   Yan, K., Wu, G., Lafleur, T. & Jarvis, C. Production, properties and catalytic hydrogenation of furfural to fuel additives and value-added chemicals. *Renewable and Sustainable Energy Reviews* **38**, 663-676 (2014).

16   Hoydonckx, H., Van Rhijn, W., Van Rhijn, W., De Vos, D. & Jacobs, P. Furfural and derivatives. *Ullmann's encyclopedia of industrial chemistry* (2007).

17   Nagaraja, B. *et al.* A highly efficient Cu/MgO catalyst for vapour phase hydrogenation of furfural to furfuryl alcohol. *Catalysis communications* **4**, 287-293 (2003).

18   Jiménez-Gómez, C. P. *et al.* Gas-phase hydrogenation of furfural to furfuryl alcohol over Cu/ZnO catalysts. *Journal of Catalysis* **336**, 107-115 (2016).

19   Bhogeswararao, S. & Srinivas, D. Catalytic conversion of furfural to industrial chemicals over supported Pt and Pd catalysts. *Journal of Catalysis* **327**, 65-77 (2015).

20   Sitthisa, S. & Resasco, D. E. Hydrodeoxygenation of Furfural Over Supported Metal Catalysts: A Comparative Study of Cu, Pd and Ni. *Catalysis Letters* **141**, 784-791, doi:DOI 10.1007/s10562-011-0581-7 (2011).

21   Sitthisa, S., Sooknoi, T., Ma, Y., Balbuena, P. B. & Resasco, D. E. Kinetics and mechanism of hydrogenation of furfural on Cu/SiO 2 catalysts. *Journal of catalysis* **277**, 1-13 (2011).

22   Li, X., Jia, P. & Wang, T. Furfural: A promising platform compound for sustainable production of C4 and C5 chemicals. *ACS Catalysis* **6**, 7621-7640 (2016).

23   Vorotnikov, V., Mpourmpakis, G. & Vlachos, D. G. DFT study of furfural conversion to furan, furfuryl alcohol, and 2-methylfuran on Pd (111). *Acs Catalysis* **2**, 2496-2504 (2012).

24   Sitthisa, S. *et al.* Conversion of furfural and 2-methylpentanal on Pd/SiO 2 and Pd–Cu/SiO 2 catalysts. *Journal of catalysis* **280**, 17-27 (2011).

25   Wang, S., Vorotnikov, V. & Vlachos, D. G. A DFT study of furan hydrogenation and ring opening on Pd (111). *Green Chemistry* **16**, 736-747 (2014).

26   Sitthisa, S., An, W. & Resasco, D. E. Selective conversion of furfural to methylfuran over silica-supported Ni Fe bimetallic catalysts. *Journal of catalysis* **284**, 90-101 (2011).

27   Hronec, M. *et al.* Cyclopentanone: A raw material for production of C 15 and C 17 fuel precursors. *Biomass and Bioenergy* **63**, 291-299 (2014).

28   Hronec, M. *et al.* Carbon supported Pd–Cu catalysts for highly selective rearrangement of furfural to cyclopentanone. *Applied Catalysis B: Environmental* **181**, 210-219 (2016).

29   Yang, Y. *et al.* Conversion of furfural into cyclopentanone over Ni–Cu bimetallic catalysts. *Green Chemistry* **15**, 1932-1940 (2013).

30   Hronec, M., Fulajtarová, K. & Liptaj, T. Effect of catalyst and solvent on the furan ring rearrangement to cyclopentanone. *Applied Catalysis A: General* **437**, 104-111 (2012).

31   Hronec, M. & Fulajtarová, K. Selective transformation of furfural to cyclopentanone. *Catalysis Communications* **24**, 100-104 (2012).

32   Hronec, M., Fulajtárova, K. & Soták, T. Highly selective rearrangement of furfuryl alcohol to cyclopentanone. *Applied Catalysis B: Environmental* **154**, 294-300 (2014).

33   Williams, C. L. *et al.* Cycloaddition of Biomass-Derived Furans for Catalytic Production of Renewable p-Xylene. *ACS Catalysis* **2**, 935-939, doi:10.1021/cs300011a (2012).

35   Gumidyala, A., Wang, B. & Crossley, S. Direct carbon-carbon coupling of furanics with acetic acid over Brønsted zeolites. *Science Advances* **2**, e1601072 (2016).

37   Bui, T. V., Crossley, S. & Resasco, D. E. C-C Coupling for Biomass-Derived Furanics Upgrading to Chemicals and Fuels. *Chemicals and Fuels from Bio-Based Building Blocks*, 431-494 (2016).

38   Kawabata, T., Kato, M., Mizugaki, T., Ebitani, K. & Kaneda, K. Monomeric metal aqua complexes in the interlayer space of montmorillonites as strong lewis acid catalysts for heterogeneous carbon–carbon bond-forming reactions. *Chemistry–A European Journal* **11**, 288-297 (2005).

40   Fischer, J. & Hölderich, W. F. Baeyer–Villiger-oxidation of cyclopentanone with aqueous hydrogen peroxide by acid heterogeneous catalysis. *Applied Catalysis A:*

General **180**, 435-443, doi:http://dx.doi.org/10.1016/S0926-860X(98)00378-0 (1999).

41 Piutti, C. & Quartieri, F. The Piancatelli Rearrangement: New Applications for an Intriguing Reaction. *Molecules* **18**, 12290-12312, doi:DOI 10.3390/molecules181012290 (2013).

46 Pham, T. N., Shi, D. & Resasco, D. E. Evaluating strategies for catalytic upgrading of pyrolysis oil in liquid phase. *Applied Catalysis B: Environmental* **145**, 10-23, doi:10.1016/j.apcatb.2013.01.002 (2014).

47 Stöcker, M. Biofuels and biomass-to-liquid fuels in the biorefinery: Catalytic conversion of lignocellulosic biomass using porous materials. *Angewandte Chemie International Edition* **47**, 9200-9211 (2008).

48 Czernik, S. & Bridgwater, A. Overview of applications of biomass fast pyrolysis oil. *Energy & Fuels* **18**, 590-598 (2004).

49 Carlson, T. R., Vispute, T. P. & Huber, G. W. Green gasoline by catalytic fast pyrolysis of solid biomass derived compounds. *ChemSusChem* **1**, 397-400 (2008).

50 Badovskaya, L. A. & Povarova, L. V. Oxidation of furans (Review). *Chemistry of Heterocyclic Compounds* **45**, 1023-1034, doi:10.1007/s10593-009-0390-8 (2009).

51 Milas, N. A. & Walsh, W. L. Catalytic Oxidations. I. Oxidations in the Furan Series. *Journal of the American Chemical Society* **57**, 1389-1393 (1935).

52 Takagaki, A., Nishimura, S. & Ebitani, K. Catalytic transformations of biomass-derived materials into value-added chemicals. *Catalysis Surveys from Asia* **16**, 164-182 (2012).

53 WANG, S., LENG, Y., LIN, F., HUANG, C. & YI, C. Catalytic oxidation of furfural in vapor-gas phase for producing maleic anhydride [J]. *Chemical Industry and Engineering Progress* **6**, 029 (2009).

54 Nielsen, E. R. Vapor phase oxidation of furfural. *Industrial & Engineering Chemistry* **41**, 365-368 (1949).

55 Kijenski, J., Winiarek, P., Paryjczak, T., Lewicki, A. & Mikolajska, A. Platinum deposited on monolayer supports in selective hydrogenation of furfural to furfuryl alcohol. *Applied Catalysis a-General* **233**, 171-182, doi:Pii S0926-860x(02)00140-0Doi 10.1016/S0926-860x(02)00140-0 (2002).

56   Zheng, H. Y. *et al.* Towards understanding the reaction pathway in vapour phase hydrogenation of furfural to 2-methylfuran. *J Mol Catal a-Chem* **246**, 18-23, doi:DOI 10.1016/j.molcata.2005.10.003 (2006).

57   Zhu, Y. L. *et al.* A new strategy for the efficient synthesis of 2-methylfuran and gamma-butyrolactone. *New J Chem* **27**, 208-210, doi:Doi 10.1039/B208849p (2003).

58   Yang, J. *et al.* Effects of calcination temperature on performance of Cu-Zn-Al catalyst for synthesizing gamma-butyrolactone and 2-methylfuran through the coupling of dehydrogenation and hydrogenation. *Catal. Commun.* **5**, 505-510, doi:DOI 10.1016/j.catcom.2004.06.005 (2004).

59   Zheng, H. Y., Yang, J., Zhu, Y. L. & Zhao, G. W. Synthesis of gamma-butyrolactone and 2-methylfuran through the coupling of dehydrogenation and hydrogenation over copper-chromite catalyst. *React Kinet Catal L* **82**, 263-269, doi:Doi 10.1023/B:Reac.0000034836.56895.A9 (2004).

60   Omotoso, T., Boonyasuwat, S. & Crossley, S. P. Understanding the role of TiO 2 crystal structure on the enhanced activity and stability of Ru/TiO 2 catalysts for the conversion of lignin-derived oxygenates. *Green Chemistry* **16**, 645-652 (2014).

61   Scholz, D., Aellig, C. & Hermans, I. Catalytic Transfer Hydrogenation/Hydrogenolysis for Reductive Upgrading of Furfural and 5-(Hydroxymethyl)furfural. *Chemsuschem* **7**, 268-275, doi:DOI 10.1002/cssc.201300774 (2014).

63   Komaya, T. *et al.* Effects of Dispersion and Metal-Metal Oxide Interactions on Fischer-Tropsch Synthesis over Ru/Tio2 and Tio2-Promoted Ru/Sio2. *Journal of Catalysis* **150**, 400-406, doi:DOI 10.1006/jcat.1994.1358 (1994).

64   Resasco, D. E. & Haller, G. L. A Model of Metal-Oxide Support Interaction for Rh on Tio2. *Journal of Catalysis* **82**, 279-288, doi:Doi 10.1016/0021-9517(83)90194-X (1983).

65   Avery, N. R. Eels Identification of the Adsorbed Species from Acetone Adsorption on Pt(111). *Surf Sci* **125**, 771-786, doi:Doi 10.1016/S0039-6028(83)80059-4 (1983).

66   Shekhar, R., Barteau, M. A., Plank, R. V. & Vohs, J. M. Adsorption and reaction of aldehydes on Pd surfaces. *Journal of Physical Chemistry B* **101**, 7939-7951, doi:Doi 10.1021/Jp971077l (1997).

67   Davis, J. L. & Barteau, M. A. Polymerization and Decarbonylation Reactions of Aldehydes on the Pd(111) Surface. *Journal of the American Chemical Society* **111**, 1782-1792, doi:Doi 10.1021/Ja00187a035 (1989).

68   Boonyasuwat, S., Omotoso, T., Resasco, D. E. & Crossley, S. P. Conversion of Guaiacol over Supported Ru Catalysts. *Catalysis Letters* **143**, 783-791, doi:DOI 10.1007/s10562-013-1033-3 (2013).

69   Omotoso, T., Boonyasuwat, S. & Crossley, S. P. Understanding the role of TiO2 crystal structure on the enhanced activity and stability of Ru/TiO2 catalysts for the conversion of lignin-derived oxygenates. *Green Chem* **16**, 645-652, doi:Doi 10.1039/C3gc41377b (2014).

70   Selvaraj, V., Vinoba, M. & Alagar, M. Electrocatalytic oxidation of ethylene glycol on Pt and Pt-Ru nanoparticles modified multi-walled carbon nanotubes. *J Colloid Interface Sci* **322**, 537-544, doi:10.1016/j.jcis.2008.02.069 (2008).

71   Iwasita, T. Electrocatalysis of methanol oxidation. *Electrochimica Acta* **47**, 3663-3674 (2002).

72   Jiang, J. & Kucernak, A. Electrooxidation of small organic molecules on mesoporous precious metal catalysts. *Journal of Electroanalytical Chemistry* **543**, 187-199, doi:10.1016/s0022-0728(03)00046-9 (2003).

73   Tan, Q. *et al.* Different Product Distributions and Mechanistic Aspects of the Hydrodeoxygenation of m-Cresol over Platinum and Ruthenium Catalysts. *ACS Catalysis* **5**, 6271-6283 (2015).

74   Rekoske, J. E. & Barteau, M. A. Isothermal reduction kinetics of titanium dioxide-based materials. *The Journal of Physical Chemistry B* **101**, 1113-1124 (1997).

75   Choi, S., Song, C. W., Shin, J. H. & Lee, S. Y. Biorefineries for the production of top building block chemicals and their derivatives. *Metabolic engineering* **28**, 223-239 (2015).

76   Zhang, W., Zhu, Y., Niu, S. & Li, Y. A study of furfural decarbonylation on K-doped Pd/Al 2 O 3 catalysts. *Journal of Molecular Catalysis A: Chemical* **335**, 71-81 (2011).

80   Zhu, X., Nie, L., Lobban, L. L., Mallinson, R. G. & Resasco, D. E. Efficient conversion of m-cresol to aromatics on a bifunctional Pt/HBeta catalyst. *Energy & Fuels* **28**, 4104-4111 (2014).

81   Nelson, R. C. *et al.* Experimental and theoretical insights into the hydrogen-efficient direct hydrodeoxygenation mechanism of phenol over Ru/TiO2. *ACS catalysis* **5**, 6509-6523 (2015).

82   Hong, S. & Rahman, T. S. Rationale for the higher reactivity of interfacial sites in methanol decomposition on Au13/TiO2 (110). *Journal of the American Chemical Society* **135**, 7629-7635 (2013).

83   Pham, T. N., Shi, D. & Resasco, D. E. Kinetics and mechanism of ketonization of acetic acid on Ru/TiO2 catalyst. *Topics in Catalysis* **57**, 706-714 (2014).

84   Madon, R. J. B., M. Experimental Criterion for the Absence of Artifacts in the Measurement of Rates of Heterogeneous Catalytic Reactions. *Ind. Eng. Chem. Fundam* **21**, 438-447 (1982).

85   Kennedy, G., Baker, L. R. & Somorjai, G. A. Selective Amplification of C☐O Bond Hydrogenation on Pt/TiO2: Catalytic Reaction and Sum-Frequency Generation Vibrational Spectroscopy Studies of Crotonaldehyde Hydrogenation. *Angewandte Chemie* **126**, 3473-3476 (2014).

86   Poenitzsch, V. *et al.* Freestanding foils of nanotube arrays fused with metals. *Journal of materials science* **49** (2014).

88   Cargnello, M. *et al.* Control of metal nanocrystal size reveals metal-support interface role for ceria catalysts. *Science* **341**, 771-773 (2013).

90   Haller, G. L. & Resasco, D. E. Metal–support interaction: Group VIII metals and reducible oxides. *Advances in Catalysis* **36**, 173-235 (1989).

91   Tauster, S., Fung, S. & Garten, R. L. Strong metal-support interactions. Group 8 noble metals supported on titanium dioxide. *Journal of the American Chemical Society* **100**, 170-175 (1978).

92   Zhao, E. W. *et al.* Strong metal–support interactions enhance the pairwise selectivity of parahydrogen addition over Ir/TiO2. *Acs Catalysis* **6**, 974-978 (2016).

93   Bhowmick, R. *et al.* Hydrogen spillover in Pt-single-walled carbon nanotube composites: formation of stable C−H bonds. *Journal of the American Chemical Society* **133**, 5580-5586 (2011).

94   Wang, L., Yang, F. H., Yang, R. T. & Miller, M. A. Effect of surface oxygen groups in carbons on hydrogen storage by spillover. *Industrial & Engineering Chemistry Research* **48**, 2920-2926 (2009).

95   Psofogiannakis, G. M. & Froudakis, G. E. DFT study of hydrogen storage by spillover on graphite with oxygen surface groups. *Journal of the American Chemical Society* **131**, 15133-15135 (2009).

96   Chen, L., Pez, G., Cooper, A. C. & Cheng, H. A mechanistic study of hydrogen spillover in MoO3 and carbon-based graphitic materials. *Journal of Physics: Condensed Matter* **20**, 064223 (2008).

97   Chen, L., Cooper, A. C., Pez, G. P. & Cheng, H. Mechanistic study on hydrogen spillover onto graphitic carbon materials. *The Journal of Physical Chemistry C* **111**, 18995-19000 (2007).

98   Wang, M. *et al.* Wafer-scale transfer of vertically aligned carbon nanotube arrays. *Journal of the American Chemical Society* **136**, 18156-18162 (2014).

99   Zhao, B., Liu, Z., Zhang, Z. & Hu, L. Improvement of oxidation resistance of ultrafine copper powders by phosphating treatment. *Journal of Solid State Chemistry* **130**, 157-160 (1997).

100   Li, J., Mayer, J. & Colgan, E. Oxidation and protection in copper and copper alloy thin films. *Journal of applied physics* **70**, 2820-2827 (1991).

101   Smith, T. Oxidation of titanium between 25 C and 400 C. *Surface Science* **38**, 292-312 (1973).

102   Hass, G. & Bradford, A. P. Optical properties and oxidation of evaporated titanium films. *JOSA* **47**, 125-129 (1957).

103   Dai, Y. *et al.* A Sinter-Resistant Catalytic System Based on Platinum Nanoparticles Supported on TiO2 Nanofibers and Covered by Porous Silica. *Angewandte Chemie* **122**, 8341-8344 (2010).

104   Campbell, C. T., Parker, S. C. & Starr, D. E. The effect of size-dependent nanoparticle energetics on catalyst sintering. *Science* **298**, 811-814 (2002).

106   Prasomsri, T., Nimmanwudipong, T. & Román-Leshkov, Y. Effective hydrodeoxygenation of biomass-derived oxygenates into unsaturated hydrocarbons by MoO 3 using low H 2 pressures. *Energy & Environmental Science* **6**, 1732-1738 (2013).

107   An, K. *et al.* Preparation of mesoporous oxides and their support effects on Pt nanoparticle catalysts in catalytic hydrogenation of furfural. *Journal of colloid and interface science* **392**, 122-128 (2013).

108   Baker, L. R. *et al.* Furfuraldehyde hydrogenation on titanium oxide-supported platinum nanoparticles studied by sum frequency generation vibrational spectroscopy: Acid–base catalysis explains the molecular origin of strong metal–support interactions. *Journal of the American Chemical Society* **134**, 14208-14216 (2012).

109   Zhang, J., Wang, B., Nikolla, E. & Medlin, J. W. Directing Reaction Pathways through Controlled Reactant Binding at Pd–TiO2 Interfaces. *Angewandte Chemie* **129**, 6694-6698 (2017).

110   Primo, A., Concepción, P. & Corma, A. Synergy between the metal nanoparticles and the support for the hydrogenation of functionalized carboxylic acids to diols on Ru/TiO 2. *Chemical Communications* **47**, 3613-3615 (2011).

Appendix A1: Effect of partially oxidized Ni sites in furfural decarbonylation/hydrogenation reactions
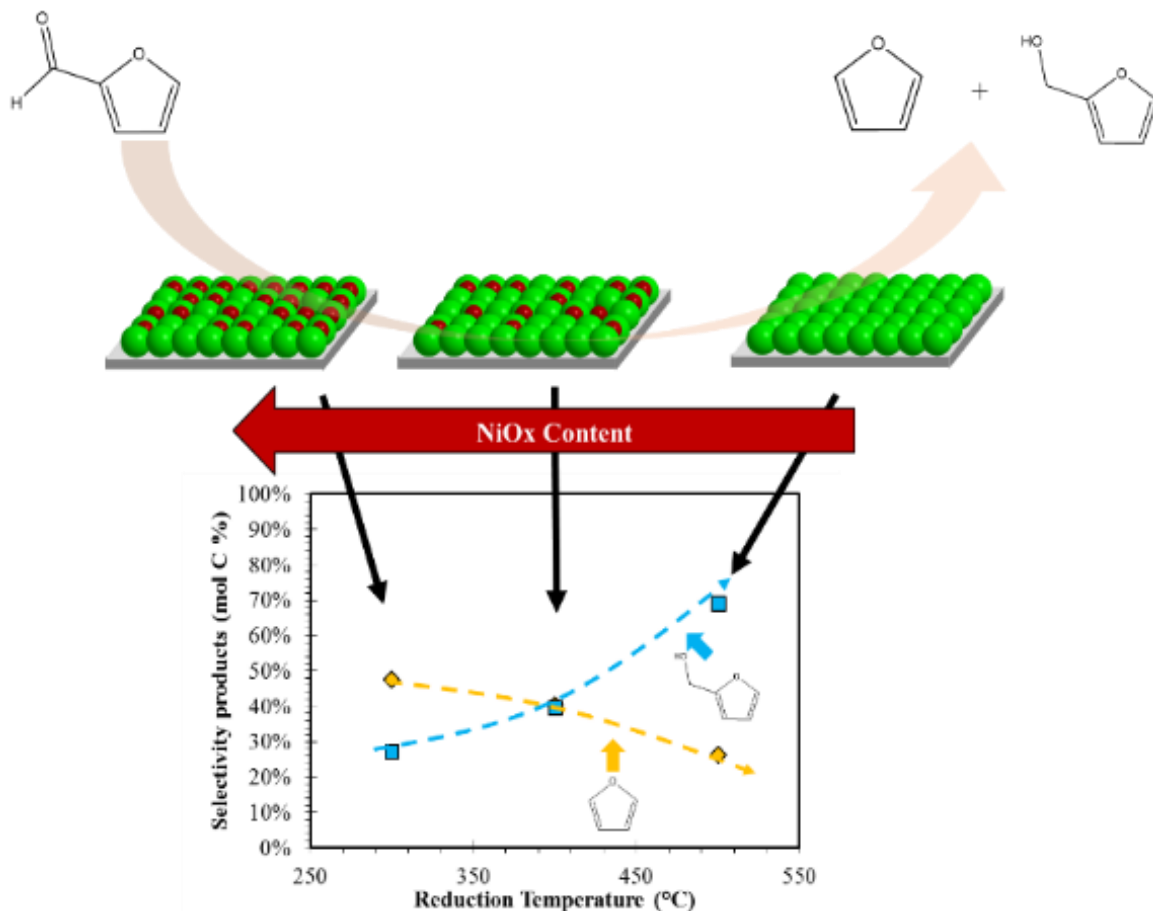
Introduction

The role of surface structure of active sites and the influence of pretreatment of the catalyst are often highly complex and difficult to be separated. Understanding those effects, allows for the achievement of the highest possible performance of the catalyst under reaction conditions[103-105]. Previous studies have demonstrated that many industrially significant reactions including catalytic combustion, ammonia production and Fischer−Tropsch synthesis, amongst others are structurally sensitive[56,106,107]. For

instance, the hydrogenation of different aldehydes such as furfural and cinnamaldehyde over Pt has been shown to strongly depend of particle size and high selectivity of the alcohol has been achieved by manipulating size in each case [104,108].

On the other hand the pretreatment conditions used in the catalyst for different reactions have also been shown to have an impact on selectivity [106]. Feng et al. studied the effect of catalyst reduction temperature on the hydrogenolysis of glycerol over Ru/TiO$_2$. The reaction activity decreased with increasing catalyst reduction temperature, which they attributed to the growth in Ru particle size and the strong metal-support interaction (SMSI), which results in partially covering of Ru metal particles by Ti2O3 species [109]. The effect of reduction temperature was also studied for CO/CO$_2$ hydrogenation over Pd-CeO$_2$ and it was found to affect the structural properties and catalytic behavior. At higher reduction temperature, the significant growth of palladium particles and the sintering of the ceria support weaken the interaction between Pd and ceria resulting in fewer CO conversions [110].

However, reduction temperature not only affects the particle size but also allows for the presence of oxide over layers of the surface [106]. For the CO oxidation on Pt **it** was suggested the reactivity of PtO$_2$ (110) was higher than that of a Pt metal surface [111,112]. Later Gong et al. [113] compared calculated CO oxidation energetics for Ru(0001), Rh(111), Pd(111), Os(1000), Ir(111), Pt(111) and their corresponding oxides. They concluded that the oxides are indeed more reactive than metal [113]. Furthermore, Min et al. [114] explained the existence of three types of oxygen species on Au(111) that can influence the CO reaction: chemisorbed oxygen not part of an ordered phase, well-ordered oxygen on the

surface of the oxide , and bulk oxide. The authors claimed that chemisorbed oxygen and the surface gold oxide species were more reactive than bulk gold oxide [106].

Furfural (FAL) is one of the most abundant products obtained from biomass and is considered as a building block for transportation fuels [68]. The carbonyl group of the furan ring can be reduced leading to furfuryl alcohol (FOL), which is the main hydrogenation product obtained from furfural. Depending on the type of metal catalyst used decarbonylation [69] and C-O bond cleavage [115] can also proceed yielding furan (FUR) or methyl furan (2MF) respectively. Both Cu and group VIII metals can be used for furfural hydrogenation, but they exhibit different catalytic mechanisms. The Cu-based catalysts are used more than group VIII metal catalysts in gas-phase reactions and favor the production of furfuryl alcohol via perpendicular adsorption mode [20,21]. The group VIII metals, especially Ni and Pd, are mainly used in liquid-phase reactions and can produce 2-methyl furan, furan, and ring opening products at high temperatures or H_2 pressures [22,23].

In this work we investigate the selectivity of furfural conversion over Ni/SiO_2 catalysts. By reduction/oxidation treatments and particle size studies we decouple the effect of NiOx presence on the surface of the catalyst and size of the clusters. The unexpected enhancement of furan yield with decreasing reduction temperature and oxidizing of the catalyst was attributed to the change in oxophilicity due to the presence of NiOx in the catalyst. Hydrogenation reaction of furfural to furfuryl alcohol showed a behavior of sensitive structure reaction, as it increases with increasing particle size. This results allowed us to have higher selectivity for either furfuryl alcohol or furan using the

same catalyst, Ni/SiO$_2$, by changing the pretreatment conditions of the catalyst and understanding better the decarbonylation chemistry.

Experimental section

Nicholas Briggs and Santiago Umbarila performed the TEM and TPR analysis.

Catalyst Preparation. Ni catalysts of 3%, 5% and 7% content were synthesized using the incipient wetness impregnation method of an aqueous solution of nickel (II) nitrate hexahydrate solution 99.999% trace metals basis, on a SiO$_2$ support (Silicon dioxide, 99.8%, from Sigma Aldrich). The catalysts were then placed in a calcination system where air was flowed at 150 ml/min through the system. The system was ramped to 100°C at 2°C/min and held at 100°C for four hours, followed by ramping to 400°C at 2°C/min and held at 400°C for four hours. The catalysts were pelletized and sieved to yield particles between the sizes of 90-250 μm.

Catalyst Characterization. Ni particle size distribution was obtained using Transmission Electron Microscopy (TEM, JEOL JEM-2100 model, equipped with a LaB$_6$ filament and operating at 200kV). For this process, the 3%, 5% and 7% catalysts were pre-reduced in hydrogen at 300 °C and 500 °C for 1 h and cooled down to room temperature in nitrogen before their dispersion in isopropanol and sonication to obtain a uniform suspension. A few drops of the suspension were deposited on TEM grids. At least 100 particles were counted in order to obtain particle size distributions.

Temperature programmed reduction (TPR) of the catalysts was investigated by flowing a gas mixture of 5 % H$_2$ in Ar at 35 ml/ min over 50 mg of sample. The

temperature was linearly increased from room temperature to 800 C at a rate of 10 °C/min. A thermal conductivity detector (TCD) (SRI 110) was used to analyze the effluent gas. A calibration curve was generated by conducting a series of TPR runs with CuO standard samples to quantify the amount of hydrogen consumed. The quantity of Ni present in the sample was calculated by integrating the TPR signal of the calcined catalyst and assuming that Ni was present as NiO. TPR experiments were also used for analyzing reduction/oxidation treatments of the catalysts.

The product samples were analyzed by online gas chromatography equipped with flame ionization detector (Agilent 5890), and HP-INNOWAX column (30 m, 0.25 μm). The products were also collected in an ice-trap and confirmed using a Shimadzu QP-2010 GCMS.

Catalytic Activity Tests. Catalytic activity was tested in a quartz tube reactor (0.25 in OD) at atmospheric pressure and 250°C. Catalyst particles (90 – 250 μm) were mixed with inert acid washed glass beads (Sigma Aldrich, Part number: G1277) with a particle size range of 212-300 μm and packed between two layers of quartz wool inside the reactor when required. In a typical experiment, pure distilled furfural (obtained from Sigma Aldrich; distilled and stored at -15 °C) with a feed flow rate of 0.5 ml/h was vaporized at the inlet zone of the reactor before introduction into a 40 ml/min hydrogen flow. The outlet stream of the reactor was heated to 250 °C to prevent condensation of compounds in the transfer lines and then flowed through a six-port valve to allow for injection into a GC for product analysis. Before introduction of the feed, the catalysts were reduced in situ at different temperatures between 300 to 500 °C for 1 h in 100 ml/min hydrogen flow.

Results and discussion

Catalyst characterization. Nickel particle size was measured using TEM and as can be seen in Figure S1 particle size increases as the amount of Ni on the catalyst is increased and as the reduction temperature is increased. The particle size for the catalysts reduced at 300°C for 3%, 5%, and 7% Ni/SiO$_2$ are 1.0 nm, 2.5 nm, and 4.2 nm, respectively. For the case of the catalysts reduced at 500°C the particle size for 3%, 5%, and 7% Ni/SiO$_2$ are 3.14 nm, 3.6 nm, and 6.3 nm, respectively. This increase in particle size is due to the sintering of the particles which increases as the reduction temperature increases. An indication of nickel oxide can be seen in the TEM images as the black spots appear to be a ligther color for the catalyst reduced at 300°C than 500°C due to nickel oxide being simialir to the silica.

Further understanding of the metallic and oxide nature of the catalyst was obtained with TPR. The 5% Ni/SiO$_2$ catalyst after calcination shows a reduction of the nickel oxide to nickel metal, Figure S2a, at 450°C and agrees with previous reports [115]. The bump next to the tail end of the main peak may be due to the presence of nickel silicates, which was observed by Montes *et al.* [116] as will be discussed in further sections depending on the temperature used to reduce the catalyst, either 300°C or 500°C, the amount of nickel oxide present can affect reaction selectivity. To quantify the amount of nickel oxide present during a reaction TPRs were run in which catalysts were reduced at 300°C and 500°C for one hour, the same way as for a reaction. By performing a TPR, after reduction of the catalyst
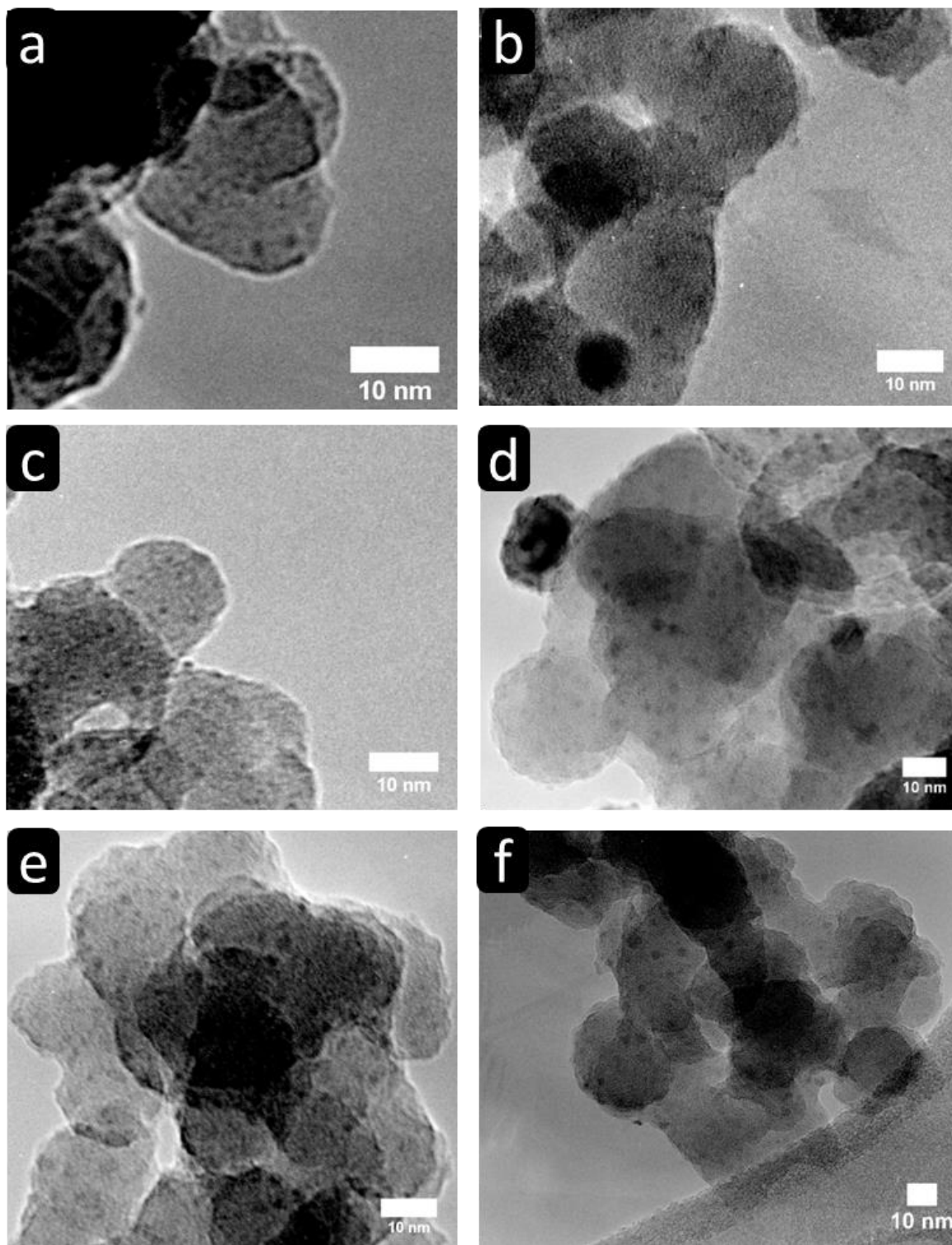
Figure S 1: (a) 3% Ni/SiO₂ reduced at 300°C, (b) 3% Ni SiO₂ reduced at 500°C, (c) 5% Ni/SiO₂ reduced at 300°C (d) 5% Ni/SiO₂ reduced at 500°C , (e) 7% Ni/SiO₂ reduced at 300°C and (f) 7% Ni/SiO₂ reduced at 500°C.

at a set temperature, the amount of remaining nickel oxide can be quantified. As can be seen in Figure S2b there is no remaining nickel oxide when reducing the catalyst at 500°C, but roughly 13.7% of the nickel oxide remains when the catalyst is reduced at 300°C. This residual nickel oxide plays a critical role in controlling reaction selectivity as will be discussed in further sections. At similar conditions Manukyan et al. observed NiOx too in their reduction study [117].
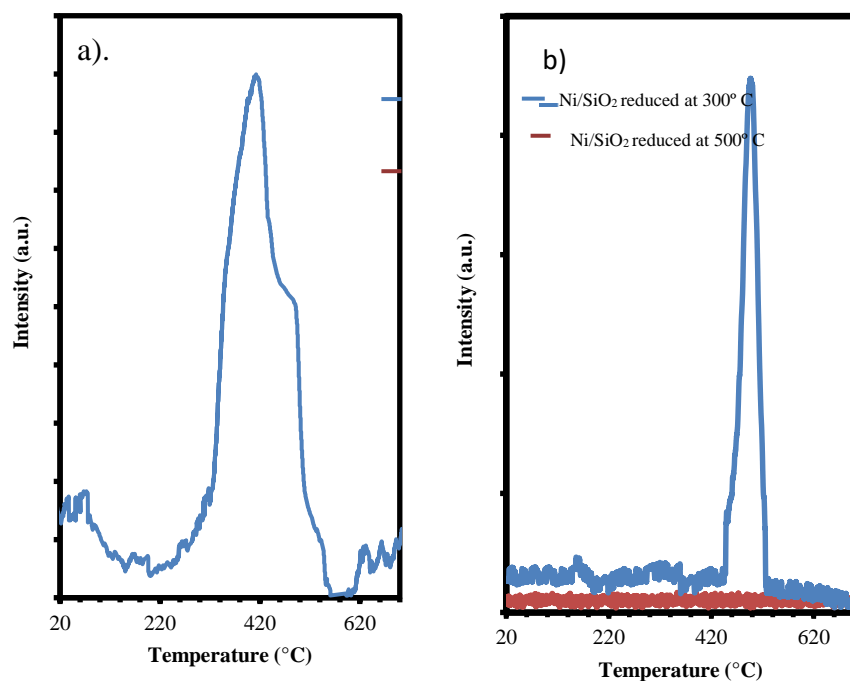

Figure S 2: a) TPR profile for 5% Ni/SiO₂ catalyst after nickel impregnation on the support and calcination. b) TPR profile for 5% Ni/SiO₂ catalyst after being reduced at either 300°C or 500°C for one hour

Effect of reduction temperature

Gas phase furfural conversion under hydrogen leads to the formation of multiple compounds through different reactions such as decarbonylation, hydrogenation, ring opening and ring rearrangement [20]. At the experimental conditions of this study, two primary reactions dominate the reaction pathway: the hydrogenation of C=O bond to yield furfuryl alcohol (FOL) which can undergo hydrogenolysis to methylfuran (MF) and subsequent ring opening to 2-pentanone (2PNO) and decarbonylation to form furan (FUR) which leads to the ring opening reaction which produces C4 products such as butanal, butanol and butane as secondary relevant products [9]. However, the selectivity of the furfural conversion was observed to strongly depend of the reduction temperature having a clear competition between decarbonylation/hydrogenation reactions.

As shown in Figure S3 a and b, with decreasing reduction temperature, or in other words with increasing NiO content in the catalyst, the selectivity of FUR and C4 increases too, which makes the C-C cleavage reaction dominate. On the other hand, at the highest reduction temperature used, there is a clear shift in selectivity from FUR to FOL and hydrogenation of the C-O bond is the dominant reaction. Most of the studies in literature of furfural hydrogenation over Ni/SiO$_2$ utilize reduction temperatures of 450 °C or more for long times obtaining FOL as the dominant product or a small enhancement in FUR selectivity. For instance Tomishige *et al.* [118] studied the total reduction of furfural to tetrahydrofurfuryl alcohol (THFOL) over Ni/SiO$_2$ at different reduction temperatures from 673 to 873 K and they observed increases of both alcohols, FOL and THFOL with temperature. They concluded the conversion of FOL to THFA is sensitive to the structure

of the catalyst since Ni particles with a smaller size give higher TOF values [118]. Resasco *et al.* [115] investigated the conversion of furfural over Ni/SiO$_2$ and Ni-Fe/SiO$_2$ using a temperature reduction of 450 °C. For Ni/SiO$_2$ the dominant product of the reaction at all W/F was FUR however when the Fe was introduced the selectivity shifted to form 2MF [20]. This shows that oxophilic additions to a metal that decarbonylates, destabilizes the tendency of the O to lift from the surface and stabilize the acyl intermediate.

Figure 3 b also shows a decrease of conversion with increasing reduction temperature due to sintering of the particles also observed by TEM. This indicates that not only the presence of the oxide can be affecting the selectivity of the decarbonylation/hydrogenation reactions but also the effect of particle size. Therefore decoupling of particle size and oxide content is analyzed in the next section.

Decoupling of oxide content and particle size effects

The change of particle with increasing reduction temperature can potentially influence the selectivity of the furfural reaction by changing the surface of the catalyst [106]. Iglesia *et al.* [119] showed by kinetics and DFT of alkanols/alkanals over different metals that C-O hydrogenolysis occurs preferentially on atoms with high-coordination number that prevail on larger clusters while C-C hydrogenolysis is favored over low-coordinated atoms . Furthermore, Somorjai et al. [104] claimed furfural conversion to FOL is a highly structure sensitive reaction. Their experiments in gas phase over Pt nanoparticles showed selectivity for FOL increases with increasing particle size (≤2.9 nm) while at small particle sizes the dominant product of the reaction was FUR.

To analyze the effect of particle size in our reactions three different Ni/SiO$_2$ catalyst of 3%, 5% and 7% were investigated at 300 °C and 500 °C reduction temperatures. The rate per metal exposed (mol/m^2.h) was calculated to avoid discrepancies due to particle size and the reactions were run at similar conversions. As shown in Figure S3 c, the ratio between FUR/FOL decreases dramatically for the catalysts reduced at 300 °C that have NiOx on the surface and not for a specific trend with particle size. This can be observed in Figure S3 d, where the FOL rate behaves as a structure sensitive reaction as some studies have shown in literature and increases with increasing particle size. However, FUR is clearly affected by the presence of oxide.

Reduction/Oxidation treatments

To further understand the role of the NiO in the decarbonylation reaction of furfural to FUR reduction/oxidation treatments were analyzed over the 3%, 5% and 7% Ni/SiO$_2$ catalysts. Each catalyst was fully reduced at 500 °C, and exposed to air at 400 °C for different times. To ensure at this conditions the catalysts were not completely reduced, the samples were analyzed by doing the same reaction process in the TPR. The 5% Ni/SiO$_2$ fully reduced at 500 °C and exposed to air for 30 mins at 400 °C at these conditions the content of NiOx of the catalyst is 39.3%.
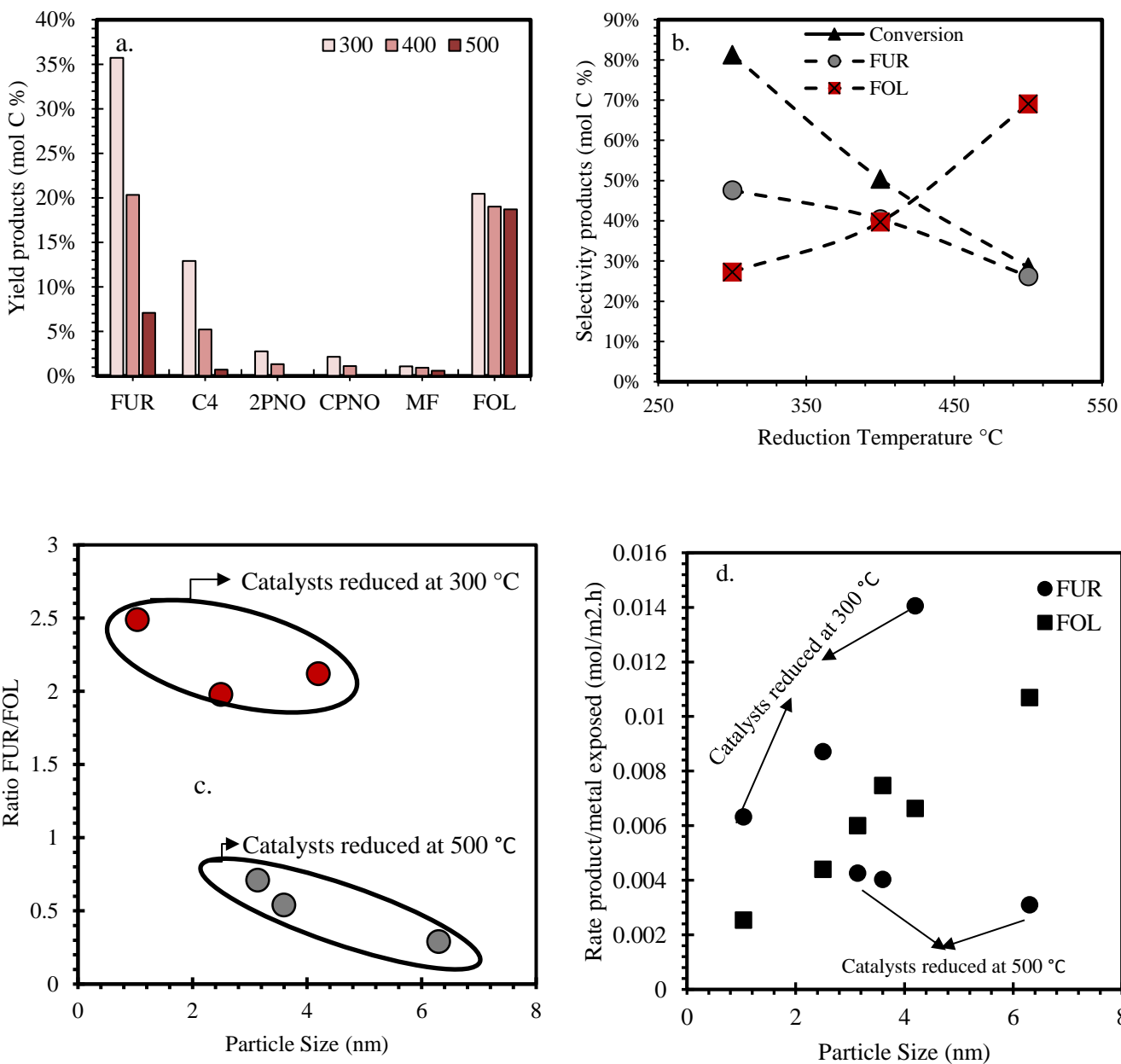
Figure 3 a) Product Distribution for furfural conversion over 5% Ni/SiO₂ at different reduction temperatures b) Selectivity of furan and furfuryl alcohol for furfural reaction over 5%Ni/SiO₂ at different reaction temperatures. Trxn= 250°C, P= 1 atm, TOS= 30 mins, FAL: 0.006 mol/h. c) Ratio of FUR and FOL over the 3%, 5% and 7% Ni/SiO₂ catalysts at different reduction temperatures d) Rate of exposed metal for FUR and FOL vs particle size. Trxn: 250 °C. TOS: 30 min

The conversion for the three catalyst at different oxidation times is shown in Figure S4a. In each case there is a trend with a maximum of conversion corresponding to an optimum specific amount of NiOx present on the surface that generated the highest conversion. The reaction without reducing catalyst was carried out and very low conversion was obtained. Furthermore, the catalysts that were completely oxidized (3% for 15 min, 5% 120 min and 7% 140 min) showed a recovery in activity after 1-2 h on stream. This proves that both metal Ni and NiOx must be present during reaction to enhance the C-C cleavage reaction since for all of the reduced/oxidized catalyst FUR was the dominant product of the reaction. The change of selectivity is noticeable in Figure S 4b,c and d from FOL when the catalyst is fully reduced to FUR when the catalysts begins to become oxidized for all the cases.

The oxide effect in decarbonylation chemistry is still matter of further investigation. Based on the oxidations experiments and previous reports that showed the change in oxophilicity with oxide present in the surface, it is possible to speculate the presence NiOx facilitates the C-C bond cleavage. If the oxide layers allows for a weakening of the interaction between the carbon of the carbonyl group and the metal, the formation of acyl intermediate will be easier and therefore the furan production will be favored [16]. On the other hand, over layers of NiOx can also affect the morphology of the surface of the catalyst and it has been showed furan is preferably converted over low-coordinated atoms [24].
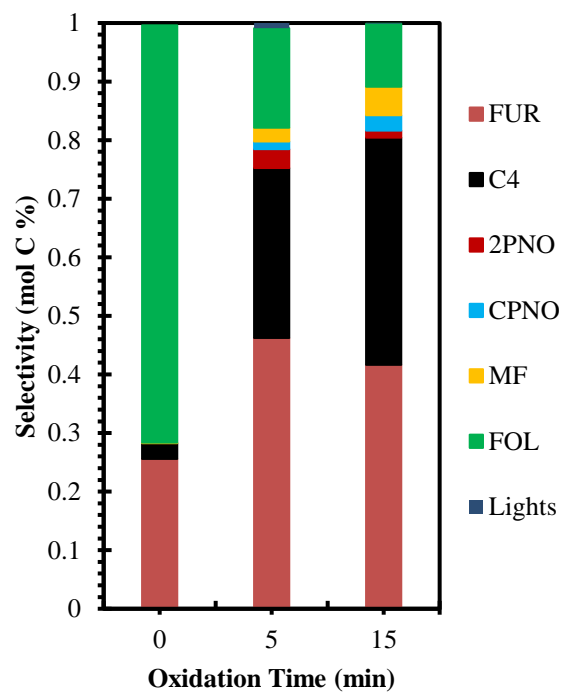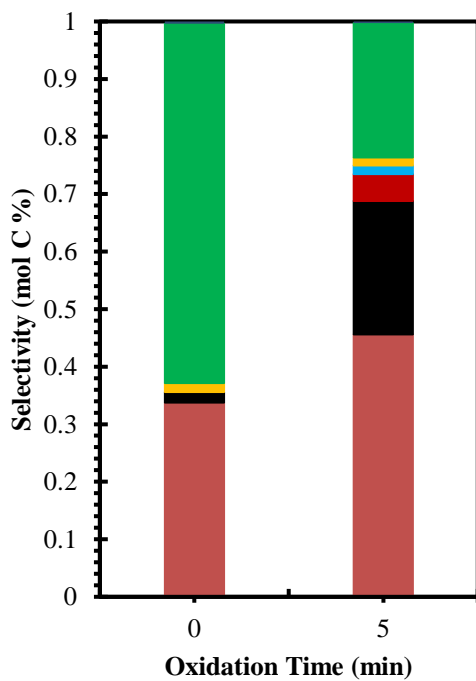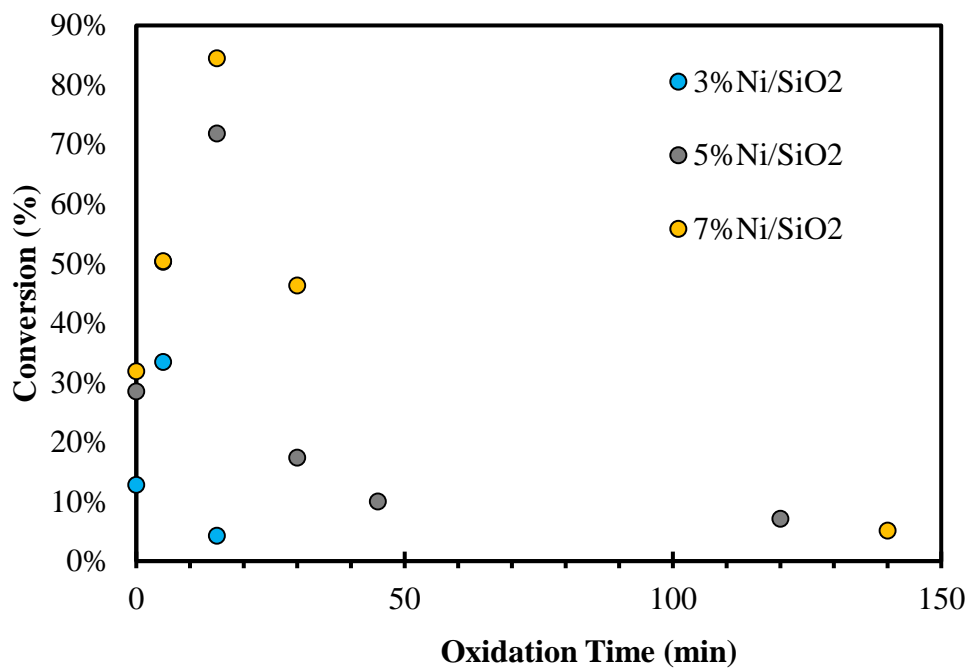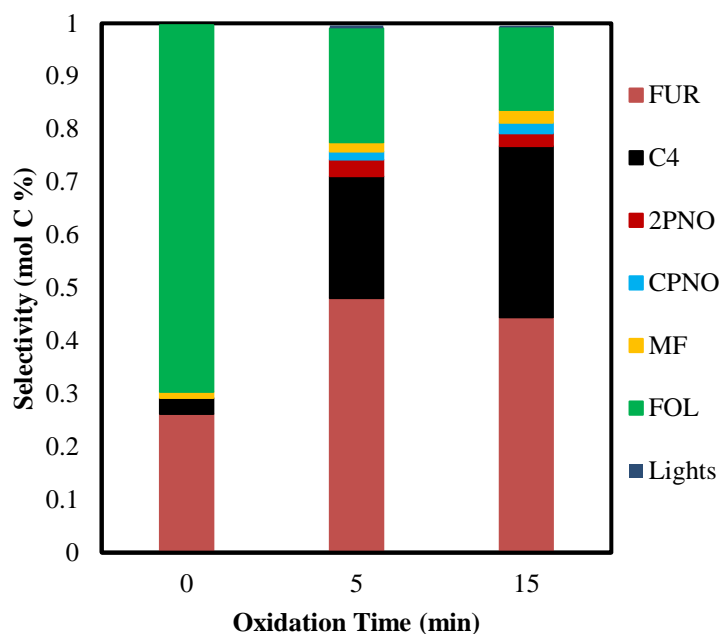
Figure 4.a) Furfural conversion vs oxidation time for the 3%, 5% and 7% Ni/SiO$_2$ catalyst. c), d), e) Product selectivity for furfural conversion over 3%, 5% and 7% Ni/SiO$_2$ oxidized catalysts respectively

Conclusions

Furfural hydrogenation in gas phase was studied over a series of silica supported Ni catalysts. The product selectivity to furfuryl alcohol and furan can be controlled by changing the pretreatment conditions of the catalyst. At low reduction temperatures, or in other words high NiOx presence, furan selectivity is enhanced while fully reduced Ni/SiO2 yields as the main product furfuryl alcohol. The hydrogenation to furfuryl alcohol was found to be a structure sensitive reaction and its rate increases with increasing particle size. The oxide effect in the decarbonylation chemistry can be attributed to different factors such as NiOx/Ni interface site that allows C-C bond cleavage or electronic effect of the oxide over layers in the metal that helps weaken the C-M bond

and enhance furan production. This results allows for high selectivity of either furfuryl alcohol or furan using the same catalyst, Ni/SiO2, by changing the pretreatment conditions of the catalyst and understanding better the decarbonylation chemistry.

References

(1   Zhang, Q., Chang, J., Wang, T. & Xu, Y. Review of biomass pyrolysis oil properties and upgrading research. *Energ Convers Manage* **48**, 87-92 (2007).

2   Yang, H., Yan, R., Chen, H., Lee, D. H. & Zheng, C. Characteristics of hemicellulose, cellulose and lignin pyrolysis. *Fuel* **86**, 1781-1788 (2007).

3   Venderbosch, R. & Prins, W. Fast pyrolysis technology development. *Biofuels, bioproducts and biorefining* **4**, 178-208 (2010).

4   Resasco, D. E. & Crossley, S. P. Implementation of concepts derived from model compound studies in the separation and conversion of bio-oil to fuel. *Catalysis Today* **257**, 185-199 (2015).

5   Meng, J., Park, J., Tilotta, D. & Park, S. The effect of torrefaction on the chemistry of fast-pyrolysis bio-oil. *Bioresource technology* **111**, 439-446 (2012).

6   Shankar Tumuluru, J., Sokhansanj, S., Hess, J. R., Wright, C. T. & Boardman, R. D. REVIEW: A review on biomass torrefaction process and product properties for energy applications. *Industrial Biotechnology* **7**, 384-401 (2011).

7   Herron, J. A. *et al.* A Systems-Level Roadmap for Biomass Thermal Fractionation and Catalytic Upgrading Strategies. *Energy Technology* (2016).

8   French, R. & Czernik, S. Catalytic pyrolysis of biomass for biofuels production. *Fuel Processing Technology* **91**, 25-32 (2010).

9   Bridgwater, A. V. Review of fast pyrolysis of biomass and product upgrading. *Biomass and bioenergy* **38**, 68-94 (2012).

10   Van der Stelt, M., Gerhauser, H., Kiel, J. & Ptasinski, K. Biomass upgrading by torrefaction for the production of biofuels: A review. *Biomass and bioenergy* **35**, 3748-3762 (2011).

11   Ebert, J. Furfural: Future feedstock for fuels and chemicals. *Ethanol Producer Magazine* (2008).

12   Werpy, T. *et al.* Top value added chemicals from biomass. Volume 1-Results of screening for potential candidates from sugars and synthesis gas. (DTIC Document, 2004).

13   Gürbüz, E. I., Wettstein, S. G. & Dumesic, J. A. Conversion of hemicellulose to furfural and levulinic acid using biphasic reactors with alkylphenol solvents. *ChemSusChem* **5**, 383-387 (2012).

14   Dias, A. S., Lima, S., Pillinger, M. & Valente, A. A. Furfural and Furfural-Based Industrial-Chemicals. *Ideas in Chemistry and Molecular Sciences: Advances in Synthetic Chemistry* **8**, 167-186 (2010).

15   Yan, K., Wu, G., Lafleur, T. & Jarvis, C. Production, properties and catalytic hydrogenation of furfural to fuel additives and value-added chemicals. *Renewable and Sustainable Energy Reviews* **38**, 663-676 (2014).

16   Hoydonckx, H., Van Rhijn, W., Van Rhijn, W., De Vos, D. & Jacobs, P. Furfural and derivatives. *Ullmann's encyclopedia of industrial chemistry* (2007).

17   Nagaraja, B. *et al.* A highly efficient Cu/MgO catalyst for vapour phase hydrogenation of furfural to furfuryl alcohol. *Catalysis communications* **4**, 287-293 (2003).

18   Jiménez-Gómez, C. P. *et al.* Gas-phase hydrogenation of furfural to furfuryl alcohol over Cu/ZnO catalysts. *Journal of Catalysis* **336**, 107-115 (2016).

19   Bhogeswararao, S. & Srinivas, D. Catalytic conversion of furfural to industrial chemicals over supported Pt and Pd catalysts. *Journal of Catalysis* **327**, 65-77 (2015).

20   Sitthisa, S. & Resasco, D. E. Hydrodeoxygenation of furfural over supported metal catalysts: a comparative study of Cu, Pd and Ni. *Catalysis letters* **141**, 784-791 (2011).

21   Sitthisa, S., Sooknoi, T., Ma, Y., Balbuena, P. B. & Resasco, D. E. Kinetics and mechanism of hydrogenation of furfural on Cu/SiO 2 catalysts. *Journal of catalysis* **277**, 1-13 (2011).

22   Vorotnikov, V., Mpourmpakis, G. & Vlachos, D. G. DFT study of furfural conversion to furan, furfuryl alcohol, and 2-methylfuran on Pd (111). *Acs Catalysis* **2**, 2496-2504 (2012).

23   Sitthisa, S. *et al.* Conversion of furfural and 2-methylpentanal on Pd/SiO 2 and Pd–Cu/SiO 2 catalysts. *Journal of catalysis* **280**, 17-27 (2011).

24   Wang, S., Vorotnikov, V. & Vlachos, D. G. A DFT study of furan hydrogenation and ring opening on Pd (111). *Green Chemistry* **16**, 736-747 (2014).

25   Li, X., Jia, P. & Wang, T. Furfural: A promising platform compound for sustainable production of C4 and C5 chemicals. *ACS Catalysis* **6**, 7621-7640 (2016).

26   Sitthisa, S., An, W. & Resasco, D. E. Selective conversion of furfural to methylfuran over silica-supported Ni-Fe bimetallic catalysts. *Journal of Catalysis* **284**, 90-101, doi:DOI 10.1016/j.jcat.2011.09.005 (2011).

27   Hronec, M. *et al.* Cyclopentanone: A raw material for production of C 15 and C 17 fuel precursors. *Biomass and Bioenergy* **63**, 291-299 (2014).

28   Hronec, M. *et al.* Carbon supported Pd–Cu catalysts for highly selective rearrangement of furfural to cyclopentanone. *Applied Catalysis B: Environmental* **181**, 210-219 (2016).

29   Yang, Y. *et al.* Conversion of furfural into cyclopentanone over Ni–Cu bimetallic catalysts. *Green Chemistry* **15**, 1932-1940 (2013).

30   Hronec, M., Fulajtarová, K. & Liptaj, T. Effect of catalyst and solvent on the furan ring rearrangement to cyclopentanone. *Applied Catalysis A: General* **437**, 104-111 (2012).

31   Hronec, M. & Fulajtarová, K. Selective transformation of furfural to cyclopentanone. *Catalysis Communications* **24**, 100-104 (2012).

32   Hronec, M., Fulajtárova, K. & Soták, T. Highly selective rearrangement of furfuryl alcohol to cyclopentanone. *Applied Catalysis B: Environmental* **154**, 294-300 (2014).

33   Williams, C. L. *et al.* Cycloaddition of biomass-derived furans for catalytic production of renewable p-xylene. *Acs Catalysis* **2**, 935-939 (2012).

34   Gumidyala, A., Wang, B. & Crossley, S. Direct carbon-carbon coupling of furanics with acetic acid over Brønsted zeolites. *Science Advances* **2**, e1601072 (2016).

35   Bui, T. V., Crossley, S. & Resasco, D. E. C-C Coupling for Biomass-Derived Furanics Upgrading to Chemicals and Fuels. *Chemicals and Fuels from Bio-Based Building Blocks*, 431-494 (2016).

36   Kawabata, T., Kato, M., Mizugaki, T., Ebitani, K. & Kaneda, K. Monomeric metal aqua complexes in the interlayer space of montmorillonites as strong lewis acid catalysts for heterogeneous carbon–carbon bond-forming reactions. *Chemistry–A European Journal* **11**, 288-297 (2005).

37   Fischer, J. & Hölderich, W. F. Baeyer–Villiger-oxidation of cyclopentanone with aqueous hydrogen peroxide by acid heterogeneous catalysis. *Applied Catalysis A: General* **180**, 435-443, doi:http://dx.doi.org/10.1016/S0926-860X(98)00378-0 (1999).

38   Piutti, C. & Quartieri, F. The Piancatelli Rearrangement: New Applications for an Intriguing Reaction. *Molecules* **18**, 12290-12312, doi:DOI 10.3390/molecules181012290 (2013).

39   Pham, T. N., Shi, D. & Resasco, D. E. Evaluating strategies for catalytic upgrading of pyrolysis oil in liquid phase. *Applied Catalysis B: Environmental* **145**, 10-23, doi:10.1016/j.apcatb.2013.01.002 (2014).

40   Stöcker, M. Biofuels and biomass-to-liquid fuels in the biorefinery: Catalytic conversion of lignocellulosic biomass using porous materials. *Angewandte Chemie International Edition* **47**, 9200-9211 (2008).

41   Czernik, S. & Bridgwater, A. Overview of applications of biomass fast pyrolysis oil. *Energy & Fuels* **18**, 590-598 (2004).

42   Carlson, T. R., Vispute, T. P. & Huber, G. W. Green gasoline by catalytic fast pyrolysis of solid biomass derived compounds. *ChemSusChem* **1**, 397-400 (2008).

43   Badovskaya, L. A. & Povarova, L. V. Oxidation of furans (Review). *Chemistry of Heterocyclic Compounds* **45**, 1023-1034, doi:10.1007/s10593-009-0390-8 (2009).

44   Milas, N. A. & Walsh, W. L. Catalytic Oxidations. I. Oxidations in the Furan Series. *Journal of the American Chemical Society* **57**, 1389-1393 (1935).

45   Takagaki, A., Nishimura, S. & Ebitani, K. Catalytic transformations of biomass-derived materials into value-added chemicals. *Catalysis Surveys from Asia* **16**, 164-182 (2012).

46   WANG, S., LENG, Y., LIN, F., HUANG, C. & YI, C. Catalytic oxidation of furfural in vapor-gas phase for producing maleic anhydride [J]. *Chemical Industry and Engineering Progress* **6**, 029 (2009).

47   Nielsen, E. R. Vapor phase oxidation of furfural. *Industrial & Engineering Chemistry* **41**, 365-368 (1949).

48   Kijenski, J., Winiarek, P., Paryjczak, T., Lewicki, A. & Mikolajska, A. Platinum deposited on monolayer supports in selective hydrogenation of furfural to furfuryl alcohol. *Applied Catalysis a-General* **233**, 171-182, doi:Pii S0926-860x(02)00140-0

Doi 10.1016/S0926-860x(02)00140-0 (2002).

49   Zheng, H. Y. *et al.* Towards understanding the reaction pathway in vapour phase hydrogenation of furfural to 2-methylfuran. *J Mol Catal a-Chem* **246**, 18-23, doi:DOI 10.1016/j.molcata.2005.10.003 (2006).

50   Zhu, Y. L. *et al.* A new strategy for the efficient synthesis of 2-methylfuran and gamma-butyrolactone. *New J Chem* **27**, 208-210, doi:Doi 10.1039/B208849p (2003).

51   Yang, J. *et al.* Effects of calcination temperature on performance of Cu-Zn-Al catalyst for synthesizing gamma-butyrolactone and 2-methylfuran through the coupling of dehydrogenation and hydrogenation. *Catal. Commun.* **5**, 505-510, doi:DOI 10.1016/j.catcom.2004.06.005 (2004).

52   Zheng, H. Y., Yang, J., Zhu, Y. L. & Zhao, G. W. Synthesis of gamma-butyrolactone and 2-methylfuran through the coupling of dehydrogenation and hydrogenation over copper-chromite catalyst. *React Kinet Catal L* **82**, 263-269, doi:Doi 10.1023/B:Reac.0000034836.56895.A9 (2004).

53   Omotoso, T., Boonyasuwat, S. & Crossley, S. P. Understanding the role of TiO 2 crystal structure on the enhanced activity and stability of Ru/TiO 2 catalysts for the conversion of lignin-derived oxygenates. *Green Chemistry* **16**, 645-652 (2014).

54   Scholz, D., Aellig, C. & Hermans, I. Catalytic Transfer Hydrogenation/Hydrogenolysis for Reductive Upgrading of Furfural and 5-(Hydroxymethyl)furfural. *Chemsuschem* **7**, 268-275, doi:DOI 10.1002/cssc.201300774 (2014).

55   Sitthisa, S., Sooknoi, T., Ma, Y. G., Balbuena, P. B. & Resasco, D. E. Kinetics and mechanism of hydrogenation of furfural on Cu/SiO2 catalysts. *Journal of Catalysis* **277**, 1-13, doi:DOI 10.1016/j.jcat.2010.10.005 (2011).

56   Komaya, T. *et al.* Effects of dispersion and metal-metal oxide interactions on Fischer-Tropsch synthesis over Ru/TiO2 and TiO2-promoted Ru/SiO2. *Journal of Catalysis* **150**, 400-406 (1994).

57   Resasco, D. E. & Haller, G. L. A Model of Metal-Oxide Support Interaction for Rh on Tio2. *Journal of Catalysis* **82**, 279-288, doi:Doi 10.1016/0021-9517(83)90194-X (1983).

58   Avery, N. R. Eels Identification of the Adsorbed Species from Acetone Adsorption on Pt(111). *Surf Sci* **125**, 771-786, doi:Doi 10.1016/S0039-6028(83)80059-4 (1983).

59   Shekhar, R., Barteau, M. A., Plank, R. V. & Vohs, J. M. Adsorption and reaction of aldehydes on Pd surfaces. *Journal of Physical Chemistry B* **101**, 7939-7951, doi:Doi 10.1021/Jp971077l (1997).

60   Davis, J. L. & Barteau, M. A. Polymerization and Decarbonylation Reactions of Aldehydes on the Pd(111) Surface. *Journal of the American Chemical Society* **111**, 1782-1792, doi:Doi 10.1021/Ja00187a035 (1989).

61   Boonyasuwat, S., Omotoso, T., Resasco, D. E. & Crossley, S. P. Conversion of guaiacol over supported Ru catalysts. *Catalysis letters* **143**, 783-791 (2013).

62   Omotoso, T., Boonyasuwat, S. & Crossley, S. P. Understanding the role of TiO2 crystal structure on the enhanced activity and stability of Ru/TiO2 catalysts for the conversion of lignin-derived oxygenates. *Green Chem* **16**, 645-652, doi:Doi 10.1039/C3gc41377b (2014).

63   Selvaraj, V., Vinoba, M. & Alagar, M. Electrocatalytic oxidation of ethylene glycol on Pt and Pt-Ru nanoparticles modified multi-walled carbon nanotubes. *J Colloid Interface Sci* **322**, 537-544, doi:10.1016/j.jcis.2008.02.069 (2008).

64   Iwasita, T. Electrocatalysis of methanol oxidation. *Electrochimica Acta* **47**, 3663-3674 (2002).

65   Jiang, J. & Kucernak, A. Electrooxidation of small organic molecules on mesoporous precious metal catalysts. *Journal of Electroanalytical Chemistry* **543**, 187-199, doi:10.1016/s0022-0728(03)00046-9 (2003).

66   Tan, Q. *et al.* Different Product Distributions and Mechanistic Aspects of the Hydrodeoxygenation of m-Cresol over Platinum and Ruthenium Catalysts. *ACS Catalysis* **5**, 6271-6283 (2015).

67   Rekoske, J. E. & Barteau, M. A. Isothermal reduction kinetics of titanium dioxide-based materials. *The Journal of Physical Chemistry B* **101**, 1113-1124 (1997).

68   Choi, S., Song, C. W., Shin, J. H. & Lee, S. Y. Biorefineries for the production of top building block chemicals and their derivatives. *Metabolic engineering* **28**, 223-239 (2015).

69   Zhang, W., Zhu, Y., Niu, S. & Li, Y. A study of furfural decarbonylation on K-doped Pd/Al 2 O 3 catalysts. *Journal of Molecular Catalysis A: Chemical* **335**, 71-81 (2011).

70   Zhu, X., Nie, L., Lobban, L. L., Mallinson, R. G. & Resasco, D. E. Efficient conversion of m-cresol to aromatics on a bifunctional Pt/HBeta catalyst. *Energy & Fuels* **28**, 4104-4111 (2014).

71   Nelson, R. C. *et al.* Experimental and theoretical insights into the hydrogen-efficient direct hydrodeoxygenation mechanism of phenol over Ru/TiO2. *ACS catalysis* **5**, 6509-6523 (2015).

72   Hong, S. & Rahman, T. S. Rationale for the higher reactivity of interfacial sites in methanol decomposition on Au13/TiO2 (110). *Journal of the American Chemical Society* **135**, 7629-7635 (2013).

73   Pham, T. N., Shi, D. & Resasco, D. E. Kinetics and mechanism of ketonization of acetic acid on Ru/TiO2 catalyst. *Topics in Catalysis* **57**, 706-714 (2014).

74   Madon, R. J. B., M. Experimental Criterion for the Absence of Artifacts in the Measurement of Rates of Heterogeneous Catalytic Reactions. *Ind. Eng. Chem. Fundam* **21**, 438-447 (1982).

75   Vannice, M. A. & Joyce, W. H. *Kinetics of catalytic reactions*. Vol. 134 (Springer, 2005).

76   Pham, T., Shi, D. & Resasco, D. Kinetics and Mechanism of Ketonization of Acetic Acid on Ru/TiO Catalyst. *Topics in Catalysis* **57** (2014).

77   Kennedy, G., Baker, L. R. & Somorjai, G. A. Selective Amplification of C□ O Bond Hydrogenation on Pt/TiO2: Catalytic Reaction and Sum-Frequency Generation Vibrational Spectroscopy Studies of Crotonaldehyde Hydrogenation. *Angewandte Chemie* **126**, 3473-3476 (2014).

78   Poenitzsch, V. *et al.* Freestanding foils of nanotube arrays fused with metals. *Journal of materials science* **49** (2014).

79   Cargnello, M. *et al.* Control of metal nanocrystal size reveals metal-support interface role for ceria catalysts. *Science* **341**, 771-773 (2013).

80   Omotoso, T. O., Baek, B., Grabow, L. C. & Crossley, S. P. Experimental and First-Principles Evidence for Interfacial Activity of Ru/TiO2 for the Direct Conversion of m-Cresol to Toluene. *ChemCatChem* (2017).

81   Resasco, D. & Haller, G. A model of metal-oxide support interaction for Rh on TiO2. *Journal of Catalysis* **82**, 279-288 (1983).

82   Haller, G. L. & Resasco, D. E. Metal–support interaction: Group VIII metals and reducible oxides. *Advances in Catalysis* **36**, 173-235 (1989).

83   Tauster, S., Fung, S. & Garten, R. L. Strong metal-support interactions. Group 8 noble metals supported on titanium dioxide. *Journal of the American Chemical Society* **100**, 170-175 (1978).

84   Zhao, E. W. *et al.* Strong metal–support interactions enhance the pairwise selectivity of parahydrogen addition over Ir/TiO2. *Acs Catalysis* **6**, 974-978 (2016).

85   Bhowmick, R. *et al.* Hydrogen spillover in Pt-single-walled carbon nanotube composites: formation of stable C− H bonds. *Journal of the American Chemical Society* **133**, 5580-5586 (2011).

86   Wang, L., Yang, F. H., Yang, R. T. & Miller, M. A. Effect of surface oxygen groups in carbons on hydrogen storage by spillover. *Industrial & Engineering Chemistry Research* **48**, 2920-2926 (2009).

87   Psofogiannakis, G. M. & Froudakis, G. E. DFT study of hydrogen storage by spillover on graphite with oxygen surface groups. *Journal of the American Chemical Society* **131**, 15133-15135 (2009).

88   Chen, L., Pez, G., Cooper, A. C. & Cheng, H. A mechanistic study of hydrogen spillover in MoO3 and carbon-based graphitic materials. *Journal of Physics: Condensed Matter* **20**, 064223 (2008).

89   Chen, L., Cooper, A. C., Pez, G. P. & Cheng, H. Mechanistic study on hydrogen spillover onto graphitic carbon materials. *The Journal of Physical Chemistry C* **111**, 18995-19000 (2007).

90   Wang, M. *et al.* Wafer-scale transfer of vertically aligned carbon nanotube arrays. *Journal of the American Chemical Society* **136**, 18156-18162 (2014).

91   Zhao, B., Liu, Z., Zhang, Z. & Hu, L. Improvement of oxidation resistance of ultrafine copper powders by phosphating treatment. *Journal of Solid State Chemistry* **130**, 157-160 (1997).

92   Li, J., Mayer, J. & Colgan, E. Oxidation and protection in copper and copper alloy thin films. *Journal of applied physics* **70**, 2820-2827 (1991).

93   Smith, T. Oxidation of titanium between 25 C and 400 C. *Surface Science* **38**, 292-312 (1973).

94   Hass, G. & Bradford, A. P. Optical properties and oxidation of evaporated titanium films. *JOSA* **47**, 125-129 (1957).

95   Dai, Y. *et al.* A Sinter-Resistant Catalytic System Based on Platinum Nanoparticles Supported on TiO2 Nanofibers and Covered by Porous Silica. *Angewandte Chemie* **122**, 8341-8344 (2010).

96   Campbell, C. T., Parker, S. C. & Starr, D. E. The effect of size-dependent nanoparticle energetics on catalyst sintering. *Science* **298**, 811-814 (2002).

97   Pham, T. N., Sooknoi, T., Crossley, S. P. & Resasco, D. E. Ketonization of carboxylic acids: mechanisms, catalysts, and implications for biomass conversion. *Acs Catalysis* **3**, 2456-2473 (2013).

98   Prasomsri, T., Nimmanwudipong, T. & Román-Leshkov, Y. Effective hydrodeoxygenation of biomass-derived oxygenates into unsaturated hydrocarbons by MoO 3 using low H 2 pressures. *Energy & Environmental Science* **6**, 1732-1738 (2013).

99   An, K. *et al.* Preparation of mesoporous oxides and their support effects on Pt nanoparticle catalysts in catalytic hydrogenation of furfural. *Journal of colloid and interface science* **392**, 122-128 (2013).

100   Baker, L. R. *et al.* Furfuraldehyde hydrogenation on titanium oxide-supported platinum nanoparticles studied by sum frequency generation vibrational spectroscopy: Acid–base catalysis explains the molecular origin of strong metal–support interactions. *Journal of the American Chemical Society* **134**, 14208-14216 (2012).

101   Zhang, J., Wang, B., Nikolla, E. & Medlin, J. W. Directing Reaction Pathways through Controlled Reactant Binding at Pd–TiO2 Interfaces. *Angewandte Chemie* **129**, 6694-6698 (2017).

102   Primo, A., Concepción, P. & Corma, A. Synergy between the metal nanoparticles and the support for the hydrogenation of functionalized carboxylic acids to diols on Ru/TiO 2. *Chemical Communications* **47**, 3613-3615 (2011).

103   Boudart, M. Catalysis by supported metals. *Advances in catalysis* **20**, 153-166 (1969).

104   Pushkarev, V. V., Musselwhite, N., An, K., Alayoglu, S. & Somorjai, G. A. High structure sensitivity of vapor-phase furfural decarbonylation/hydrogenation reaction network as a function of size and shape of Pt nanoparticles. *Nano letters* **12**, 5196-5201 (2012).

105   Somorjai, G. A. & Park, J. Y. Molecular factors of catalytic selectivity. *Angewandte Chemie International Edition* **47**, 9212-9228 (2008).

106   Cuenya, B. R. Synthesis and catalytic properties of metal nanoparticles: Size, shape, support, composition, and oxidation state effects. *Thin Solid Films* **518**, 3127-3150 (2010).

107   Bennett, C. & Che, M. Some geometric aspects of structure sensitivity. *Journal of Catalysis* **120**, 293-302 (1989).

108   Durndell, L. J. *et al.* Selectivity control in Pt-catalyzed cinnamaldehyde hydrogenation. *Scientific reports* **5** (2015).

109   Feng, J. *et al.* Hydrogenolysis of glycerol to glycols over ruthenium catalysts: Effect of support and catalyst reduction temperature. *Catalysis Communications* **9**, 1458-1464 (2008).

110   Shen, W.-J. *et al.* Effect of reduction temperature on structural properties and CO/CO 2 hydrogenation characteristics of a Pd-CeO 2 catalyst. *Applied Catalysis A: General* **217**, 231-239 (2001).

111   Ackermann, M. *et al.* Structure and reactivity of surface oxides on Pt (110) during catalytic CO oxidation. *Physical review letters* **95**, 255505 (2005).

112   Hendriksen, B. & Frenken, J. CO oxidation on Pt (110): scanning tunneling microscopy inside a high-pressure flow reactor. *Physical Review Letters* **89**, 046101 (2002).

113   Gong, X.-Q., Liu, Z.-P., Raval, R. & Hu, P. A systematic study of CO oxidation on metals and metal oxides: density functional theory calculations. *Journal of the American Chemical Society* **126**, 8-9 (2004).

114   Min, B., Alemozafar, A., Pinnaduwage, D., Deng, X. & Friend, C. Efficient CO oxidation at low temperature on Au (111). *The Journal of Physical Chemistry B* **110**, 19833-19838 (2006).

115   Sitthisa, S., An, W. & Resasco, D. E. Selective conversion of furfural to methylfuran over silica-supported Ni Fe bimetallic catalysts. *Journal of catalysis* **284**, 90-101 (2011).

116   Montes, M. *et al.* Influence of metal-support interactions on the dispersion, distribution, reducibility and catalytic activity of Ni/SiO2 catalysts. *Applied catalysis* **12**, 309-330 (1984).

117   Manukyan, K. V. *et al.* Nickel Oxide Reduction by Hydrogen: Kinetics and Structural Transformations. *The Journal of Physical Chemistry C* **119**, 16131-16138 (2015).

118   Nakagawa, Y., Nakazawa, H., Watanabe, H. & Tomishige, K. Total Hydrogenation of Furfural over a Silica-Supported Nickel Catalyst Prepared by the Reduction of a Nickel Nitrate Precursor. *ChemCatChem* **4**, 1791-1797 (2012).

119   Gürbüz, E. I., Hibbitts, D. D. & Iglesia, E. Kinetic and Mechanistic Assessment of Alkanol/Alkanal Decarbonylation and Deoxygenation Pathways on Metal Catalysts. *Journal of the American Chemical Society* **137**, 11984-11995 (2015).

Appendix A2: Supporting information chapter 1: Stabilization of furanics to cyclic ketone building blocks in the vapor phase
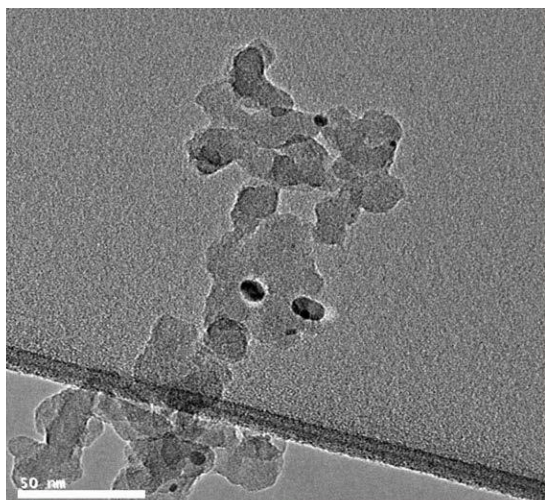
Supplementary Information

Ru/SiO₂

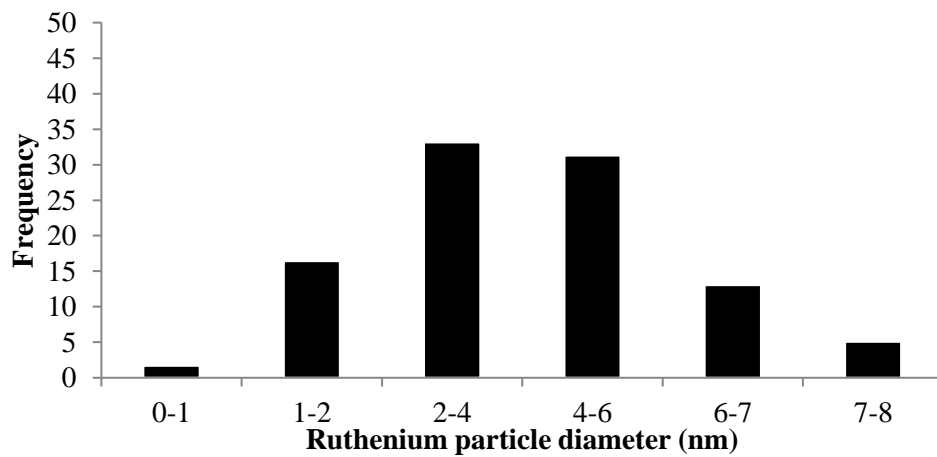**Figure S 5Representative TEM image for 5.3% Ru/SiO2**

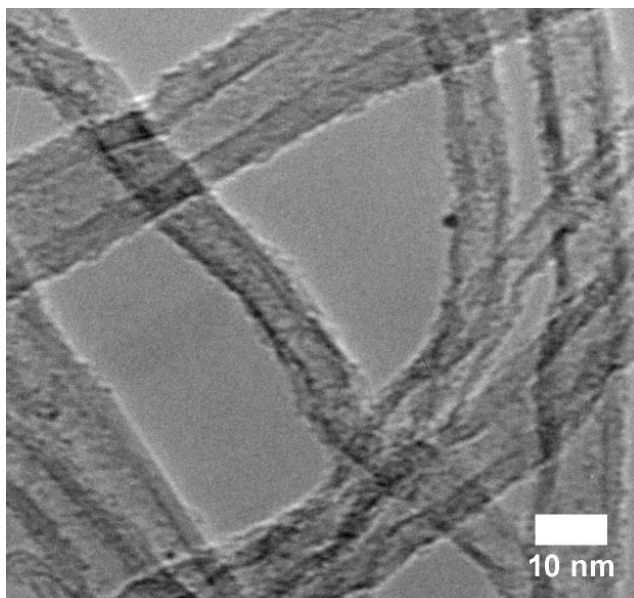**Figure S 6 Particle size distribution of 5.3 % Ru/SiO2 catalyst pre-reduced at 400 °C for one hour prior to imaging**

Ru/CNT
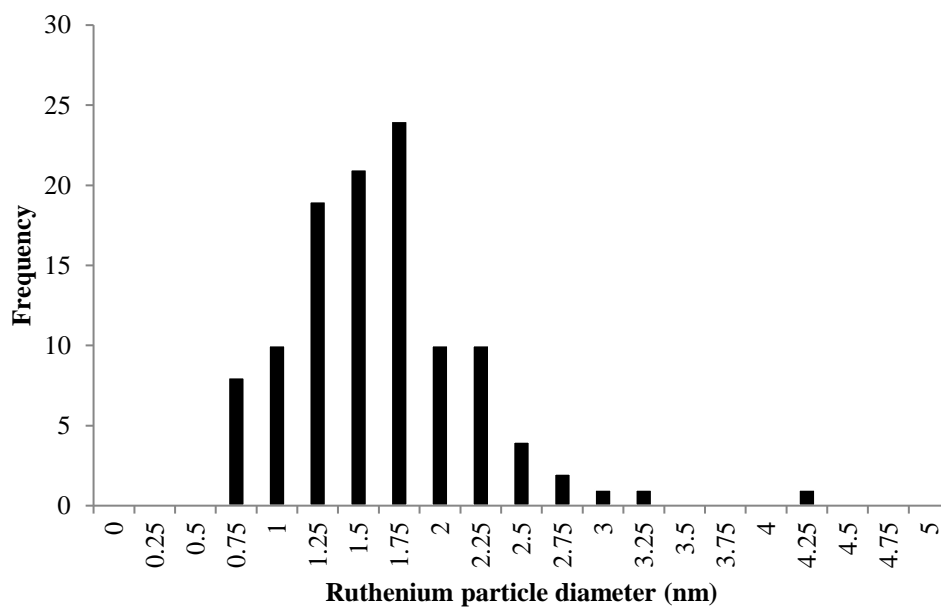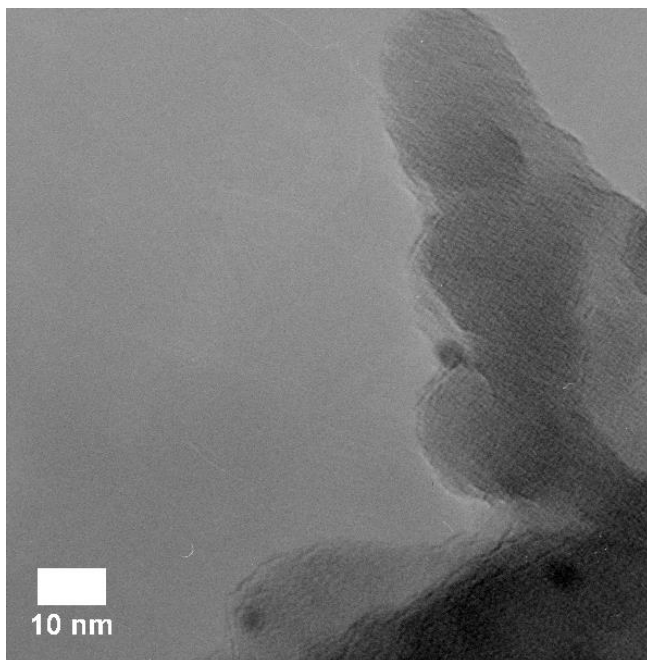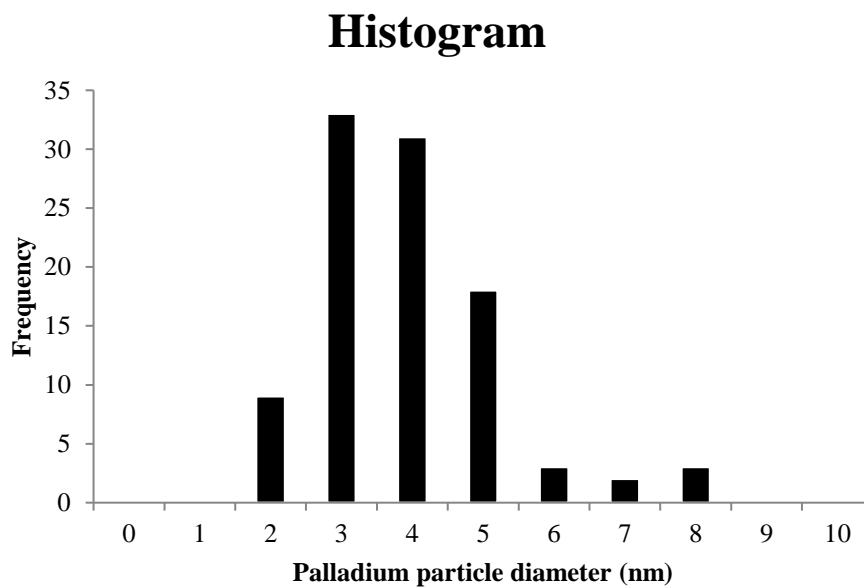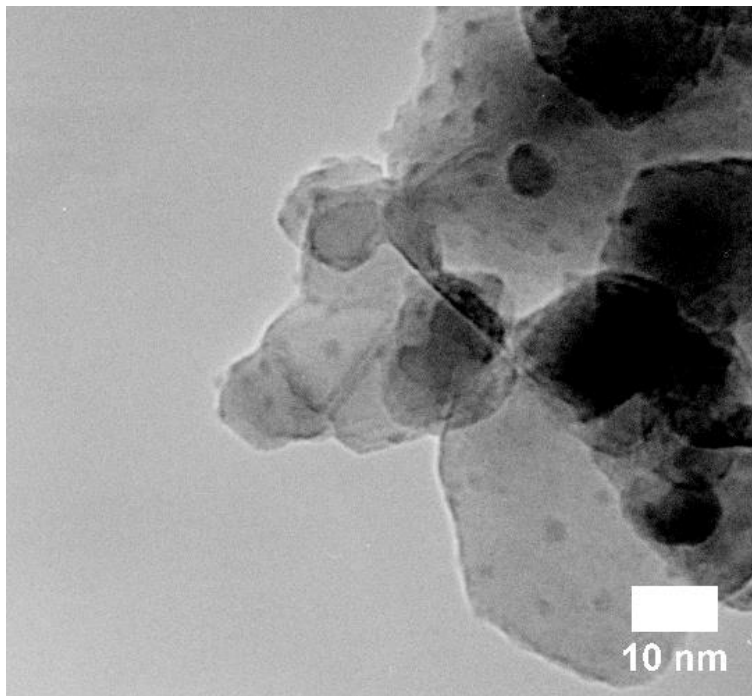

Figure S 7 Representative TEM image for 1% Ru/CNT

Figure S 8 Particle size distribution of 1% Ru/CNT catalyst pre-reduced at 400 °C for one hour prior to imaging

Pd/SiO₂

Figure S 9 Representative TEM image for 1% Pd/SiO2

Histogram

Figure S 10 Particle size distribution of 1% Pd/SiO2 catalyst pre-reduced at 400 °C for one hour prior to imaging

Pd/TiO₂

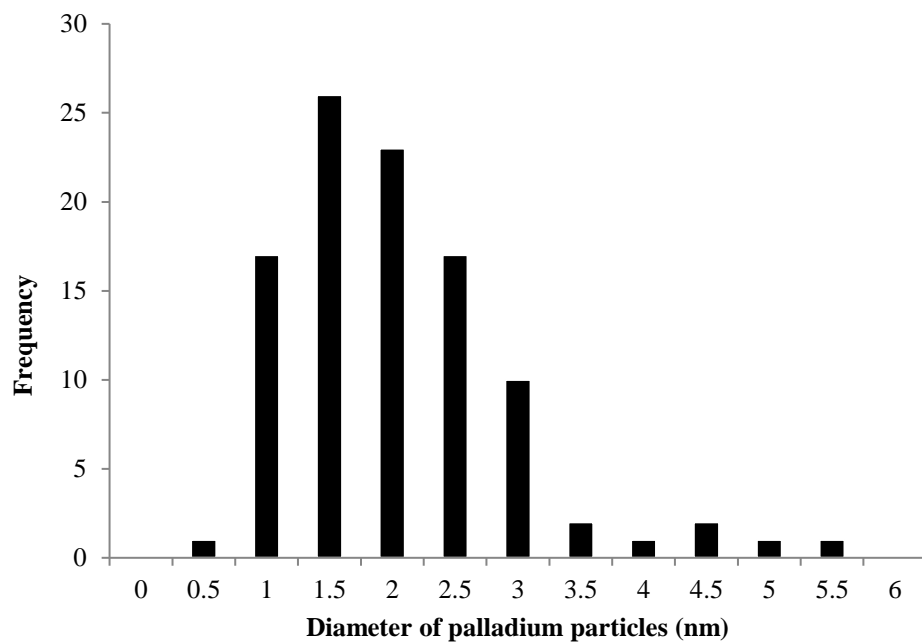**Figure S 11 Representative TEM image for 1% Pd/TiO₂**

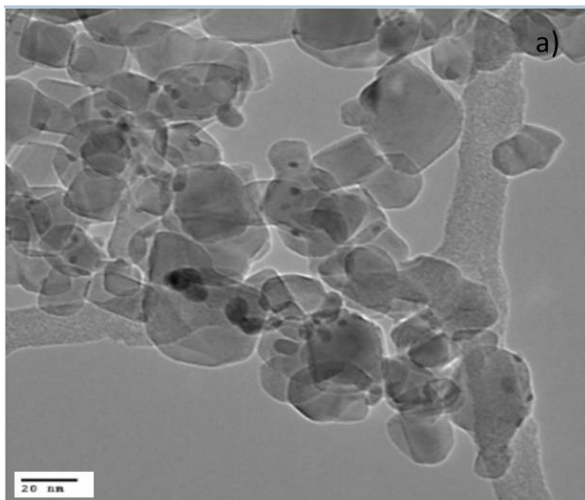**Figure S 12 Particle size distribution of 1 % Pd/TiO₂ catalyst pre-reduced at 400 °C for one hour prior to imaging**

Ru/TiO₂

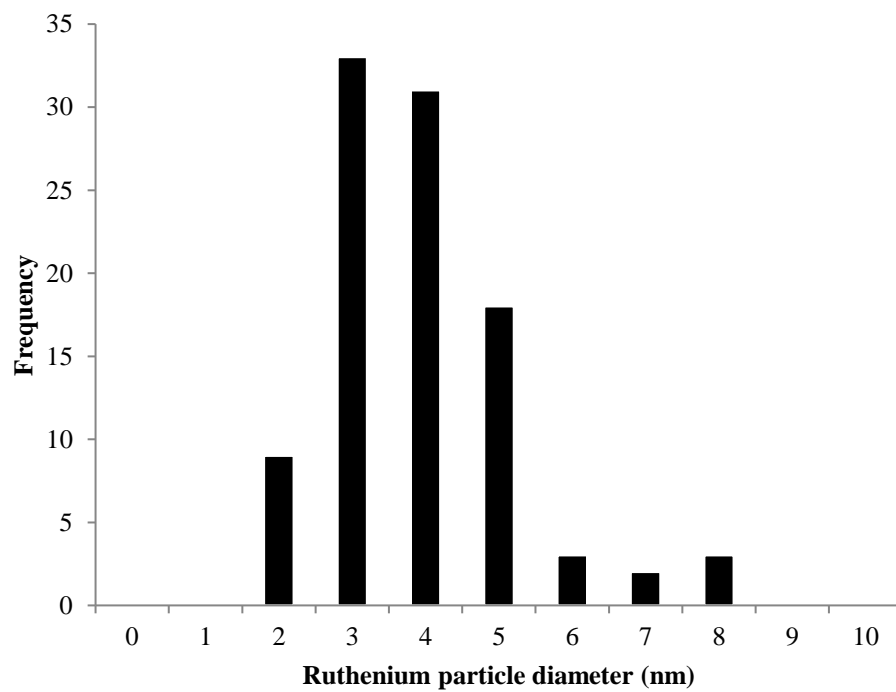**Figure S 13 Representative TEM image for 4.4% Ru/TiO₂**

Figure S 14 Particle size distribution of 4.4% Ru/TiO₂
catalyst pre-reduced at 400 °C for one hour prior to imaging

Table S 15 Particle size characterization and Surface area for the different catalyst tested

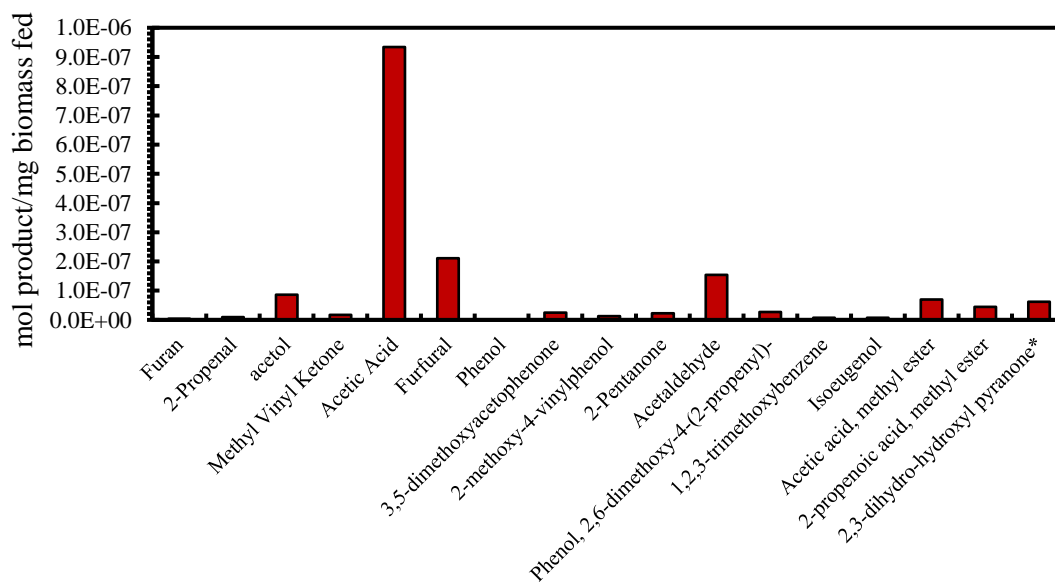| Catalyst	Loading (wt %)	BET Surface Area (m²/g)	Average Particle size (d_p)
Ru/TiO₂	4.4	55	3.6
Ru/SiO₂	5.3	126	4.1
Ru/CNT	1		1.5
TiO₂	-	60	-
Pd/SiO₂	1		3.4
Pd/TiO₂	1		1.7

Oak Torrefaction Experiments

Figure S 16 1st Pulse distribution of torrefaction blank with oak 270℃ and 20 min. * Formal name: 4-hydoxy-5,6-dihydro-(2H)-pyran-2-one

Number of pulses	1	2	3	4	5	6	7
Furfural + Pyranone balance	94.5%	83.4%	96.1%	108.1%	106.2%	105.8%	93.8%
Furfural balance	112.8%	117.7%	122.0%	114.4%	139.9%	131.4%	132.6%

Table S 2 Mass balance for furfural products and unreacted furfural respect to furfural + 2,3-dihydro-hydroxyl pyranone (4-hydoxy-5,6-dihydro-(2H)-pyran-2-one) mass in the blank and respect to furfural alone in the blank